MISSOURI UNIVERSITY OF SCIENCE
AND TECHNOLOGY (MS&T)

RPSEA SUBCONTRACT# 11123-14
DR. BAOJUN BAI
PRINCIPAL INVESTIGATOR

STUDY AND PILOT TEST OF PREFORMED PARTICLE GEL CONFORMANCE CONTROL COMBINED WITH SURFACTANT TREATMENT

Final Report

Covering the period from November 2012 to August 2015

Prime Contractor's Technical Point of Contact:
Baojun Bai
Phone: 573-341-4016; Email: baib@mst.edu

Missouri University of Science and Technology

August 2015

Study and Pilot Test of Preformed Particle Gel Conformance Control Combined with Surfactant Treatment

RPSEA Subcontract# 11123-14

Final Report August 2015

Completed by

Baojun Bai, Shari Dunn-Norman, Mingzhen Wei, Parthasakha Neogi

Farag Muhammed, Yue Qiu, Songyuan Liu, Abdulmohsin Imqam, Ali Alhuraishawy, Jiaming Geng, Xindi Sun, Lingbo Liu, Zainab Alabdulmhsen

Leading Organization

Missouri University of Science and Technology, Rolla MO

Participants

Blue Top Energy, LLC, Girard, Kansas (Small Producer)

Colt Energy Inc., Mission, Kansas (Small Producer)

TMD Energy Inc., Brentwood, Tennessee (Small Producer)

Baker Hughes Inc, Houston, Texas (Service Company)

EXECUTIVE SUMMARY

The objectives of the project are to: (1) test, through extensive laboratory and field pilot tests, the extent to which the coupled method of particle gel conformance control and surfactant treatment can improve both sweep efficiency and microscopic efficiency, thus improving overall oil production for small producers, and (2) evaluate whether PPG treatment and the coupled process can be used to control water production and improve oil recovery for the well candidates owned by small producers.

The project involves a series of laboratory experiments to comprehensively evaluate the proposed novel enhanced oil recovery (EOR) process, to screen the best PPGs and surfactants compatible with the formation fluids provided by the small producer collaborators, and to select screen tracers for field applications. We have executed a few pilot tests in injection wells located in Kansas operated by Blue Top Energy LLC and Colt Energy Inc. The format of this final report is as follows:

Section (1) reports the technology status of particle gel treatment technologies for conformance control in mature oilfields. The existing technologies are briefly reviewed and the proposed technology and mechanism are represented in this section.

Section (2) reports the core-flooding experiments that were conducted in the Missouri S&T laboratory. Two series of experiments were executed to test whether the combined method can be used in injection wells. Experimental results showed that the mixture injection of PPG and surfactant could result in higher oil recovery than any single method or sequential injection of PPG and surfactant.

Section (3) focuses on the screening experiments conducted to select the best PPG and surfactant for candidate wells. Several families of surfactants and nanoparticles were evaluated for their ability to emulsify heavy oil. Crude oil samples from the oilfields in western Missouri and southeastern Kansas were used for the tests. Results showed the non-ionic surfactant IGEPAL® CO-530 could form stable emulsions with the heavy oils at reservoir temperature but the emulsion could breakdown when the temperature increased to above 45 °C, which could significantly reduce the cost of deemulsifying crude oil. This section also examined the compatibility of PPGs with the selected surfactants and formation water. The swelling ratio and

strength of PPGs were measured with and without surfactant. After evaluation, the Cerogel™ PPGs 780 and 746 were selected to be used for pilot tests.

Section (4) provides the method to select a well candidate for PPG treatment and the coupled method of PPG treatment and surfactant injection. We collected data of 874 successful PPG treatments from papers and oil companies and conducted data analysis. Then a comprehensive evaluation method was developed based on the weight of each factor that impact the well selection, including injection well injectivity, reservoir heterogeneity and the production performance of adjacent wells. An interface-friendly software tool was developed to screen the well candidates for PPG treatment, which is available to be downloaded in the web www.PPGEOR.org.

Section (5) shows the preparation, operation and result analysis for the pilot tests which were carried out in four leases by our small producer collaborators, Blue Top Energy LLC and Colt Energy Inc. All of the pilot tests showed that PPG could be successfully injected into the selected wells. The water injection pressures after treatment were significantly improved. The treatments also significantly reduce the directional channel problems evidenced by the delayed breakthrough time of tracers or the pressure response of adjacent producers. Both companies reported to have observed water cut reduction and oil production rate increase from the treatments though detailed information was not provided.

Section (6) presents the technology transfer efforts from this research group. We published 12 papers in either peer-reviewed journals or at SPE conferences. We also made 14 presentations and gave five invited talks in conferences, companies, and institutions. One website was developed to provide more information with regard to preformed particle gel conformance control technologies.

TABLE OF CONTENTS

PAGE

EXECUTIVE SUMMARY ..... **I**

TABLE OF CONTENTS ..... **III**

LIST OF ILLUSTRATIONS ..... **VI**

LIST OF TABLES ..... **XI**

1. TECHNOLOGY STATUS REPORT **12**

1.1 Summary 12

1.2 Existing Gel Treatment Technologies 12

1.2.1 Gel Treatments 12

1.2.2 Surfactant EOR 15

1.3 Proposed Coupled Method 16

2. CORE FLOODING EXPERIMENTS TO TEST THE EFFECTIVENESS OF THE COMBINATION METHOD **19**

2.1 Experiments 19

2.2 Materials 19

2.2.1 Experiment Apparatus Design 21

2.2.2 Open Fracture Experiments Procedure 24

2.3 Results and Discussion 25

2.3.1 First Set of Experiments—PPG Swollen in 1.0 Wt.% NaCl Solution 25

2.3.2 Second Set of Experiments—PPG Swollen in Surfactant Aqueous Solution 27

2.4 Summary 33

3. SCREEN THE BEST PPGS AND SURFACTANTS FOR THE WELL CANDIDATES **34**

3.1 A Systematic Evaluation for Heavy Oil Emulsion Method for EOR 35

3.1.1 Materials 35

3.1.2 Procedures 38

3.1.3 Results and Discussion 41

3.1.4 Summary 49

3.2 Surfactant and Nanoparticle Emulsion Stability for Larsen Oil 49

3.2.1 Introduction 49

3.2.2 Emulsion Stability by Crude Oil and Surfactants 50

3.2.3 Summary 58

3.3 Optical Experiments of Surfactants to Oil and Water Emulsion 60
3.3.1 Introduction 61
3.3.2 Method and Materials 65
3.3.3 Results and Discussion 67
3.3.4 Summary 82
3.4 Select the Best PPG Compatible with the Selected Surfactant(s) and Formation Water 82
3.4.1 Materials and Methods 83
3.4.2 Results and Discussion 84
3.4.3 Summary 96
4. WELL CANDIDATE SELECTION 97
4.1 Introduction 97
4.2 Data Analysis 98
4.2.1 Reservoir Conditions 98
4.2.2 Injection Well Conditions 101
4.2.3 Corresponding Production Wells Conditions 104
4.3 Methodology 106
4.3.1 Determining the Weight Factors of Each Index 106
4.3.2 The Comprehensive Evaluation Method 109
4.4 Illustrated Case 110
4.4.1 Determining the Weight Factors of Each Index 111
4.4.2 Evaluation Results by Comprehensive Evaluation Method 113
4.5 Summary 114
5. PILOT TESTS IN SMALL PRODUCER LEASES 115
5.1 Background on the Pilot Areas 115
5.1.1 Cherokee Group Basin 117
5.1.2 The Humboldt-Chanute Field 117
5.1.3 The Neosho Falls-Leroy Field 121
5.2 Pilot Tests Preparation, Operation, and Results Evaluation 123
5.2.1 Pilot Tests in E. Larsen Lease 124
5.2.2 L. L. Baker Lease 135
5.2.3 Field Testing in Crotts Lease 137

5.2.4 Murray B Lease 141
5.3 Summary and Lessons 144
6. TECHNICAL TRANSFER.....145
6.1 Research Website 145
6.2 Publications 145
6.3 Presentations 146
6.4 Invited Talks 147
REFERENCES 148

LIST OF ILLUSTRATIONS

Page

Figure 1-1 Effect of particle size and strength on permeability reduction (rock permeability = 85 md). 17
Figure 2-1. Sandstone slabs prepared for the experiments. 21
Figure 2-2. Apparatus for the saline extraction process. 21
Figure 2-3. Schematic diagram of the semi-fractured model. 23
Figure 2-4. Schematic diagram of the semi-transparent model. 23
Figure 2-5. Picture of the semi-transparent fracture model. 24
Figure 2-6. Injection pressure profile at different stages of the fracture model. 26
Figure 2-7. Oil recovery factor during treatment with PPG swollen in 1 wt.% NaCl. 27
Figure 2-8. Injection pressure profile at different stages of the fracture model. 28
Figure 2-9. Oil recovery factor during treatment with PPG swollen in surfactant. 29
Figure 2-10. PPG placement inside the fracture followed by brine injection. 31
Figure 2-11. Sandstone core surface at the end of the experiment. 31
Figure 2-12. Core surface after the experiments. 32
Figure 2-13. PPG particles before and after injection into the fracture. 32
Figure 3-1. UV absorbance calibration curve for IGEPAL® CO-530. 41
Figure 3-2. Adsorption isotherms for IGEPAL® CO-530. 41
Figure 3-3. Stability of emulsions created by NEODOL® surfactants. 42
Figure 3-4. Stability of emulsions created by Tomadol® nonionic surfactants. 42
Figure 3-5. Stability of emulsions created by TERGITOL® nonionic surfactants. 43
Figure 3-6. Stability of emulsions created by some nonionic surfactants. 43
Figure 3-7. Stability of emulsions created by anionic surfactant. 44
Figure 3-8. Stability of emulsions created by three cationic surfactants. 44
Figure 3-9. Effect of temperature on the stability of heavy oil and formation brine emulsion. 45
Figure 3-10. Effect of surfactant concentration on the stability of heavy oil and formation brine emulsion. 45

Figure 3-11. Effect of oil-to-brine ratio on the stability of heavy oil and formation brine emulsion. 46
Figure 3-12. Effect of IGEPAL® CO-530 and alkaline NaOH on wettability. 46
Figure 3-13. Heavy oil recovery by core flooding test using IGEPAL® CO-530 surfactant with and without the addition of alkaline solution of NaOH. 47
Figure 3-14. IGEPAL® CO-530 and A-Hauser crude oil emulsions with different ratios at 25˚C. 51
Figure 3-15. IGEPAL® CO-530 and A-Hauser crude oil emulsions with different ratios at 40˚C. 51
Figure 3-16. SDS and A-Hauser crude oil emulsions with different ratios at 25°C. 51
Figure 3-17. CTAB and A-Hauser crude oil emulsions with different ratios at 25°C. 52
Figure 3-18. Al_2O_3/IGEPAL® CO-530 and A-Hauser crude oil emulsions with different ratios at 40°C. 53
Figure 3-19. Al_2O_3/IGEPAL® CO-530 and A-Hauser crude oil emulsions with different ratios at 40°C. 53
Figure 3-20. Al_2O_3/SDS and A-Hauser crude oil emulsions with different ratios at 25°C. 54
Figure 3-21. Al_2O_3/SDS and A-Hauser crude oil emulsions with different ratio at 25°C after 24 hours. 54
Figure 3-22. Al_2O_3/CTAB and A-Hauser crude oil emulsions with different ratios at 25°C after 24 hours. 55
Figure 3-23. SiO_2/ IGEPAL® CO-530 and A-Hauser crude oil emulsions with different ratios at 25°C. 56
Figure 3-24. SiO_2/SDS and A-Hauser crude oil emulsions with different ratios at 25°C. 57
Figure 3-25. SiO_2/CTAB and A-Hauser crude oil emulsions with different ratios at 25°C. 58
Figure 3-26. Ternary phase diagram of an oil-surfactant water system, based on a $C_{12}E_{10}$-oleic acid water system. 62
Figure 3-27. Phase diagram: Water (aqueous phase), oil, surfactant and the structure of microemulsion. 62
Figure 3-28. Classification of emulsifiers according to HLB values. 62
Figure 3-29. Relationship between phase behavior and IFT values. 63

Figure 3-30. A hypothetical ternary phase diagram representing three components of the system. 64
Figure 3-31. Schematic presentation of most frequently occurring surfactant associates. 65
Figure 3-32. Emission spectrum of Nile Red in different solvents: (a) n-hexane; (b) ethyl acetate; (c) methanol; (d) water. 66
Figure 3-33. Natural florescence of crude oil 5-8. 66
Figure 3-34. Surfactant selection and its HLB value. 67
Figure 3-35. Schematic of the experimental apparatus. 67
Figure 3-36. Emulsion types using decane and crude oil together with 3 different surfactants. 68
Figure 3-37. Emulsion types using water and crude oil together with 2 different surfactants. 68
Figure 3-38. Microscopic image of the middle layer using surfactant Span 80 with (a) decane and (b) crude oil. 69
Figure 3-39. Bicontinuous water and oil phase using IGEPAL® CO-530 and (a) decane and (b) crude oil. 70
Figure 3-40. Oil in water emulsion with SDS and (a) decane and (b) crude oil. 71
Figure 3-41. Microscopic image of the upper layer using Span 80 with crude oil. 72
Figure 3-42. Microscopic image of the middle layer using Span 80 with decane. 72
Figure 3-43. (a) Microscopic image of emulsion using SDS with decane and the measurement of droplets threshold, (b) Automated measurement of region of interest using an intensity threshold from 142 to 172, (c) Automated measurement of region of interest using an intensity threshold from 172 to 215. 74
Figure 3-44. Dispersed phase size distribution for 85% water, 10% decane and 5% Span 80. 75
Figure 3-45. Dispersed phase size distribution for 85% water, 10% decane, and 5% SDS. 76
Figure 3-46. Dispersed phase size distribution for 85% water, 10% crude oil, and 5% Span 80. 76
Figure 3-47. Dispersed phase size distribution for 85% water, 10% crude oil, and 5% SDS. 77
Figure 3-48. Procedures of surfactant flooding using a two-window micro-tube. 79
Figure 3-49. Crude oil water flooding process and the residual oil caused by high oil viscosity. 80
Figure 3-50. A 3-D reconstruction of residual oil distribution after water flooding. 80
Figure 3-51. Oil emulsion forming and flowing within micro-tube using 1% SDS surfactant. 81
Figure 3-52. Entrance image after (a) surfactant flooding, and (b) gas flooding. 81
Figure 3-53. Effect of brine concentration and temperature on the swelling ratio of PPG1. 85

Figure 3-54. Effect of brine concentration on the swelling ratio of PPG2. 86
Figure 3-55. Effect of brine concentration and temperature on the swelling ratio of PPG3. 86
Figure 3-56. Effect of brine concentration on the swelling ratio of PPG4. 87
Figure 3-57. Effect of brine concentration on the swelling ratio of PPG5. 87
Figure 3-58. Effect of brine concentration on the swelling ratio of PPG6. 88
Figure 3-59. Effect of brine concentration on the swelling ratio of PPG7. 88
Figure 3-60. Strength (storage moduli, G') of seven PPGs swollen in 1.0 wt% NaCl. 89
Figure 3-61. Effect of salinity on Cerogel™ strength at ambient temperature. 90
Figure 3-62. Swelling ratio of Cerogel™ at ambient temperature (25°C). 91
Figure 3-63. Swelling ratio of Cerogel™ at 60°C. 91
Figure 3-64. Swelling ratio of Cerogel™ at 80°C. 92
Figure 3-65. Effect of surfactant (200 ppm) on Cerogel™ strength at ambient temperature. 93
Figure 3-66. Effect of surfactant (200 ppm) on Cerogel™ strength at 80°C. 93
Figure 3-67. Effect of surfactant (500 ppm) on Cerogel™ strength at ambient temperature. 94
Figure 3-68. Effect of surfactant (500 ppm) on Cerogel™ strength at 80°C. 94
Figure 3-69. Effect of surfactant (1000 ppm) on Cerogel™ strength at ambient temperature. 95
Figure 3-70. Effect of surfactant (1000 ppm) on Cerogel™ strength at 80°C. 95
Figure 4-1. Distribution of reservoir temperatures. 99
Figure 4-2. Distribution of reservoir salinity. 99
Figure 4-3. Distribution of reservoir permeability. 100
Figure 4-4. Lorenz coefficient for injection flow distribution. 100
Figure 4-5. Distribution of reservoir permeability heterogeneity. 101
Figure 4-6. Distribution of injection profile heterogeneity. 101
Figure 4-7. Distribution of injection pressure. 102
Figure 4-8. Distribution of injection rate. 102
Figure 4-9. Pressure draw-down curve. 103
Figure 4-10. Distribution of pressure index (PI). 104
Figure 4-11. Distribution of liquid production. 104
Figure 4-12. Distribution of water cut. 105
Figure 5-1. Map showing the Cherokee Group basin. 117
Figure 5-2. Location of Humboldt-Chanute field. 119

Figure 5-3. Annual oil production from Humboldt-Chanute field. 120
Figure 5-4. Production history and decline curve analysis of Neosho Falls-Leroy Field (Source: KGS website). 122
Figure 5-5. Location of Humboldt-Chanute Field. 123
Figure 5-6. Flow chart of typical surface equipment for the novel EOR methods. 124
Figure 5-7. Production plot for E. Larsen lease (Source: KGS website). 125
Figure 5-8. Well distribution at E. Larson lease. 125
Figure 5-9. Crude oil viscosity and API° of E. Larsen lease. 126
Figure 5-10. Nitrate test kit, 0-50 mg/L NO_3-N. 127
Figure 5-11. Tracer test results from four production wells. 128
Figure 5-12. Step rate test on injector Well 7. 129
Figure 5-13. Cement unit used for the PPG and surfactant treatment in E. Larsen lease. 130
Figure 5-14. Bags of Cerogel™. 131
Figure 5-15. PPG and surfactant were mixed before injection into Well 7. 132
Figure 5-16. Real time injection pressure during PPG and surfactant treatment in Well 7. 133
Figure 5-17. Wellhead pressure gage reading of Well 7 before and after the treatment. 133
Figure 5-18. Draw down pressure before and after PPG treatment. 134
Figure 5-19. Production history for L. L. Baker lease (Source: KGS website). 136
Figure 5-20. Well distribution in L. L. Baker lease. 137
Figure 5-21. Production history for Crotts lease (Source: KGS website). 138
Figure 5-22. Well distribution in Crotts lease. 139
Figure 5-23. The cement pump to inject PPG dispersion. 140
Figure 5-24. Monitored real-time injection pressure of PPG injection. 141
Figure 5-25. Production history for Murray B lease (Source: KGS website). 141
Figure 5-26. Well distribution in Murray B lease. 142
Figure 5-27. Real time injection pressure during PPG treatment of Well 11 in Murray lease. 143

LIST OF TABLES

Page

Table 2-1. Parameters of Berea sandstone cores. 20
Table 3-1. Compositions of reservoir formation brine. 36
Table 3-2. Recipe for Synthetic Formation Brine. 36
Table 3-3. Commercial and chemical name for the surfactants investigated. 37
Table 3-4. Viscosity, standard deviation and experimental error. 38
Table 3-5. Oil recovery test results with water-wet and oil-wet sandpacks. 47
Table 3-6. Stability results of surfactants at 25°C and 40°C. 59
Table 3-7. Stability results of surfactants with Al_2O_3 at 25°C and 40°C. 59
Table 3-8. Chemical additives system expectations and results. 60
Table 3-9. HLB group number. 63
Table 3-10. Statistical analysis of the size distribution in different emulsions. 78
Table 3-11. Evaluated PPG Samples 83
Table 4-1. Criteria for well selection. 105
Table 4-2. The relative importance values of pair-wise comparisons. 108
Table 4-3. The value of the random index (RI). 109
Table 4-4. Water injection well raw data. 111
Table 4-5. Normalized index matrix and entropy-based weights of factors. 112
Table 4-6. Pairwise comparison matrix and AHP-based weight factors. 113
Table 4-7. Final well ranking. 114
Table 5-1. Stratigraphic chart of oil-producing formations in Kansas. 116
Table 5-2. Summary of the production history of Humboldt-Chanute field. 119
Table 5-3. Reservoir characteristics of Bartlesville sandstone formation. 121
Table 5-4. Leases selected for the oilfield pilot tests. 123
Table 5-5. Properties of PPGs used in the pilot test. 124
Table 5-6. Properties of injection water. 126

1. TECHNOLOGY STATUS REPORT

1.1 Summary

This project aims to systematically investigate a novel technology that couples PPG and surfactant into one enhanced oil recovery (EOR) process. When surfactants and PPG are injected into a well together, the PPG will preferentially enter fractures or fracture-like channels to reduce their permeability, while the surfactant solution will squeeze into non-swept matrices or zones/areas to reduce the interfacial tension (IFT) and alter the wettability. Gel treatments alone can only improve the sweep efficiency, and surfactant EOR can only improve the microscopic displacement efficiency. Together, however, they can significantly reduce water production and improve both the displacement and sweep efficiency, thus yielding a more cost-effective EOR method.

The ultimate objective of this project is to provide a comprehensive understanding of the combined technology and, through laboratory experiments and field demonstration tests, to identify where and how the technology can be applied most acceptably. This chapter summarizes the current status of relevant technologies.

1.2 Existing Gel Treatment Technologies

Excess water production and low oil production rates are two major issues that lead to early well abandonment and unrecoverable hydrocarbon in mature wells owned by small producers. Oil recovery is the product of the displacement efficiency (ED) and the sweep efficiency (ES). EOR methods focus either on increasing the ED by reducing residual oil saturation or the ES by correcting reservoir heterogeneity. Gel treatment and surfactant EOR are two principle EOR methods. Each has limitations that can largely be avoided by combining the two methods.

1.2.1 Gel Treatments

Gel injections usually are intended to reduce the volume of water produced with the oil, but they also can result in improved ES [1]. When successful, these gel systems divert a portion of the injected water into areas not previously swept by water. However, gels are designed to improve

only the ES [2]. A new trend in gel treatments is to apply preformed gels because they can overcome some distinct drawbacks inherent in in-situ gelation systems, such as a lack of gelation time control, uncertainness of gelling due to shear degradation, chromatographic fractionation of gelant compositions, and dilution by formation water.

1.2.1.1 Using Preformed Gels to Control Conformance Has Become a New Trend for Gel Treatments

Gel treatments are widely applied to improve conformance and reduce water channeling in mature reservoirs. Two kinds of gels, in-situ crosslinking gels and preformed particle gels (PPGs) are applied for control conformance. For in-situ gel, a mixture of a polymer and a cross-linker (called pre-gel or gelant) is injected into a target formation, where the two react at reservoir temperature to form a gel that fully or partially seals the formation. PPGs recently have been developed and applied to control conformance. They can overcome some of the drawbacks inherent in an in-situ gelation system, such as lack of gelation time control, gelling uncertainty due to shear degradation, chromatographic fractionation, and dilution by formation water [3, 4, 5]. PPG is formed at a surface facility before injection, so no gelation occurs in the reservoir. PPGs usually have only one component during injection and display little sensitivity to the physico-chemical conditions in a reservoir, such as pH, salinity, multivalent ions, hydrogen sulfide, and temperature [4, 5]. Commercially available particle gels come in various sizes, including micro- to millimeter-sized PPGs [4, 5, 6], microgels [7], pH-sensitive cross-linked polymers [8, 9], and swelling submicron-sized polymers [10, 11]. Their major differences lie in the particle size, swelling time, and swelling ratio. The literature indicates that PPGs, microgels, and submicron-sized polymers have been economically applied to reduce water production and improve oil recovery in mature oilfields. In one case, microgels were applied to approximately 10 gas storage wells to reduce water production [7]. In another case, submicron-sized particles were applied to more than 60 wells [12]. In China, millimeter-sized PPGs have been applied to over 5,000 wells in water floods and polymer floods to reduce the permeability of fractures and super-high-permeability channels [13].

1.2.1.2 Advantages of PPG Treatment

PPGs have been widely accepted and are seeing more use by operators due to their unique advantages over traditional in-situ gels, including that they

- Are synthesized prior to formation contact, thus overcoming distinct drawbacks inherent in in-situ gelation systems, such as uncontrolled gelation times, variations in gelation due to shear degradation, and gelant changes caused by contact with reservoir minerals and fluids.

- Are strength- and size-controlled, environmentally friendly, and stable in the presence of almost all reservoir minerals and formation water salinities.

- Can preferentially enter into fractures or fracture-feature channels while minimizing gel penetration into unswept zones/matrices. Gel particles with the appropriate size and properties should transport through fractures or fracture-feature channels but should not penetrate into conventional rocks.

- Usually have only one component during injection. Thus, PPG treatment is a simpler process that does not require many of the injection facilities and instruments that often are needed to dissolve and mix polymers and crosslinkers for conventional in-situ gels.

- Can be prepared with produced water without influencing gel stability. In contrast, traditional in-situ gels are often very sensitive to salinity, multivalent cations, and H_2S in the produced water. This not only saves fresh water but also protects the environment.

1.2.1.3 Achievements from Previous RPSEA Project, "Preformed Particle Gels for Conformance Control" Project No: 017123-02

The project entitled "Preformed Particle Gel for Conformance Control" was funded by RPSEA in August 2008, and was completed in March 2011. The goal of the project was to develop methods for optimizing PPG treatments in order to increase oil recovery and reduce water production by improving the water flood sweep efficiency. The following achievements were realized from the RPSEA-funded project:

- Field application examples from different reservoirs were summarized and analyzed. The results showed that PPGs can be injected successfully not only into reservoirs that have been identified as having fractures, but also into reservoirs that have been water flooded

for a long time and have not been identified as having fractures. This useful information acquired from the field experience will facilitate well candidate selection and PPG treatment design.

- The factors influencing PPG injectivity, including the channel permeability, particle strength, and injection rate, were quantified using screen models, tubing models, and transparent fracture models. These solid data will provide important theoretical support to optimize PPG treatment design.

- A series of size-distributed, novel PPGs for use under various reservoir conditions were successfully developed, and some have been commercialized and made available to small producers. The particle size can be adjusted from a few micrometers to a few millimeters, and the swelling ratio can be adjusted over the course of a few days.

1.2.2 Surfactant EOR

Surfactant EOR reduces residual oil in the swept area and improves the ED by reducing the capillary and IFT between oil and water. Surfactants can be injected either from an injection well (called flooding) or a production well (called huff-puff or soaking). The major problem with surfactant injection is that the surfactant primarily enters fractures or super-permeable zones/streaks, which will cause the surfactant to break through early or have little opportunity to enter low-permeability zones or matrices to clean the large amount of oil remaining there.

Recent studies have shown that the EOR mechanism behind this method for heavy oil also contributes to a significant oil viscosity reduction resulting from the formation of W/O emulsions [13, 14]. One concern regarding the emulsification method is the emulsion stability. However, it has been reported that some nanoparticles, such as CAB-O-Sil®TS-530, can be used to stabilize the emulsion. Several pilot tests have shown that surfactant flooding can increase oil recovery by 10 to 20 percent after water flooding [15]. However, early surfactant breakthrough often can occur due to flow short-circuiting. This occurs because surfactant flooding is always performed in mature oilfields where reservoir heterogeneity has been aggravated due to previous oil

production and water injection [16, 17]. Early breakthrough wastes surfactants and increases lifting costs.

Surfactant soaking is used mainly to alter reservoir wettability from oil-wet to water-wet for oil recovery improvement, mostly in carbonate and heavy oil reservoirs. During field application first, a surfactant solution is injected into a production well, and then the well must be shut off for a few days to allow the surfactant to enter unswept regions by spontaneous imbibition instead of entering only the fractures or high-permeability channels, as is its preference. Lastly, the well is put back into production. This method can significantly improve oil recovery at a lab scale, but it is a slow recovery process because spontaneous imbibition is limited by the rate of molecular diffusion. Stoll et al. [18] indicated that spontaneous imbibition would not prove economically feasible unless external forces enabled forced imbibition.

1.3 Proposed Coupled Method

Surfactant EOR can increase the ED but has little or no effect on the ES. PPGs have been applied successfully to control conformance in more than 4,000 wells in China; however, the technology can only be used to plug fractures or super-K channels to improve the ES and has little effect on the ED. We investigated coupling PPG treatment and surfactant injection into one process, thus bypassing the limitations of each method when used individually. The combined method will improve both the ED and the ES and thus the overall cost-effectiveness of EOR.

Two findings from the last RPSEA-supported study [19] suggest that PPG is a better gel for the combination process. The first finding showed that particle gel will only enter high-permeability zones/streaks or fractures and will not form face plugging on the surface of low permeabilityzones or fracture surfaces if the particle sizes and strengths are properly selected; thus, PPGs cause little damage to low-permeability oil zones, as shown inFigure 1-1**.** Another finding, obtained during a preliminary study of the compatibility of PPG and surfactant, indicated that (1) surfactant can greatly reduce PPG strength when mixed together, but the strength can be recovered after the surfactant is removed; and (2) some surfactants cannot enter the pores in a particle gel network, and thus, no surfactant is lost to the gel. These two new findings set PPGs apart from bulk gels. Compared with a single PPG treatment, the coupled EOR process has the following distinct advantages:

- PPG injectivity can improve drastically because the presence of surfactant can greatly reduce the PPG strength.

- The reduced PPG strength can be recovered after the treatment when the water is diluted during water flooding, which will increase the PPG's plugging efficiency.

- The surfactant solution mixed with the PPG will be squeezed from gel particles into low-permeability zones/areas where crude oils are trapped by capillary force. The surfactant solution can dramatically reduce the capillary force (IFT between oil and water) and release the crude oil.

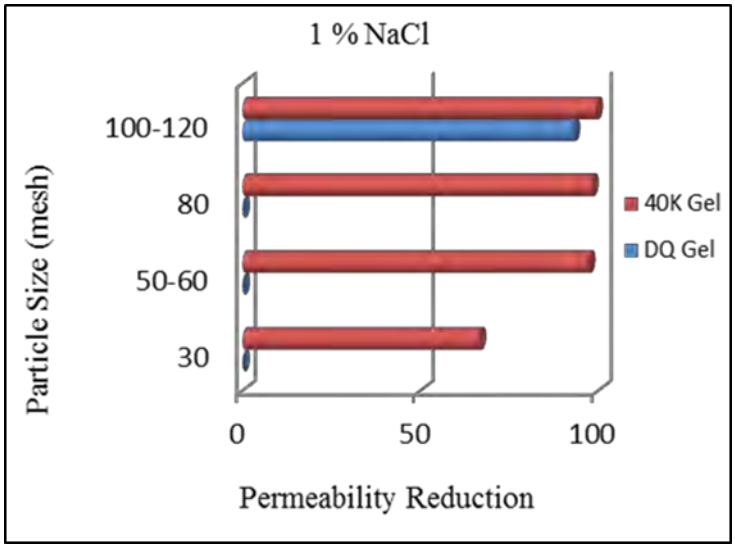

Figure 1-1 Effect of particle size and strength on permeability reduction (rock permeability = 85 md).

A 40K gel is a weak particle gel, whereas DQ (define DQ as it is the first time this appears in the report) is a strong particle gel. As illustrated in Figure 1-1, DQ does not damage the rock's permeability when it has a mesh size of 30, 50-60, or 80, but it does cause damage when its size is 100-120. However, 40K will damage the rock's permeability in all cases.

The combined injection of PPG and surfactant will result in a higher injection pressure gradient in the reservoir because of the high flow resistance resulting from the particle. This increased pressure will produce an additional force to drive surfactant into the matrix or low-permeability areas, thus making forced imbibition practical. The successful development of this technology

will provide a more cost-effective method for improving oil recovery and reducing water production for small producers.

2. CORE FLOODING EXPERIMENTS TO TEST THE EFFECTIVENESS OF THE COMBINATION METHOD

Laboratory experiments were run to test whether the coupled method could be used in injection wells. The purpose of the experiments was to test the extent to which the proposed coupled method could reduce water production through channels and improve oil production from unswept areas or zones. The following subsections describe the experimental models and results.

2.1 Experiments

2.2 Materials

Brine: 1.0 wt.% NaCl was used for flooding and preparing swollen PPG.

PPG: A commercial PPG, Cerogel™ PPG-746 from ChemEOR, was used for the experiments. The dry PPG samples had a size of 60 to 70 mesh.

Surfactant: IGEPAL® CO-530, a commercial nonionic surfactant, was used for the experiments.

Oil: A heavy mineral oil (paraffin oil) with a viscosity of 165 cp was used to represent heavy oil.

Sandstone core: Berea sandstone cores with an average porosity of 21.8% and a permeability of 154 mD were used for the experiments (Figure 2-1). Table 2-1 summarizes the parameters of the six core slabs used. The cores were treated with toluene and silane to change their wettability from water to oil-wet using the following wettability alteration procedures:

Sink the sandstone core slabs in an acid base to clean them for 12 hours.

Wash the cores using distilled water, and then leave them in deioninzed (DI) water bath at ambient temperature for 12 hours.

Dry the cores in an oven at 125°C (257°F) for 12 hours.

1. Vacuum the cores, place them in a container, add toluene to cover them, and then add 2 .0 wt.% of Octadecyl Dimethyl-dimethoxy-silane as a salinization agent.

2. Use an extraction process similar to that used by the US Bureau of Mines (USBM) to ensure that the solution saturates into all connected pores in the cores, as Figure 2-2 illustrates.

3. Rinse the sandstone cores using toluene.

4. Dry the cores under 120°C (257°F) for 24 hours. Then, vacuum the cores and saturate them fully with oil after the porosity, permeability, and pore volume are determined.

Table 2-1. Parameters of Berea sandstone cores.

Sample #	Length (cm)	Width (cm)	Thickness (cm)	Bulk volume (cc)	Pore volume (cc)	Dry weight (gram)	Porosity (%)	Permeability (md)
1	22.6	4.735	2.133	228.3	49.76	478.08	21.8	154
2	22.55	4.81	2.108	228.6	49.83	467.69		
3	22.36	4.739	2.095	222.1	48.41	452.79		
4	22.45	4.7493	2.119	225.9	49.25	467.91		
5	22.4	4.80	2.10	226.1	49.30	480.18		
6	22.5	4.6	2.1	229.3	49.98	469.66		

Figure 2-1. Sandstone slabs prepared for the experiments.

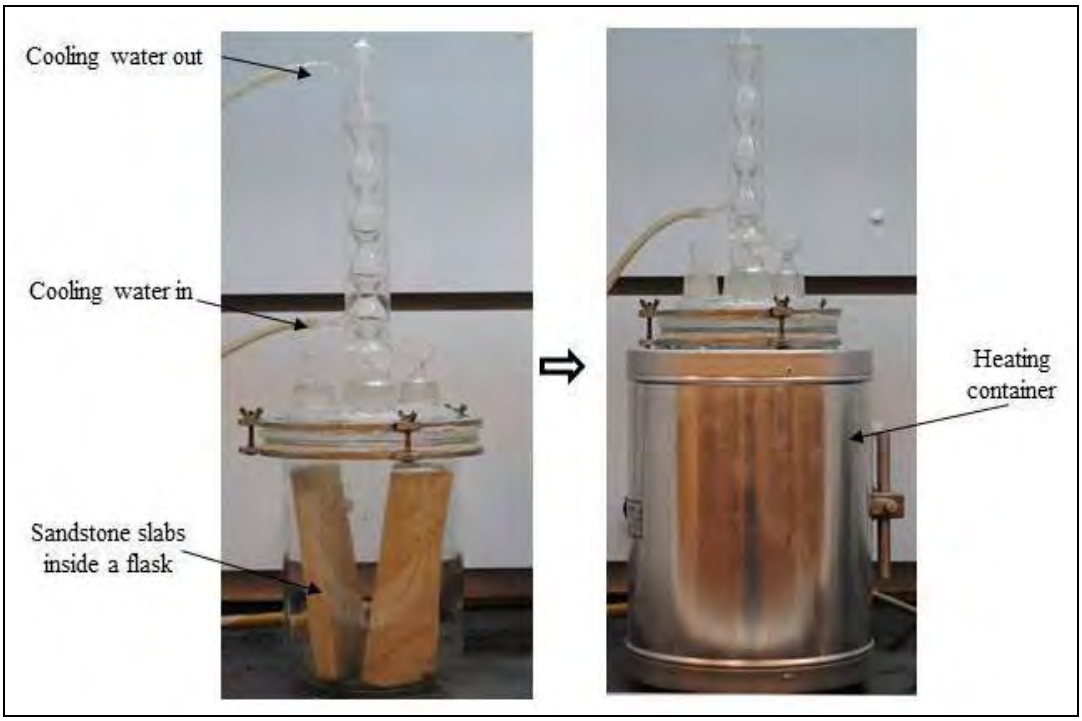

Figure 2-2. **Apparatus for the saline extraction process.**

2.2.1 Experiment Apparatus Design

Semi-transparent fracture model: Figure 2-3 through Figure 2-5 show the schematics and picture of the model used in the experiments. The model was constructed of two acrylic plates with a

rubber O-ring between them. Bolts and nuts were used to fix the two plates and shims to control the fracture width.

A long square pocket (2.0 in. wide, 9.0 in. long, and 1.0 in. deep) was drilled in the center of one side of one acrylic plate; a piece of Berea sandstone core was fixed into this pocket using epoxy. The model is transparent on one side to clearly visualize the movement of the PPG and surfactant. In the plate on the fracture side, four equally spaced holes were drilled for pressure recording and injection/discharge.

Pressure sensors were mounted in the first three holes to acquire the pressure change during the experiments, as seen in Figure 2-3**.** On the other plate, one hole was drilled to serve as an outlet to discharge fluid. The effluent from the fracture and matrix (for open fracture mode) and from the matrix alone (for closed fracture mode) were recorded separately to calculate the oil recovery factor and water cut.

Figure 2-3. Schematic diagram of the semi-fractured model.

shows the schematic diagram of the semi-transparent model. A fracture width of 2.5 mm (0.098 inch) was used in the experiment.

Dual-porosity system: This model uses a dual-porosity (matrix and fracture porosity) reservoir system. The fracture porosity (Φ_f) was calculated using the following formula:

$$\Phi_f = \frac{fracturevolume}{totalvolume} = \frac{V_f}{V_T} \quad \text{..... (2-1)}$$

The matrix porosity (Φ_m) also was different from the core porosity Φ_{core} measured as:

$$\Phi_m = \Phi_{core}(1 - \Phi_f) \quad \text{..... (2-2)}$$

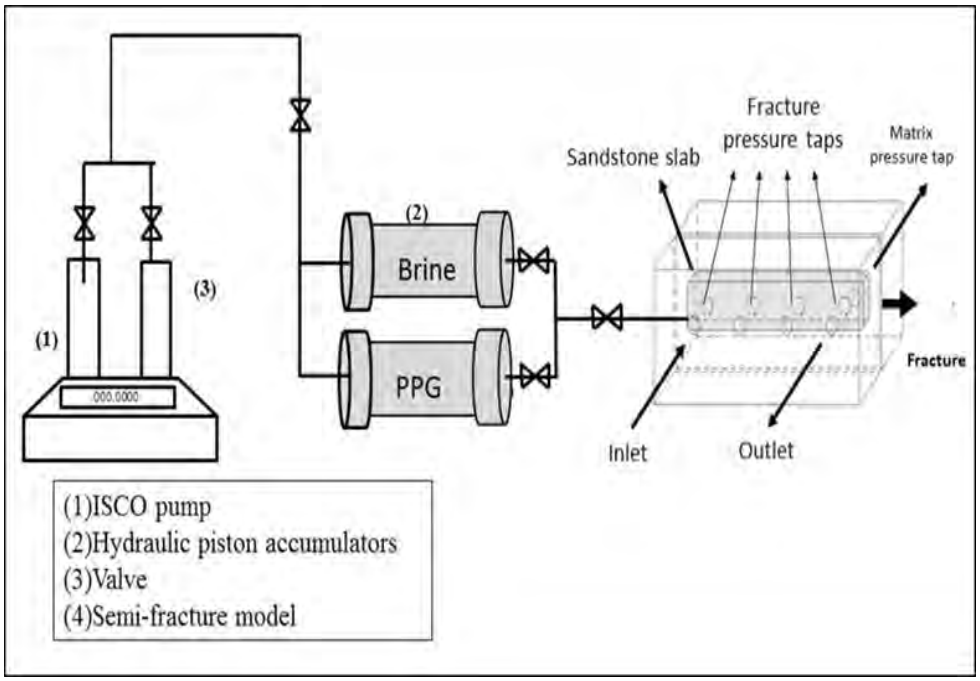

Figure 2-3. Schematic diagram of the semi-fractured model.

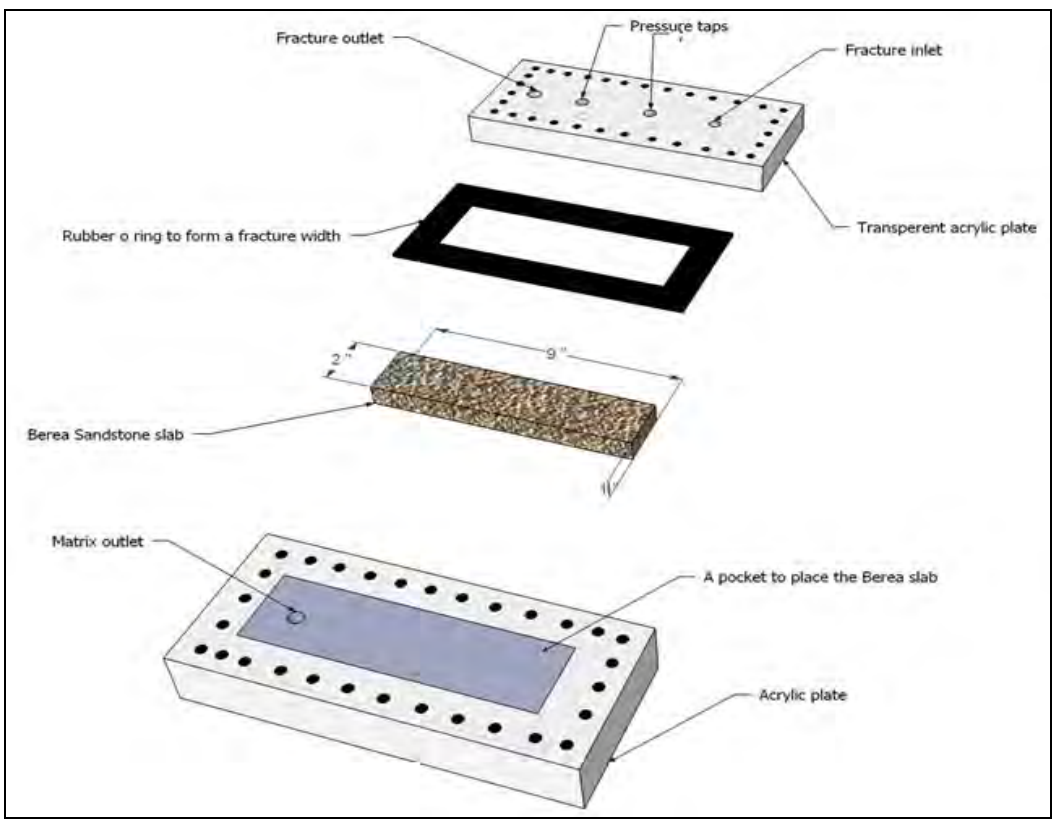

Figure 2-4. Schematic diagram of the semi-transparent model.

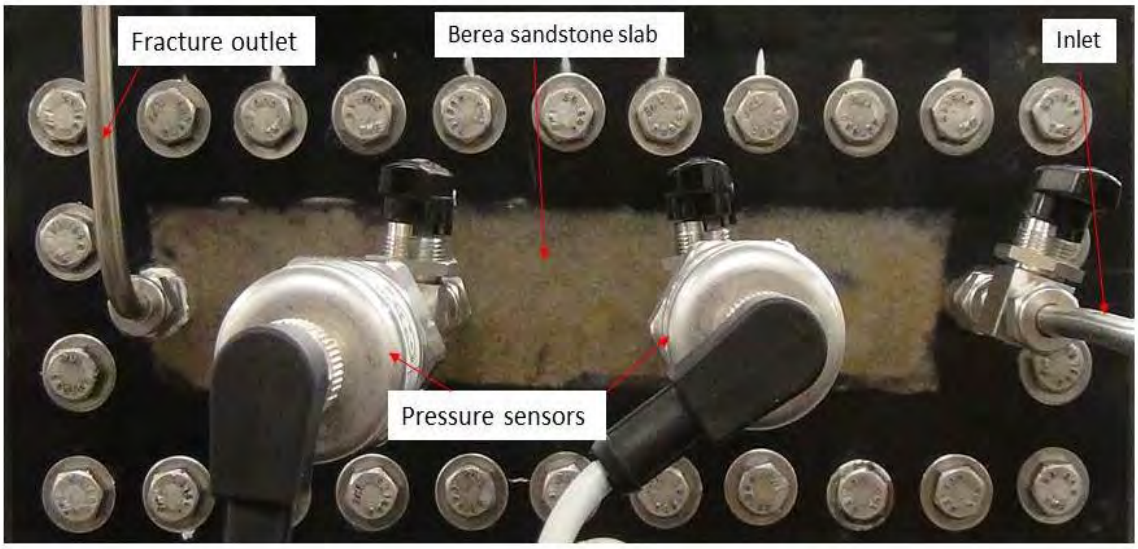

Figure 2-5. Picture of the semi-transparent fracture model.

2.2.2 Open Fracture Experiments Procedure

Each experiment was conducted in four steps, as follows:

Initial water flooding. Brine (1.0 wt.% NaCl) was injected into the fracture inlet to simulate secondary recovery conditions and detect any oil production from the matrix outlet.

PPG treatment. Two sets of experiments were conducted to examine the PPG treatment process and its ability to improve oil recovery and reduce water production. In the first treatment, the PPG was swollen in 1.0 wt.% NaCl aqueous solution. The swollen PPG was injected through the fracture, followed by surfactant (1.0 wt. % IGEPAL® CO-530) injection. In the second treatment, PPG was swollen in an aqueous solution of surfactant (1.0 wt.% IGEPAL® CO-530). Then, the mixture of PPG and surfactant was injected, followed by brine injection.

Surfactant treatment. In the first set of experiments, the PPG was swollen in an aqueous solution of 1.0 wt.% NaCl. After placing this swollen PPG, 1.0 wt. % of IGEPAL® CO-530 surfactant was injected using the same flow rate (2.0 ml/min) to investigate the ability of the surfactant to filter into and release the oil from the matrix by changing or modifying the

wettability of the matrix rock. In the other set of experiments, the surfactant was used as the swelling media for PPG and thus was injected into the model at the same time as the PPG.

Final brine flooding. A final batch of brine was injected into the model to test the PPG plugging efficiency and how much additional oil could be recovered due to the treatment. The same flow rate (2.0 ml/min) was used in all of the core-flooding stages.

In summary, the following procedures were used during the experiments:

1. An oil-wet core was vacuumed for six hours, and then, the core was saturated with a mineral oil and aged for 48 hours in an oven at 90 °C (194 °F).

2. To simulate a water-flooding process, 1.0 wt.% NaCl brine was injected through the inlet of the fracture. The water cut (f_w) and oil recovery (RF) were measured from the outlets of both the fracture and the matrix, separately. Brine injection was stopped when the water cut reached 100%.

3. PPG, swollen in 1.0 wt.% NaCl brine solution, was extruded into the fracture. The propagation of the PPG through the fracture was monitored. The f_w and RF were recorded from the fracture and matrix outlets, separately. The swollen PPG was injected until no more oil was produced from the matrix outlet.

4. Surfactant solution (1.0 wt.% of IGEPAL® CO-530 prepared in 1.0 wt.% NaCl) was injected through the fracture inlet. The f_w and RF were recorded during the injection process.

5. The effluent from the fracture and matrix outlets was monitored.

Note: In the second set of experiments, steps 3 and 4 were combined. PPG was swollen in 1.0 wt.% of IGEPAL® CO-530 surfactant, and the mixture of PPG and surfactant was injected into the fracture model.

2.3 Results and Discussion

2.3.1 First Set of Experiments—PPG Swollen in 1.0 Wt.% NaCl Solution

Figure 2-6 shows the injection pressure profile of the first set of experiments, in which swollen PPG and surfactant were injected separately. The pressure was acquired from the pressure taps mounted in the fracture side of the model. The plot indicates that there was no pressure build-up during the initial water flooding. This is due to the fact that the water channeled directly to the fracture outlet through the open fracture. No water penetrated into the matrix.

When the swollen PPG was injected into the model, the injection pressure began to increase during the first PV of PPG injection. After that, the pressure fluctuated, with a peak of 60 psi. When the surfactant was injected after PPG injection, the pressure dropped suddenly in a very short time because the surfactant solution created a channel in the PPG pack [20, 21]. In this case, the surfactant moved directly from the inlet to the outlet of the fracture, and no surfactant solution was squeezed into the matrix rock. This indicates that this PPG cannot totally block the fracture. A stronger PPG might be required to force the surfactant solution into the matrix.

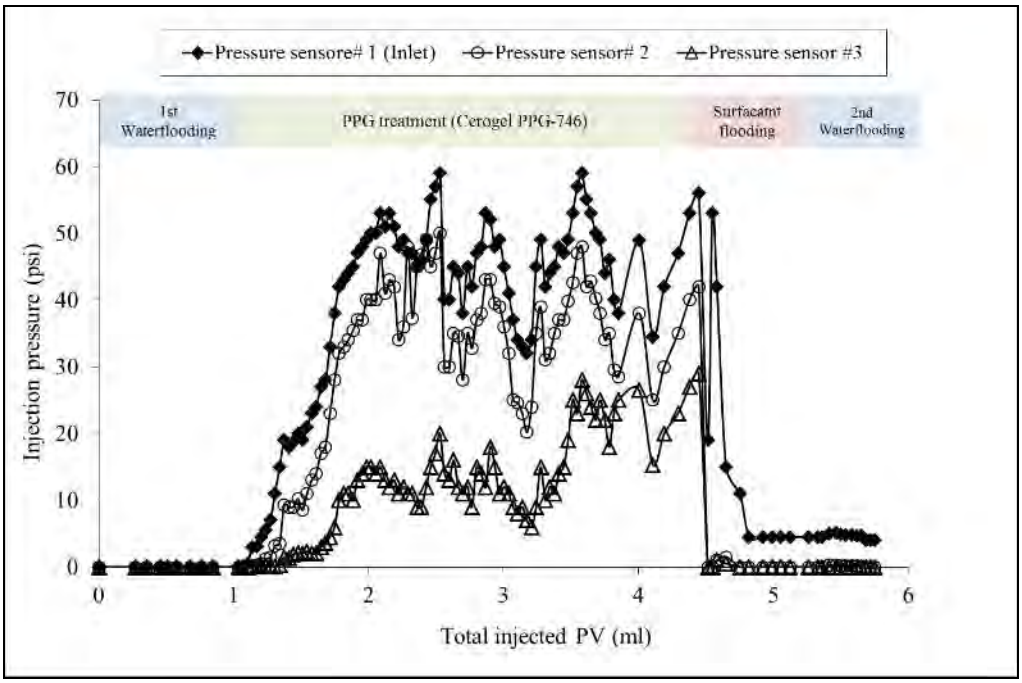

Figure 2-6. Injection pressure profile at different stages of the fracture model.

Figure 2-7 plots the oil recovery factor for the first set of experiments, in which oil was collected from the matrix outlet. During the initial water flooding, there was no effluent from the matrix outlet because all of the water was directed to the fracture outlet. Therefore, the oil recovery

from both matrices was zero. During PPG injection, the oil recovery from the matrix reached approximately 33%.

The mechanism of oil recovery from the matrix was attributed to the forced imbibition during PPG injection. The PPG did not form a non-permeable cake on the fracture surface, which allowed water to penetrate into the matrix. During PPG injection, the build-up pressure caused by PPG packing in the fracture increased the fluid flow resistance in the fracture, which could result in a more significant pressure drop from the fracture surface to the matrix outlet. Therefore, the water from the swollen PPG was forced to penetrate into the matrix.

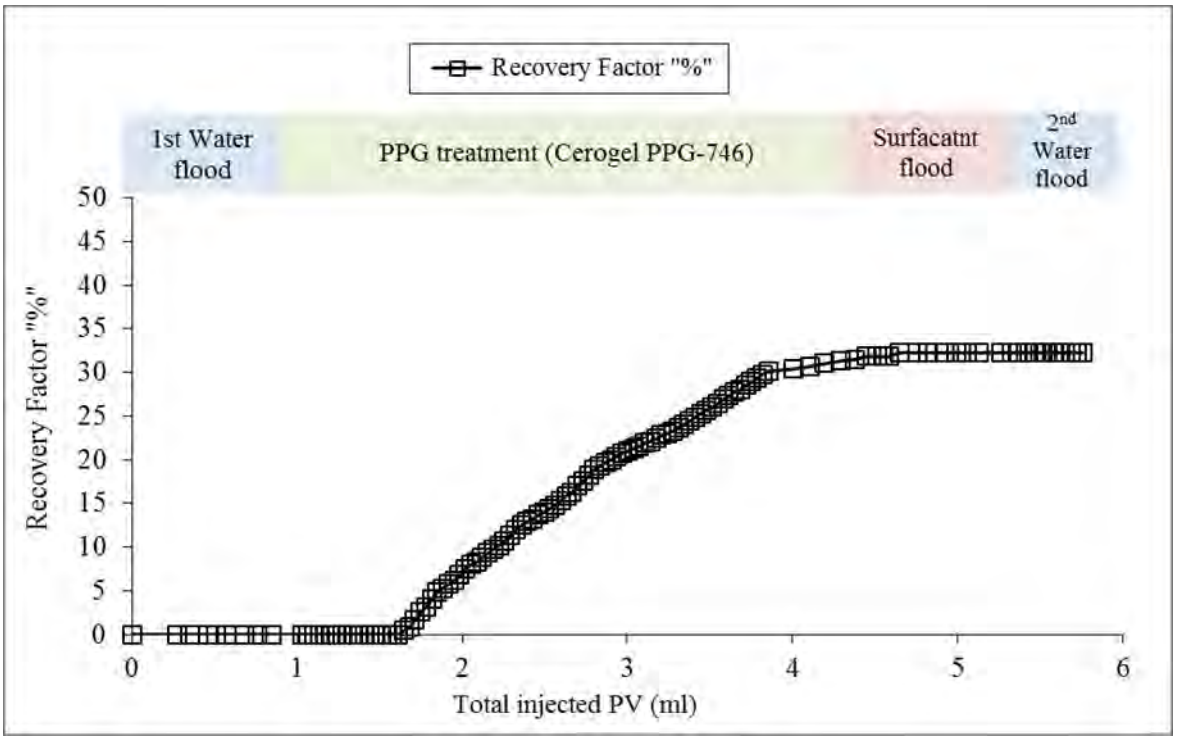

Figure 2-7. Oil recovery factor during treatment with PPG swollen in 1 wt.% NaCl.

The injected surfactant did not significantly contribute to an increase in oil recovery; only 0.1% more oil was produced. This lack of effect occurred because the surfactant created a channel through the PPG pack, which caused all of the surfactant to flow directly out through the fracture outlet. During the second water-flooding stage, no more oil was produced from the matrix either.

2.3.2 Second Set of Experiments—PPG Swollen in Surfactant Aqueous Solution

Figure 2-8 shows the injection pressure profile for the second set of experiments, in which PPG and surfactant were co-injected into the model. As the figure indicates, during the initial brine flooding, the pressure profile was similar to that in the first set of experiments; no pressure build-up was recorded. After injecting a total of 0.72 PV of water, there was no effluent from the matrix outlet, and all of the water flowed directly through the path of least resistance (fracture outlet). The injection was stopped when the water cut from the fracture outlet reached 100%. While injecting the mixture of PPG and surfactant, the PPG broke through from the fracture outlet when 1.18 PV PPG was injected. The maximum pressure was approximately 43 psi, which was less than the pressure in the first set of experiments, as shown in Figure 2-8. This could be attributed to the surfactant working as a lubricant to reduce PPGs friction and increase its injectivity. This phenomenon also was observed by Wu et al. [22], who reported that particle gel injectivity could be improved significantly through the use of proper surfactants. In the second water-flooding stage, the pressure dropped gradually because the water created a smaller channel in the PPG pack.

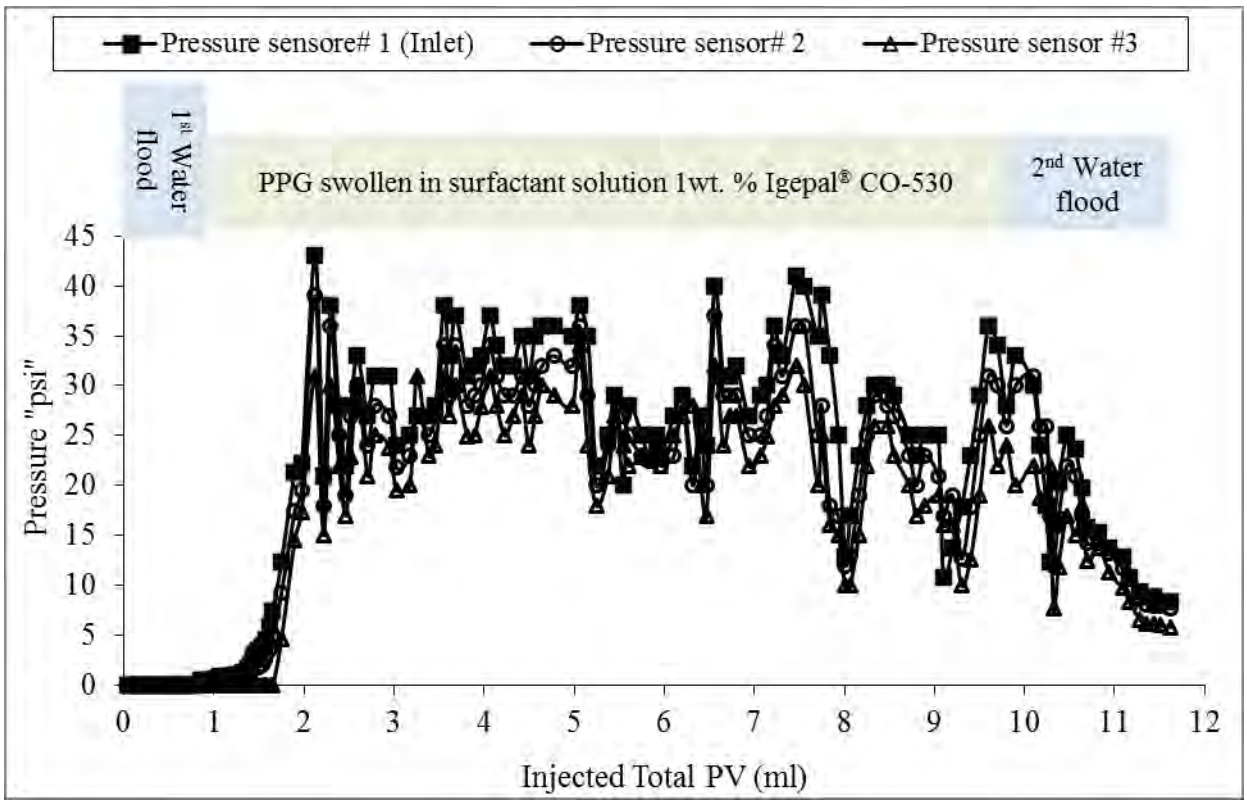

Figure 2-8. Injection pressure profile at different stages of the fracture model.

Figure 2-9 plots the oil recovery factor during the treatment with PPG swollen in surfactant. Similar to the first set of experiments, during the initial water flooding, there was no effluent from the matrix outlet because all of the water was directed to the fracture outlet. When the PPG and surfactant mixture was injected, the swollen PPG propagated through the fracture until it reached the outlet, and the effluent was found from the matrix outlet after 0.81 PV of the mixture was injected.

The maximum oil recovery was 43%, which was higher than in the first set of experiments (~33%). This was attributed to the surfactant that was forced to filter into the matrix rock, which altered its wettability from oil to water or mixed-wet. Approximately 3.1% of the oil was recovered during the water flood (after the injection of the PPG and surfactant mixture).

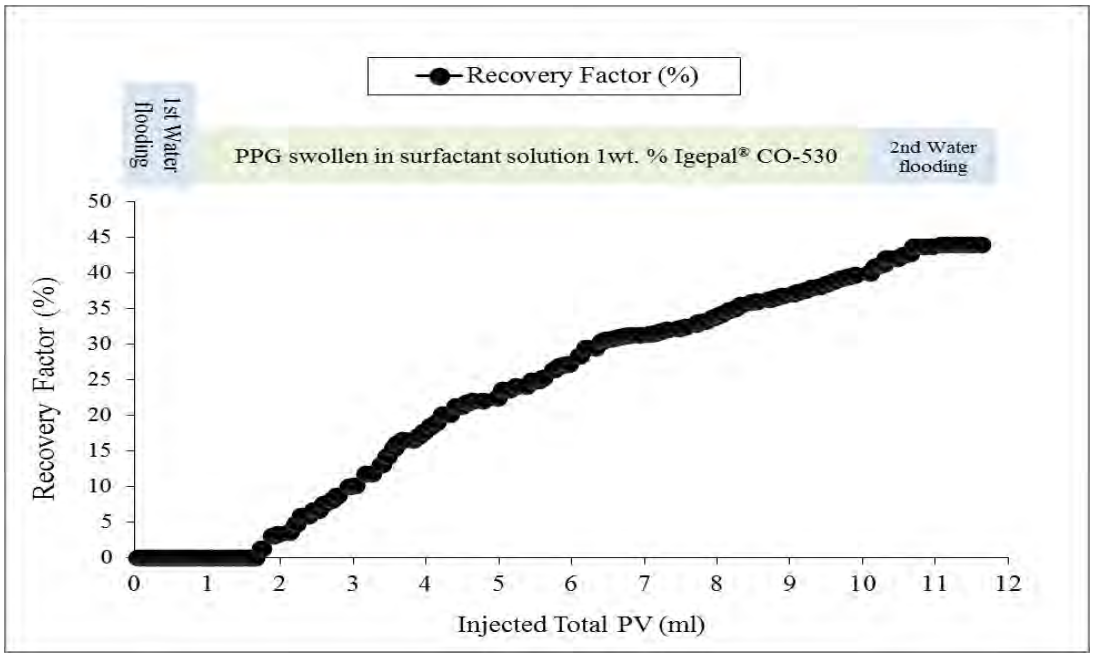

Figure 2-9. Oil recovery factor during treatment with PPG swollen in surfactant.

The semi-transparent model allows one to view the PPG propagation through the fracture, as well as water and/or surfactant penetration through the PPG pack and matrix. Previous work by Hao et al. [20] illustrated PPG propagation through a fracture and brine movement through a gel pack. They reported that the PPG moved like a piston inside the fracture, and gravity did not have a significant effect; this behavior was confirmed by our experiments.

Figure 2-10 illustrates PPG extrusion through the fracture, followed by water injection. (The brine was dyed black.) The first picture shows that the fracture was filled with PPG particles after PPG injection. The other three pictures show the movement of water into the gel pack during the second water-flooding process. As illustrated, PPGs were able to flow with the water through the fracture if they were smaller than the fracture. However, any particles larger than the fracture remained in place longer and kept the water from flowing. Eventually, only a small amount of the larger particles remained in the fracture, and the others exited the fracture outlet. In this experiment, approximately 60% of PPGs were washed out from the fracture outlet.

Figure 2-11 shows the surface of the core after PPG treatment; some of the particles remained on that core surface and were not washed out of the fracture. Only the big particles were left inside the fracture; they did not adhere to the surface of the sandstone core, and after opening the model, they were easily removed. This indicates that the PPG did not penetrate inside the matrix's porous media, nor did it form a filter cake. Figure 2-12 illustrates that the PPG did not damage the matrix's surface because it did not form a filter cake. The picture shows the areas where water (dark) penetrated into the core, thus indicating that PPG can force water so as to improve the ES.

Figure 2-13 shows the size of the swollen particles before and after they extruded through the fracture. The change in size serves as evidence that the PPG was dehydrated and shrank as it moved through the fracture. Some particles even collapsed and broke into small pieces due to the compaction or squeezing of the particles inside the fracture.

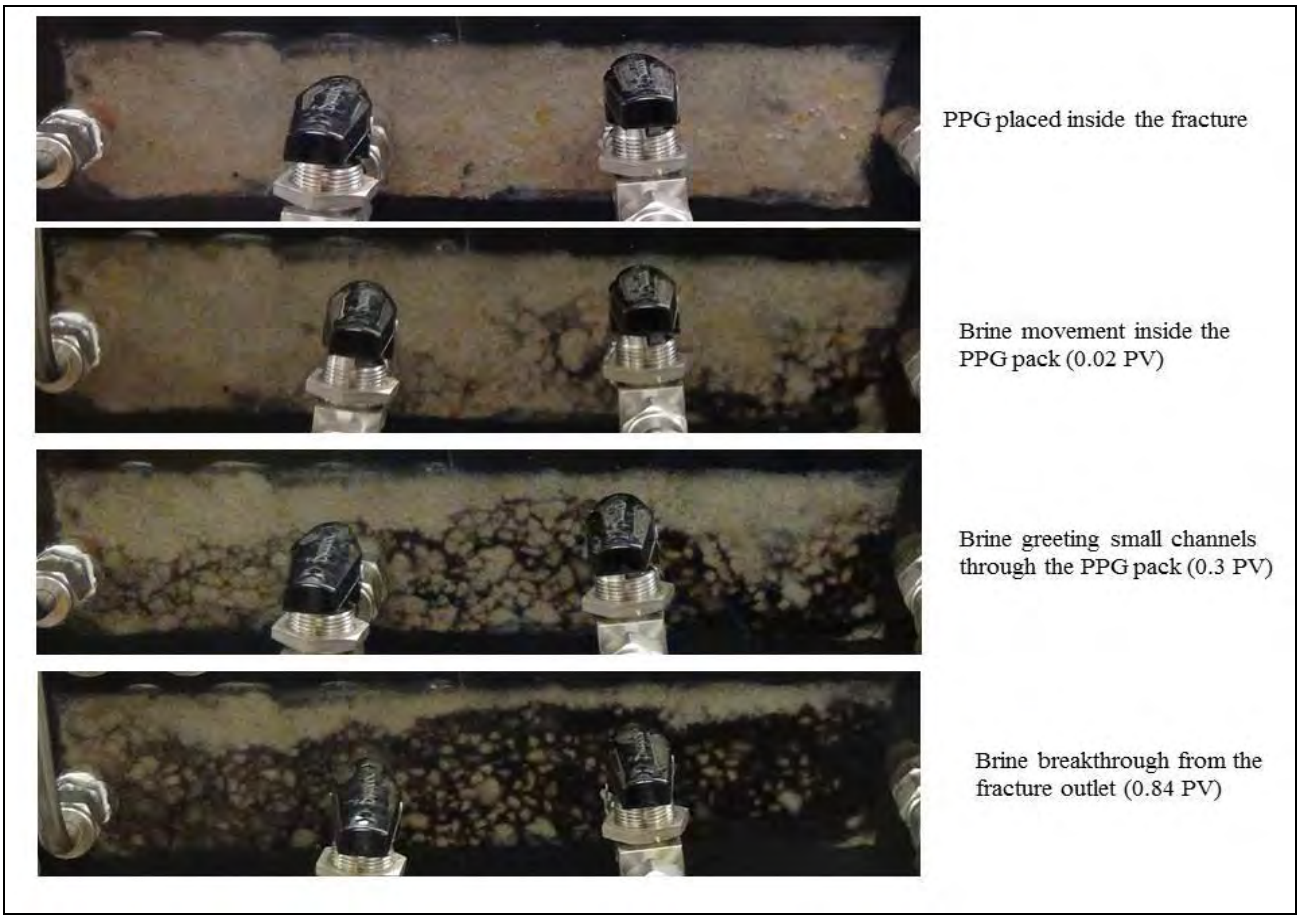

Figure 2-10. PPG placement inside the fracture followed by brine injection.

Figure 2-11. Sandstone core surface at the end of the experiment.

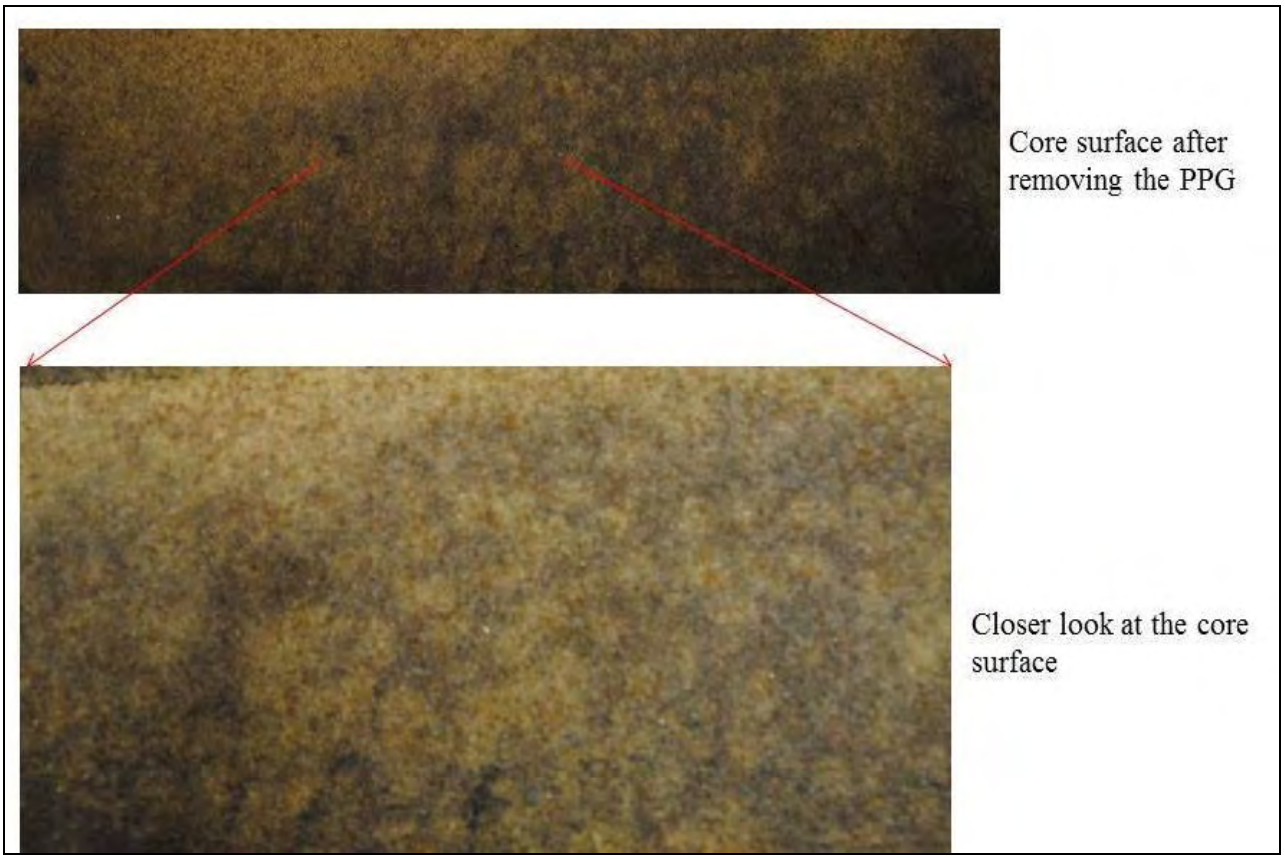

Figure 2-12. Core surface after the experiments.

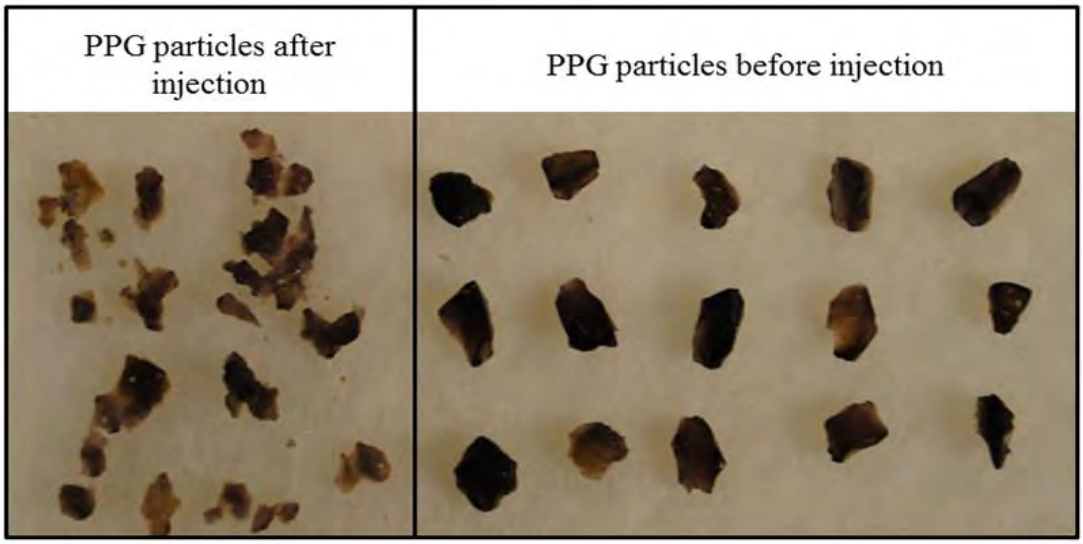

Figure 2-13. PPG particles before and after injection into the fracture.

2.4 Summary

Two sets of fracture flooding tests were conducted using open fracture models. PPG and surfactant were injected into the fracture model separately in the first set, whereas in the second set, PPG and surfactant were injected simultaneously into the model by injecting swollen PPG into a surfactant solution. The results reveal the following information:

- Millimeter-sized particle gel can only enter high-permeability zones/streaks or fractures and cannot form face plugging on the surface of low-permeability zones or fractures; thus, these PPGs cause little damage to unswept oil zones/areas.

- The surfactant solution mixed with PPG is squeezed from gel particles into low-permeability zones/areas where crude oil is trapped by capillary force. The surfactant solution can dramatically reduce the capillary force (IFT between oil and water) and release the crude oil.

- The combined injection of PPG and surfactant will result in a higher injection pressure gradient in the reservoir because of the high flow resistance resulting from the particles. This increased pressure will produce an additional force to drive surfactant into the matrix or low-permeability areas, thus making forced imbibition practical.

- The successful development of this technology will provide a more cost-effective method for improving oil recovery and reducing water production for small producers.

3. SCREEN THE BEST PPGS AND SURFACTANTS FOR THE WELL CANDIDATES

This chapter is divided into three parts that focus on the screening experiments to select the best PPG and surfactant for small producers.

The first part presents a systematic method to evaluate the potential of emulsions for enhanced oil recovery, including surfactant screening, emulsion stability test, adsorption tests, and core flooding tests. Results indicated that the nonionic surfactant IGEPAL® CO-530 could form a very stable emulsion for heavy oil and synthetic brine at reservoir temperature. Through the emulsion, the viscosity of the heavy oil can be reduced from 18,518 cp to 2.5 cp at 25°C. The mobility of the heavy oil can be improved significantly. The emulsion created by the surfactant IGEPAL® CO-530 was very stable at 25°C, but at 40°C, this emulsion separated automatically into two layers within two hours without the addition of any de-emulsion agent. This behavior provides great advantages for applications of this technology.

The second part shows the evaluation results of the emulsion stability formed by IGEPAL® CO-530, nanoparticles, and a few other surfactants, with the crude oil from the field of our pilot tests. Results showed IGEPAL® CO-530 is good enough to provide a stable emulsion for the pilot test, although nanoparticles can make the emulsion even more stable. The produced emulsion from IGEPAL® CO-530 could be broken down at lower temperature than nanoparticles stabilized emulsion.

The third part gives the direct observation results of the emulsification process of the heavy oil and surfactants in porous media through micromodel experiments using confocal microscope.

This last part examined the compatibility of PPGs with the selected surfactants and formation water. The swelling ratio and strength of PPGs were measured with and without surfactant. After evaluation, the Cerogel™ PPG was selected to be used in pilot tests.

3.1 A Systematic Evaluation for Heavy Oil Emulsion Method for EOR

The objective of this research is to select surfactants that can form stable O/W emulsions with the heavy oil from small producers. In the study, more than 30 commercial surfactants were evaluated for their emulsion stability. The viscosity reduction of heavy oil, the wettability alteration of the sand surface, and the adsorption of the surfactant on silica and kaolinite clay were also investigated.

3.1.1 Materials

Heavy oil sample: The heavy oil sample was provided by a small producer. The viscosity was measured as 28,834 cp at 25°C.

Formation water sample: The original formation water also was provided by the small producer and came from the same oilfield in Vernon County, Missouri. Its composition was analyzed by St. Louis Fluid System Technologies in Missouri. The brine composition is listed in Table 3-1. The synthetic brine used in this study was prepared based on the composition of the original formation water. Table 3-2 shows the recipe for the synthetic brine.

Surfactant samples: More than 30 commercial surfactants were tested in this study. These surfactants can be categorized as anionic, cationic, or nonionic. Their commercial and chemical names are listed in Table 3-3.

Silica and kaolinite clay: Silica powder was purchased from U.S. Silica (Pacific, MO), and the kaolinite came from Phelps County, Missouri.

Table 3-1. Compositions of reservoir formation brine.

Composition	A.W.	PPM	Ions	Total Charge
Potassium	39.1	49.1	K^+	1.256×(+1)
Sodium	23.0	1950.0	Na^+	84.783×(+1)
Calcium	40.1	95.4	Ca^{2+}	2.379×(+2)
Magnesium	24.3	40.0	Mg^{2+}	1.646×(+2)
Barium	137.3	2.08	Ba^{2+}	0.015×(+2)
Chloride	35.5	3000.0	Cl^-	84.507×(-1)
Sulfate	96.1	142.0	SO_4^{2-}	1.478×(-2)
Bicarbonate	100.0	1060	HCO_3^-	10.60×(-1)
Check pH	Adjust pH to 7.0		TDS	6338 PPM

Table 3-2. Recipe for Synthetic Formation Brine.

Salt	M.W.	g/L	Ions	mg/L
NaCl	58.5	4.400	Total Na^+	2041.1
$NaHCO_3$	84.0	0.890	K^+	49.1
KCl	74.6	0.094	Ca^{2+}	95.4
Na_2SO_4	142.1	0.230	Mg^{2+}	40.0
$CaCl_2{\cdot}2H_2O$	147.0	0.351	Total Cl^-	3000.0
$MgCl_2{\cdot}6H_2O$	203.3	0.335	SO_4^{2-}	142.0
			HCO_3^-	1060.0
Check pH	Adjust pH to 7.0		TDS	6427.6 ppm

Table 3-3. Commercial and chemical name for the surfactants investigated.

Surfactant Name	Chemical Description	HLB
NEODOL® 1-5	Linear C11 primary alcohol with 5 moles of ethylene oxide(EO)	11.2
NEODOL® 1-7	Linear C11 primary alcohol with 7 moles of EO	12.8
NEODOL® 1-9	Linear C11 primary alcohol with 9 moles of EO	13.9
NEODOL® 25-7	Linear C12-C15 primary alcohol with 7 moles of EO	12.3
NEODOL® 25-9	Linear C12-C15 primary alcohol with 9 moles of EO	13.1
Tomadol® 25-12	Linear C12-C15 primary alcohol with 7 moles of EO	12.3
Tomadol® 45-7	Linear C12-C15 primary alcohol with 9 moles of EO	13.1
Tomadol® 45-13	Linear C12-C15 primary alcohol with 12 moles of EO	14.4
TERGITOL® 15-S-3	Linear C14-C15 primary alcohol with 7 moles of EO	11.6
TERGITOL® 15-S-9	Linear C14-C15 primary alcohol with 13 moles of EO	14.4
TERGITOL® 15-S-12	C12-14 secondary alcohol ethoxylate with 3 moles of EO	8.3
TERGITOL® 15-S-20	C12-14 secondary alcohol ethoxylate with 9 moles of EO	13.3
TERGITOL® NP-10	C12-14 secondary alcohol ethoxylate with 12 moles of EO	14.7
IGEPAL® CO-530	C12-14 secondary alcohol ethoxylate with 20 moles of EO	15.7
Triton® X-405	Ethoxylated nonylphenol with 10 moles of EO	13.2
Calamide®CW-100	Ethoxylated nonylphenol with 5 moles of EO	10.8
Calamide® CWT	Ethoxylated octylphenol with 40 moles of EO	17.6
Calamide® F	Modified coconut diethanolamide	N/A
Calsoft® LAS-99	Modified coconut amidesoap superamide	N/A
Calimulse® EM-99	Vegetable oil diethanolamide	N/A
Calimulse® PRS	Benzensulfonic acid, C10-C16 alkyl derivitives	Acid
ARQUAD® T-50	Benzensulfonic acid, C10-C16 alkyl derivitives	Acid
Ethomeen® C/12	Benzensulfonic acid, dodecyl branched	Acid
Ethomeen® S/12	Block copolymers of propylene, ethylene oxides	N/A
Aerosol® MA-80	Block copolymers of propylene, ethylene oxides	7.0
Alfoterra® 23	Ammonium nonylphenol ethoxylate sulfate, 4 EO	Anionic
Alfoterra® 48	Sodium lauryl ether sulfate, 30 EO	Anionic
Tomadol® 600	Sodium lauryl sulfate (SDS)	Anionic
Tomadol® 901	C10-C16 ethoxylated alcohol	10.6
Tomadol® 91-6	C9-C11, C10-C16 ethoxylated alcohols	12.1
Tomadol® 91-8	C9-C11 ethoxylated alcohol	14.3

3.1.2 Procedures

Preparation of synthetic brine: Based on the compositions of the original formation water listed in Table 3-1, the recipe for the synthetic brine was designed, as listed in Table 3-2. Salt was weighed, and a total of 3000 grams was added to distilled water. The synthetic brine was stirred for one hour. A pH meter and NaOH (0.200 M) solution were used to adjust the synthetic brine to pH = 7.3, at which point it was ready to use.

Viscosity measurement for the oil sample: The viscosity of the heavy oil was measured at 25°C, 50°C, 60°C ,70°C and 80°C and at three different shear rates using a Brookfield DV-II+Pro viscometer. The viscosity results of the heavy oil are listed in Table 3-4.

Table 3-4. Viscosity, standard deviation and experimental error.

T (°C)	Ave. η (cP)	Std. (±Δη)	Δη %	Δη/°C
20.0	24343.0	767.4	3.2	N/A
25.0	18518.0	409.4	2.2	1762.4
30.5	11325.8	289.6	2.6	1481.7
40.0	4966.3	174.6	3.5	704.6
50.0	2047.8	16.5	0.8	259.8
70.0	544.6	6.2	1.1	44.2
80.0	302.0	7.2	2.4	21.1

Emulsion stability test for surfactant screening: In this study, 30 commercial surfactants were selected for screening to test their ability to create an emulsion of heavy oil and formation brine. All surfactant solutions were prepared at 1.0 wt. % with the synthetic brine. To create the O/W emulsion, 2.0 grams of heavy oil and 18.0 grams of each surfactant solution were mixed in separate transparent glass bottles, which were then shaken for 30 seconds by hand at room temperature. Then, the bottles were placed on a rack to await natural phase separation, referred to as the emulsion stability test. The rapid and automatic separation of oil and brine indicated an unstable emulsion system. In such cases, the top layer of the oil turned black, while the bottom layer of brine turned white or cloudy brown. Very stable emulsion systems were indicated by the bottles that remained uniformly black, showing no dividing line between the oil and brine. To quantify the stability of the emulsions, the height of the brine layer in the bottle was measured

every half hour for the first 24 hours, once per hour for the second 24 hours, and once every two hours for the third 24 hours. The thicker the brine layer, the less stable the emulsion system. Furthermore, the ratio of the oil layer height to the total height of brine and heavy oil in each bottle was calculated.

An oil recovery test was performed with oil-wet and water-wet sands. Before the sand could be used for the experiment, it was washed with tap water several times until the water turned clear; then, the sand was rinsed with distilled water three times. The washed sand was dried in an oven at 90°C (194°F) for two days. The dried sand was separated with sieves, and the sand between 20 and 30 mesh size was collected for testing.

Two water-wet sand samples were prepared by mixing 10.0 grams of the dry, clean sand with 1.25 grams of formation water. Then, 2.0 grams of Missouri heavy oil were added to each sample. These sand-oil mixtures were warmed at 40 °C (104 °F) for a half hour to ensure that the heavy oil mixed thoroughly with the sand. To compare the performance of the surfactant with and without alkaline in enhanced heavy oil recovery from water-wet sand, 35.0 mL of surfactant solution (IGEPAL® CO-530 at 2.00 wt.%) was added to one sample to approximately the 40 ml mark on the bottle; meanwhile, 35.00 mL of surfactant and alkaline (IGEPAL® CO-530 at 2.0 wt.%, NaOH at 0.6 wt.%) solution was added to another water-wet sample. The samples were shaken overnight at room temperature.

To compare the surfactant's ability to enhance heavy oil recovery from oil-wet and water-wet sand, two oil-wet sand samples also were prepared in a manner similar to that described above but without the addition of 1.25 grams of formation water. Similarly, 35.00 mL of surfactant solutions with and without alkaline were added separately to the two samples. The samples were shaken overnight at room temperature. These sand samples with different initial wettabilities exhibited very different heavy oil recovery rates.

AS flooding test to measure oil recovery: To make a sandpack for the AS flooding test, a core holder with a diameter of 2.6 cm and length of 24 cm was used. To pack the core, 100 grams of heavy oil was weighed out and warmed at 40 °C (104 °F) for 2 hours. In the case of water-wet sand, 200 grams of sand (30-20 mesh) was saturated with formation brine to 100%, and 65 grams of warm, heavy oil was added. No brine was added to the oil-wet sand. Next, the mixture was put

in an oven for two hours. The porosity of the sandpack was measured as 45%, and its absolute permeability to water was 2.5 Darcys. The displacement tests were conducted horizontally. Sandpack flood tests were conducted using the oil sample under ambient conditions. For each test, fresh sand (from US Silica) was packed to ensure the same initial sand wettability. The core was waterflooded using the PerkinElmer Series 100 pump. The injection rate was 0.5 mL/min, and the synthetic formation brine was injected continuously until the oil production became negligible (oil cut <1%). Then, 1.0 PV of preflush slug was injected. The preflush slug was 2.0% surfactant and 0. 6% NaOH in the formation brine. During tertiary chemical flooding, a 1.0 PV chemical slug was injected, followed by an extended water flood until oil production became negligible. The oil production was determined on a volume basis.

Adsorption measurement for selected surfactants on silica and kaolinite clay: In this study, the adsorption of surfactant on silica and kaolinite powder surfaces was measured because surfactant loss in reservoirs caused by adsorption on the rock's surface is a major problem in chemical flooding applications. The surfactant investigated was IGEPAL® CO-530. In general, less adsorption by the rock's surface indicates a better quality surfactant. At the beginning of the experiment, a series of IGEPAL® CO-530 surfactant solutions was prepared at concentrations of 20, 40, 60, 80, 100, 150, 200, 250, 300, 400, and 500 ppm. A UV-visible spectrophotometer (UVmini-1240, Shimadzu) was used to analyze the concentration of IGEPAL® CO-530. Using the prepared initial solutions, the UV absorbance (ABS) of IGEPAL® CO-530 was measured at a wavelength of 265 nm (λmax), where this surfactant's absorbance peaks; then, the ABS for all of the initial solutions was measured at 265 nm. A calibration curve for this surfactant was obtained by plotting the ABS versus the initial concentrations, as shown in Figure 3-3.

To measure the adsorption of surfactant on silica and kaolinite clay, all of the powder samples were dried in an oven at 100°C for 48 hours to remove all moisture. For each surfactant solution, a clean test tube was used to weigh 10.00 grams of the surfactant solution, and then, 0.5 grams of silica was added to the test tube. All of the tubes were shaken at room temperature for 24 hours to establish the adsorption equilibrium and then put in a centrifuge to separate the solution from the solid powder. The surfactant concentration after adsorption can be calculated through this calibration curve and the ABS. Then, the adsorption of the surfactant on the powder surface can be calculated using the following equation [25]:

$$q_e = \frac{(C_0 - C_e)*V}{W}$$

where C_0 and C_e are the initial and equilibrium concentrations of the surfactant, respectively (mg/L), V is the volume of the solution (L), and W is the weight of the powder (g). The adsorption isotherms appear in Figure 3-4.

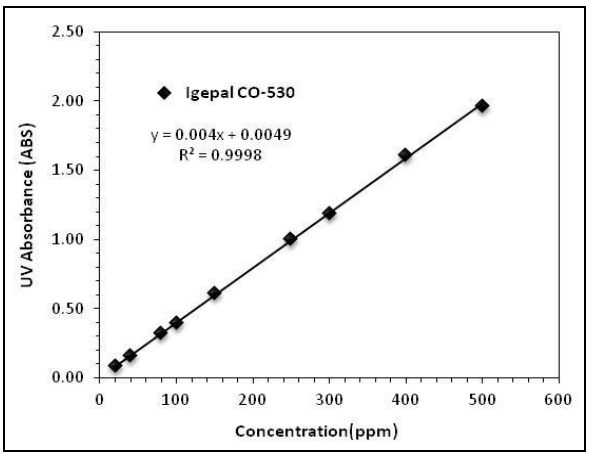

Figure 3-1. UV absorbance calibration curve for IGEPAL® CO-530.

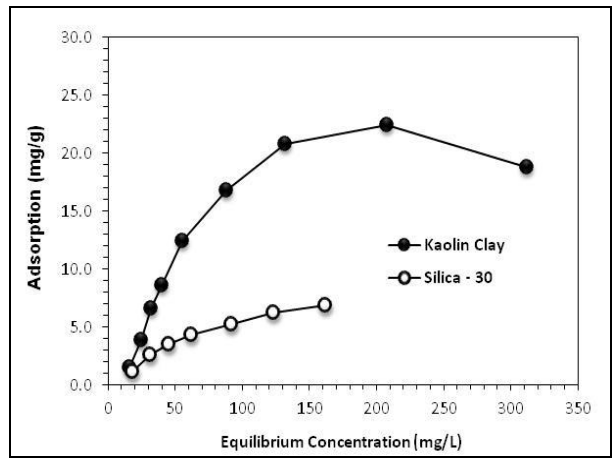

Figure 3-2. Adsorption isotherms for IGEPAL® CO-530.

3.1.3 Results and Discussion

Effect of temperature on the viscosity of heavy oil: The viscosity of crude oil decreases as the temperature increases. Even though crude oil is Newtonian, the measured viscosity is slightly different for each shear rate value, most likely because of practical or experimental errors, and this causes a slight deviation. Hence, the average value was calculated and plotted for each temperature, with error bars to distinguish the viscosity range at each temperature. At lower temperatures, e.g., below 40°C (104°F), the error percentage appears significantly larger than at higher temperatures. Perhaps the crude oil is more consistent at higher temperatures because of the reduced viscosity.

Also at lower temperatures, the viscosity of the heavy oil decreases more significantly than at higher temperatures. The API gravity of the heavy oil in the Long Farm reservoir was 17.1°. At

room temperature, 25°C (77°F), without removing the sand and water contained in the provided heavy oil sample, the viscosity of the heavy oil in the Long Farm reservoir was 28,843 cp; this value decreased rapidly as the temperature increased.

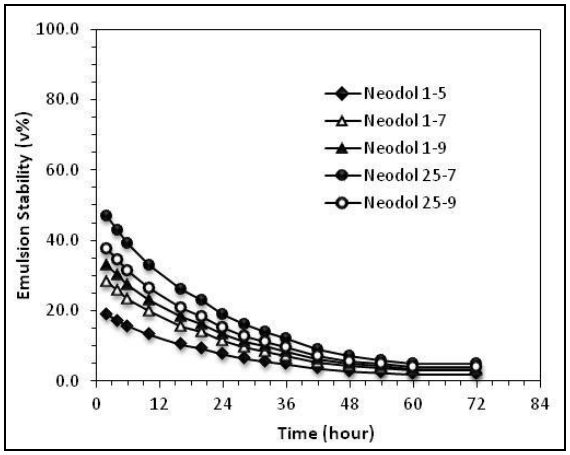

Figure 3-3. Stability of emulsions created by NEODOL® surfactants.

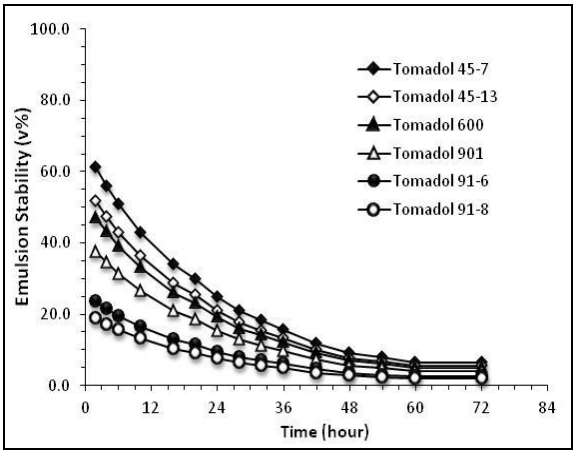

Figure 3-4. Stability of emulsions created by Tomadol® nonionic surfactants.

Emulsion of the heavy oil by surfactants, and stability of the emulsion: Figure 3-3 shows the emulsion stability of the heavy oil and synthetic brine emulsified by five nonionic surfactants, the NEODOL® series provided by Shell Chemicals. Figure 3-4 shows the emulsion stability of the heavy oil and synthetic brine emulsified by six nonionic Tomadol® surfactants, provided by Air Products and Chemicals, Inc. All of these surfactants are ethoxylated primary alcohols. The emulsions were unstable, separating into two layers of heavy oil and aqueous solution automatically within 12 hours. Only NEODOL® 25-7 and Tomadol® 45-7 remained stable for approximately 24 hours. Figure 3-5 shows the stability of the emulsions created by another five nonionic surfactants, the TERGITOL® series provided by The Dow Chemical Company, which are ethoxylated secondary alcohols. The emulsion stability yielded by these secondary alcohols was better than that yielded by the primary alcohols, but none remained stable for more than 24 hours. Figure 3-6 shows the stability of the emulsions created by another five nonionic surfactants, Triton® X-405, Calamide® CW-100, Calamide® CWT, Calamide® F and IGEPAL® CO-530, provided by different manufacturers, i.e., Pilot Chemical Company and Rhodia. Most of

these surfactants yielded emulsions that still were not very stable and separated within 24 hours; the oil and surfactant solution separated into two layers for all but the IGEPAL® CO-530 surfactant, which remained stable for more than 72 hours [26].

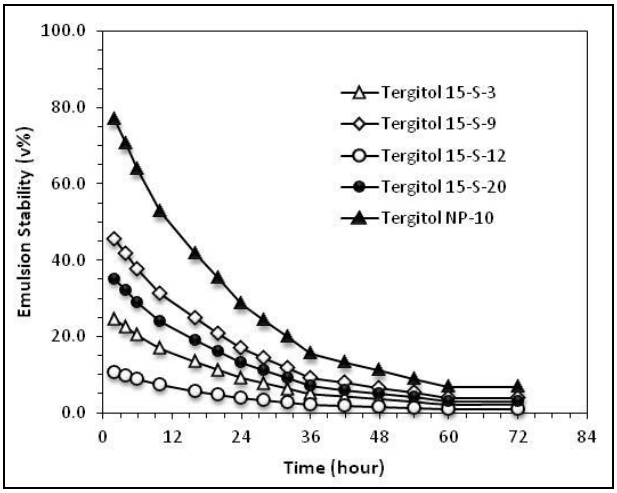

Figure 3-5. Stability of emulsions created by TERGITOL® nonionic surfactants.

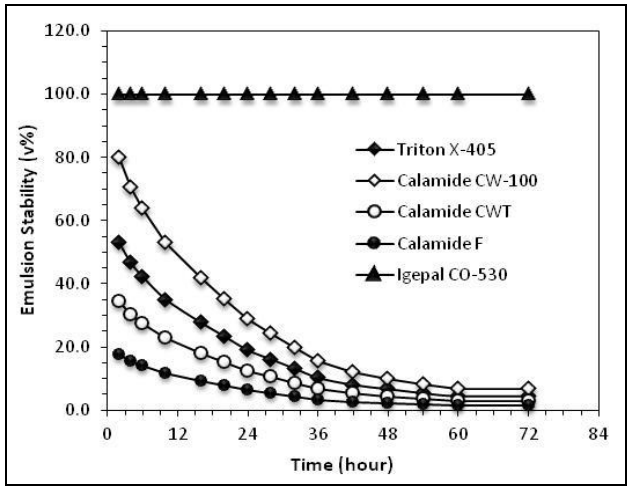

Figure 3-6. Stability of emulsions created by some nonionic surfactants.

Figure 3-7 shows the emulsion stability yielded by anionic surfactants, including Aerosol® MA-80 (Cytec Industries Inc.), Alfoterra® 23, and Alfoterra® 48 (Sasol), as well as Calsoft® LAS-99, Calimulse® EM-99, and Calimulse® PRS (Pilot Chemical Company). These six anionic surfactants created very unstable emulsions. As a result, it was expected that the IFT between the Missouri heavy oil and the formation brine would not decrease sufficiently using these anionic surfactants. Figure 3-8 shows the stability results of the emulsion with each of the three cationic surfactants, Ethomeen® S/12, Ethomeen® C/25 and ARQUAD® T-50, provided by AkzoNobel. All of the cationic surfactant samples were very unstable.

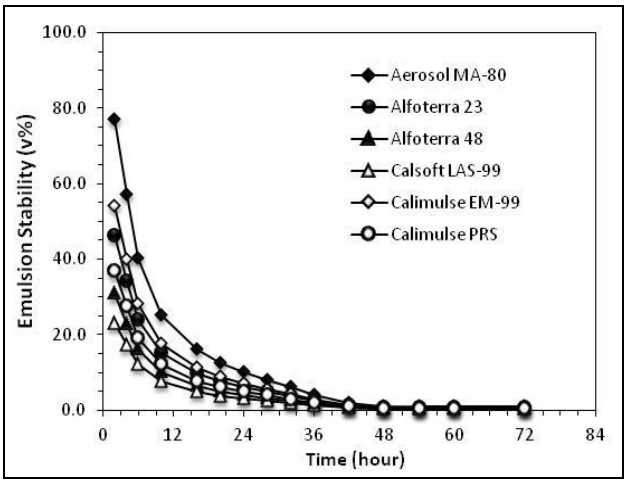

Figure 3-7. Stability of emulsions created by anionic surfactant.

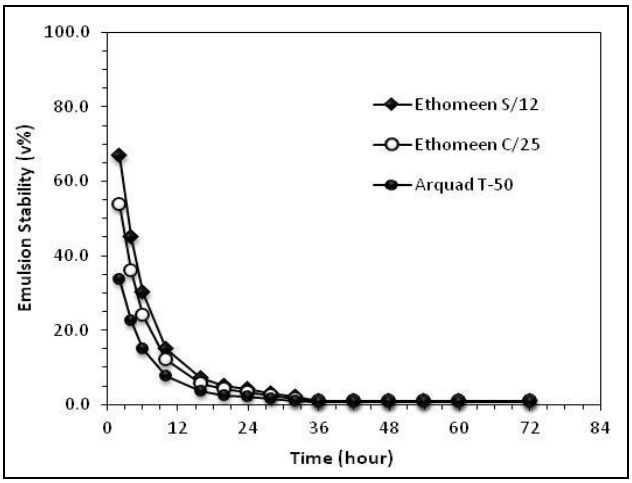

Figure 3-8. Stability of emulsions created by three cationic surfactants.

Temperature effect: The emulsion stability at an elevated temperature of 40 °C was also studied. To compare the stability results at 25 °C (77 °F) and 40 °C (104 °F), Figure 3-9 shows the percentage of height/equilibrium height (hmax) for the heavy oil/synthetic brine/surfactant emulsion at 40°C (104°F). Most emulsions with nonionic surfactants became unstable after one hour, while all of the samples with anionic and cationic surfactants became unstable immediately.

The emulsion stability of IGEPAL® CO-530 differed significantly between 25°C (77°F) and 40°C (104°F), as Figure 3-9 depicts. This emulsion was very stable at 25°C (77°F), with no separation between heavy oil and brine for more than 72 hours. At 40°C (104°F), however, the emulsion remained stable for only two hours. After that time, it became unstable and automatically separated into two layers, leaving a clear aqueous phase with oil on the top. Consequently, this surfactant can be used to generate stable oil and water emulsions at 25°C, and separates easily at 40°C (104°F).

Effect of surfactant concentration: Different concentrations of the surfactant IGEPAL® CO-530/synthetic brine were tested at 25°C (104°F). Surfactant-brine solutions, each of 18 g, with different concentrations of 0.5, 0.6, 0.7, 0.8, 0.9, 1.0, and 2.0 wt.% were mixed with 2.0 g of heavy oil, separately, and shaken by hand for one minute. Figure 3-10 shows that higher

concentrations (above 1.0 wt.%) created stable emulsions that reduced the IFT between oil and brine, but concentrations lower than 1.0 wt.% did not create stable emulsions or reduce the IFT.

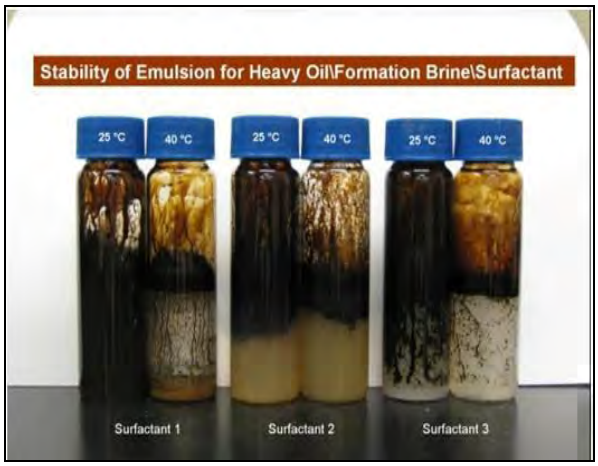

Figure 3-9. Effect of temperature on the stability of heavy oil and formation brine emulsion.

Figure 3-10. Effect of surfactant concentration on the stability of heavy oil and formation brine emulsion.

Effect of O/W ratio on stability: The influence of oil on the IGEPAL® CO-530 surfactant/synthetic brine ratio was investigated. Four samples of IGEPAL® CO-530 surfactant/brine solution at different ratios were prepared as follows:

Sample A: 4 g oil +16 g surfactant solution (20% oil to 80% IGEPAL® solution)

Sample B: 6 g oil +14 g surfactant solution (30% oil to 70% IGEPAL® solution)

Sample C: 8 g oil +12 g surfactant solution (40% oil to 60% IGEPAL® solution)

Sample D: 10 g oil +10 g surfactant solution (50% oil to 50% IGEPAL® solution)

The effect of the surfactant-to-oil ratio on the emulsion stability was also evaluated. Figure 3-11 illustrates the results of systematically changing the W/O ratio while keeping the other variables constant; the systems exhibited different stability behaviors. The results revealed that decreasing the W/O ratio caused the system to change from stable → partially stable → unstable. This information serves as a useful tool for designing optimum formulations suitable for heavy oil recovery.

Effects of the alkaline-surfactant solution on wettability: Formation sand saturated with heavy oil was used to measure the ability of surfactant and alkaline to change the sand from oil-wet to water-wet. Two oil-wet sandpack samples were saturated with heavy oil mixed with the IGEPAL® CO-350 synthetic brines, and another two samples of water-wet sand were mixed with the alkaline surfactant solution. These samples were shaken overnight. Figure 3-12 shows that the oil-wet sand can be changed into water-wet sand, and the oil can be recovered. When surfactant is combined with alkaline, it yields better recovery due to the reaction of alkaline with organic acid in the heavy oil, which further reduces the IFT.

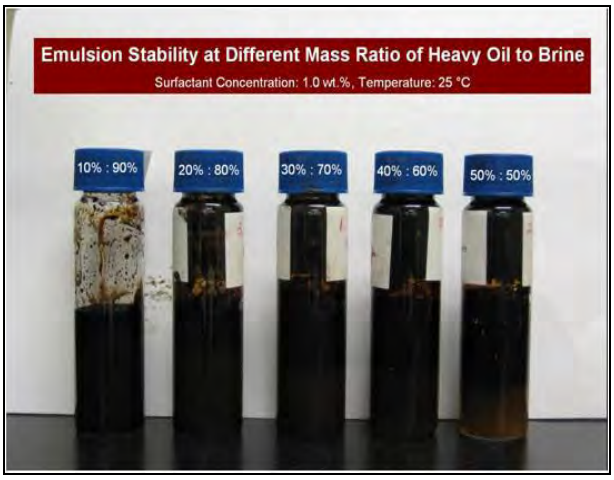

Figure 3-11. Effect of oil-to-brine ratio on the stability of heavy oil and formation brine emulsion.

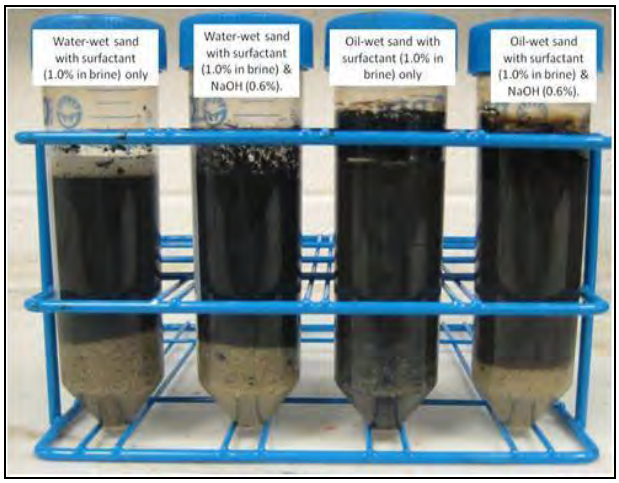

Figure 3-12. Effect of IGEPAL® CO-530 and alkaline NaOH on wettability.

Heavy oil recovery by AS flooding: As described in the previous section, injecting alkaline NaOH and IGEPAL® CO-530 can increase tertiary oil recovery. To further investigate the effect of the alkaline type on EOR efficiency, the results for sandpack flood tests with 2.0 wt.% of surfactant and 0.60 wt.% NaOH were compared. Figure 3-13 shows the oil recovery curves of these two sandpack types.

NaOH often is used in chemical flooding so that the alkaline can reduce the surfactant adsorption on the rock's surface. The incremental oil recovery was only about 10~11% OOIP, with a 1 PV injection of the chemical solution followed by an extended water flood. These results indicate

that using NaOH was necessary to obtain an optimum EOR. NaOH and the surfactant had a synergistic effect on reducing the IFT and forming O/W emulsions. The use of NaOH increased the reaction rate between the alkaline and the organic acids in the oil, leading to a significant pressure drop response [27].

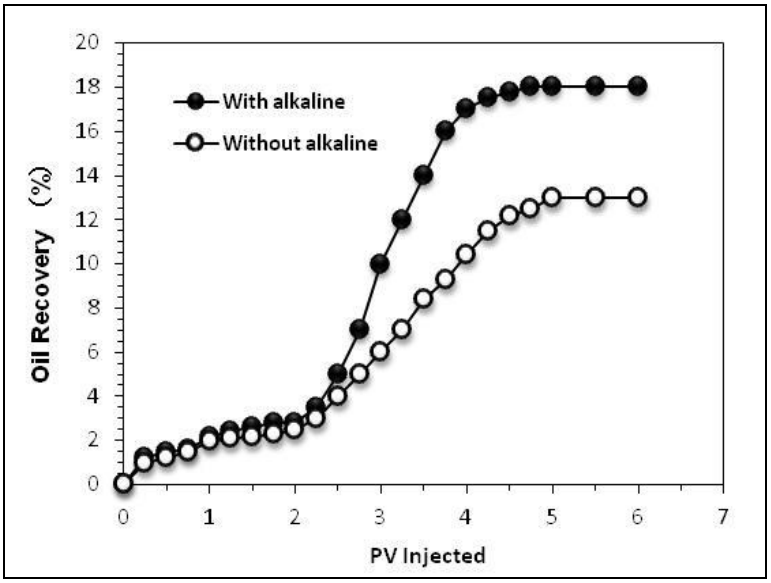

Figure 3-13. Heavy oil recovery by core flooding test using IGEPAL® CO-530 surfactant with and without the addition of alkaline solution of NaOH.

Table 3-5. Oil recovery test results with water-wet and oil-wet sandpacks.

Wettability of sandpack	2.0 wt.% of IGEPAL® CO-530 surfactant	0.60 wt.% NaOH alkaline / 2.0 wt.% of IGEPAL® CO-530 surfactant
Water-wet	90% OOIP	96% OOIP
Oil-wet	50% OOIP	70% OOIP

Oil-wet sandpack: A sandpack flood test was conducted using a 2.0 wt.% of surfactant and alkalis (0.60 wt.% NaOH) to investigate their function in the EOR process. Figure 3-12 shows that no incremental oil was recovered after AS flooding with 5% OOIP compared to water flooding with 11% OOIP. This indicates that a water channel might have been created after the water flooding. Table 3-5 lists the recovery results of AS flooding. The volumetric ES and ED, though quite low, resulted in an additional 5% (v/v) recovery of remaining oil in place (ROIP).

Water-wet sandpack: To further study the ED of alkaline and surfactant fluid, flood tests were performed on a second type of water-wet sandpack. The flooding results are listed in Table 3-5. The displacement efficiency of the water-wet sand was 17% ROIP.

Adsorption of surfactants on silica and kaolinite clay: The adsorption of the surfactant IGEPAL® CO-530 on silica and kaolinite clay was tested. These procedures were conducted with 0.1 g of kaolinite. Figure 3-2 shows the adsorption isotherms, which might correspond to the Langmuir type because of the mutual compensation of several factors that affect the shape of the isotherm. When adsorption isotherms follow the Langmuir type, the equilibrium data can be processed by employing the Langmuir equation [25]:

$$\frac{C_e}{q_e} = \frac{1}{q_{Max}} b + \frac{C_e}{q_{\max}},$$

where C_e and q_e are the surfactant concentration (mg/L) and amount absorbed (mg/g) at equilibrium, respectively; b is the Langmuir constant; and q_{max} is the maximum adsorption capacity (mg/g).

Figure 3-12 indicates that IGEPAL® CO-530 has a higher adsorption on kaolin clay than on Silica-30. The maximum adsorption of IGEPAL® CO-530 on kaolin clay is 22.13 mg per gram of clay, while the maximum adsorption of IGEPAL® CO-530 on Silica 30 is 6.9 mg per gram of silica. Several researchers have found a similar type of isotherm for the adsorption of anionic or cationic surfactants on carbons, metals and fibers [27]. Two explanations exist for this adsorption: (1) as the surfactant concentration increases, so does the ionic strength; and the depth of the surface's double layer decreases, which results in the transformation of a surface micelle; and (2) the swelling of the solid materials in the surfactant solution increases the available surface of the adsorbent. Unfortunately, no definite conclusion can be drawn at present. The lower adsorption capacity shown by Silica 30 with IGEPAL® CO-530 occurs because of the weak hydrophobic and hydrogen bond interactions between the surfactants and the adsorbent [24].

The experimental results with kaolin clay show that the adsorption of IGEPAL® CO-530 increased with the concentration, eventually plateaued, but then decreased sharply. The reason for this decrease is currently unknown.

3.1.4 Summary

The screening tests of alkalis and surfactants for the enhanced recovery of heavy oil in western Missouri were conducted by measuring the emulsion stability. Results indicated that the nonionic surfactant IGEPAL® CO-530 can form a very stable emulsion for heavy oil and synthetic brine. Through application of the emulsion, the viscosity of the heavy oil can be reduced from 18,518 cp to 2.5 cp at 25°C. The mobility of the heavy oil can be improved significantly.

The emulsion created by the surfactant IGEPAL® CO-530 was very stable at 25°C, but at 40°C, this emulsion separated automatically into two layers within two hours without the addition of any de-emulsion agent. This behavior provides great advantages for applications of this technology. Flooding tests showed that greater heavy oil recovery can be achieved with combinations of alkaline and surfactant. Adding 0.6% NaOH to the surfactant solution of IGEPAL® CO-530 can alter the wettability of the oil sand surface from oil-wet to water-wet. NaOH/surfactant systems showed a synergistic effect on the stability of the heavy oil emulsion. For Missouri heavy oil, the water-wet sandpack yielded a higher recovery than oil-wet sand. Using AS flooding, the tertiary heavy oil recovery from water-wet sandpacks reached 12% of the OOIP.

3.2 Surfactant and Nanoparticle Emulsion Stability for Larsen Oil

Nanoparticles, were tested to be added into surfactant solutions to stabilize the emulsion. A series of experiments were conducted to evaluate the nanoparticle concentration effect on emulsion stability. Whether the stabilized emulsion can be broken by a slight temperature increase or other de-emulsification methods was also evaluated.

3.2.1 Introduction

Surfactants are long chain compounds comprised of a long hydrocarbon (aliphatic) molecule that ends in a polar head group. This group can be ionic. Thus, it dissociates in water. If the group is sodium sulfate, as in sodium dodecyl sulfate (SDS), the sulfate is negatively charged and bonded to the tail. Hence, SDS is an anionic surfactant; the sodium is positively charged. Surfactants with either divalent or trivalent cations have very limited solubility and precipitate as “bathtub rings.”

Cetyltrimethyl ammonium bromide (CTAB) is a cationic surfactant. The counter ion is the bromide ion that carries a negative charge, and the surfactant ion is positively charged in the amine group. The cationic surfactants are more expensive. Nonionic surfactants are also possible when the head groups are comprised of bulky ethoxy groups. These groups are hydrophilic, as they form hydrogen bonds with water. These bonds break, however, as the temperature increases.

Surfactants are surface active. Thus, they accumulate at the oil-water interface. Both SDS and CTAB, however, are also preferentially water soluble and will stay in the aqueous phase as well. A nonionic surfactant (e.g., C12-14E20) will become oil soluble at high temperatures when its surface-active properties disappear.

Nanoparticles are less than 30 nm in diameter. They can be either hydrophilic or hydrophobic. Hydrophobic particles are very expensive and difficult to handle. Alumina (Al_2O_3) and silica (SiO_2) particles are hydrophilic particles that are easily obtained. However, alumina tends to charge positively, and silica is charged strongly negatively. These particles by themselves are not surface-active.

3.2.2 Emulsion Stability by Crude Oil and Surfactants

A heavy crude oil was obtained from an oilfield operated by Blue Top Energy LLC in southeast Kansas. A-Hauser crude oil had a viscosity of around 700 cp and an API gravity of around 20 API°. It was used with all of the series that included either the surfactants only or surfactants with Al_2O_3 nanoparticles.

3.2.2.1 Emulsion Stability by A-Hauser Crude Oil and IGEPAL® CO-530

The IGEPAL® CO-530 should stabilize emulsion only when water is continuous. Emulsion should become very unstable at a higher temperature. The emulsion samples of A-Hauser crude oil and IGEPAL® CO-530 were placed in a 25°C water bath for 24 hours to test this theory. The samples with a water to oil ratio of 1:9, 5:5, and 2.5:7.5 (in which oil was the continuous phase) became unstable within a few hours, forming two phases of separation (Figure 3-14 a, b, and c). However, samples with the water to oil ratio of 7.5:2.5 and 9:1 (in which water was the

continuous phase) were stable for several weeks without exhibiting separation (Figure 3-14 d and e).

Figure 3-14. IGEPAL® CO-530 and A-Hauser crude oil emulsions with different ratios at 25˚C.

Figure 3-15. IGEPAL® CO-530 and A-Hauser crude oil emulsions with different ratios at 40˚C.

The samples that did not exhibit separation were returned to the water bath at a higher temperature to test their ability to break the emulsion as the temperature. The temperature was increased to 40°C for another 24 hours. The sample with the water to oil ratio of 7.5:2.5 remained stable, as shown in Figure 3-15 d. However, the sample with the water to oil ratio of 7.5:2.5 became unstable and exhibited two phases, as shown in Figure 3-15 e.

3.2.2.2 Emulsion Stability by A-Hauser Crude Oil and Sodium Dodecyl Sulfate (SDS)

The samples prepared by A-Hauser crude oil and SDS at different ratios were placed in a water bath at 25°C. Figure 3-18 showed the results after 2 hours in the water bath. It is clear that all samples were not stable. Each sample exhibited two phases: an oil phase and a water phase. These samples were not tested at a higher temperature due to the instability of the emulsions at room temperature.

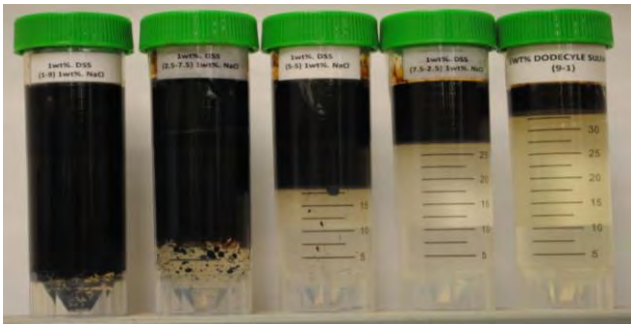

Figure 3-16. SDS and A-Hauser crude oil emulsions with different ratios at 25°C.

3.2.2.3 Emulsion Stability by A-Hauser Crude Oil and Cetylrimethyl Ammonium Bromide (CTAB)

The samples of A-Hauser crude oil that were combined with CTAB were placed in a water bath at 25°C for 24 hours. The sample with the water to oil ratio of 9:1 formed both a brown phase and a black phase, as shown in Figure 3-17 a. The samples with the water to oil ratios of 7.5:2.5, 5:5, and 2.5:7.5 formed a dark brown phase and a black phase as shown in Figure 3-17 b, c, and d, respectively. However, the sample with the water to oil ratio of 1:9 formed one phase of emulsion without separation, as shown in Figure 3-17 e. The CTAB samples were then placed in a water bath at higher temperatures (40, 50, and 60°C). No break occurred in the emulsions, indicating the emulsions formed by CTAB were not affected by temperature.

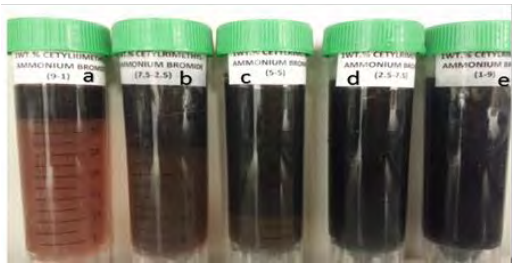

Figure 3-17. CTAB and A-Hauser crude oil emulsions with different ratios at 25°C.

3.2.2.4 Emulsion Stability by A-Hauser Crude Oil, IGEPAL® CO-530, and Al_2O_3

Adding Al_2O_3 nanoparticle to IGEPAL® CO-530 should make IGEPAL® CO-530 adsorb on alumina. Both a water continuous emulsion and an oil continuous emulsion should be more stable than IGEPAL® CO-530 alone. Unlike CTAB, only water continuous emulsion becomes unstable when the temperature increases. To test this theory, the samples of A-Hauser crude oil combined with IGEPAL® CO-530 and Al_2O_3 were placed in a 25°C water bath for 24 hours. The samples with the water to oil ratio of 7.5:2.5 and 5:5 formed unstable emulsions. The remaining samples with the water to oil ratio of 2.5:7.5 and 1:9 formed stable emulsion, and oil was the continuous phase as pictured in Figure 3-20. The sample with the water to oil ratio of 9:1 showed slight separation, evidence of a stable emulsion. The aqueous phases of the emulsion with the water to oil ratios of 7.5:2.5 and 5:5 were brown, indicating some oil droplets were

contained in the phases. The addition of Al_2O_3 nanoparticles made IGEPAL® CO-530 stabilize the emulsion more than using IGEPAL® CO-530 alone.

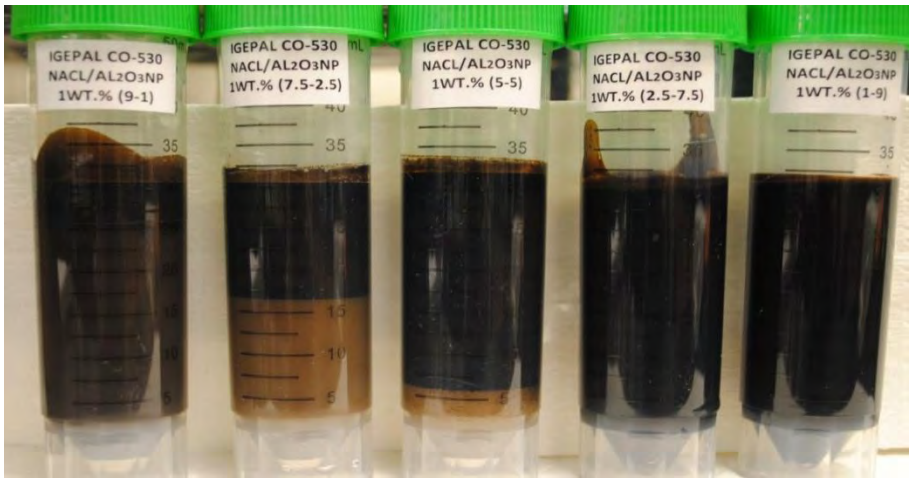

Figure 3-18. Al_2O_3/IGEPAL® CO-530 and A-Hauser crude oil emulsions with different ratios at 40°C.

The samples of Al_2O_3 and IGEPAL® CO-530 were then placed in a 40°C water bath for an additional 24 hours so that the behavior of crude oil, IGEPAL® CO-530, and Al2O3 emulsion could be investigated at higher temperatures. The emulsion with the water to oil ratio of 9:1 broke emulsion within a few hours (Figure 3-19 e). The properties of the remaining samples did not change as the temperature increased (Figure 3-19 a, b, c, and d).

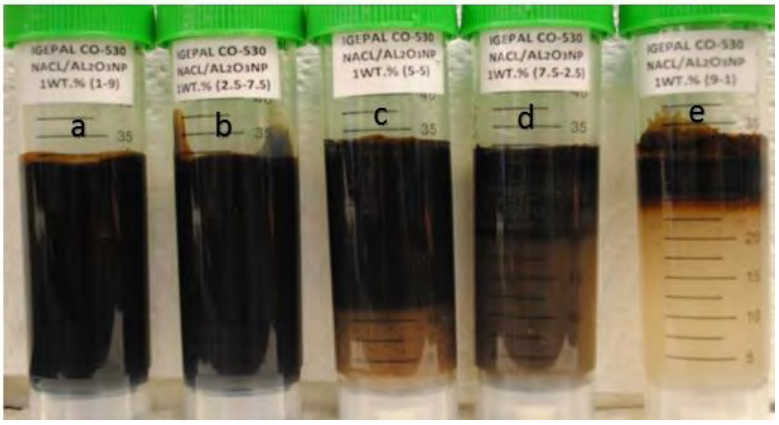

Figure 3-19. Al_2O_3/IGEPAL® CO-530 and A-Hauser crude oil emulsions with different ratios at 40°C.

3.2.2.5 Emulsion Stability by A-Hauser Crude Oil, SDS, and Al2O3

SDS adsorbs on alumina. Such particles are partially hydrophobic and, hence, surface-active. Water continuous emulsions are expected to be more stable than SDS alone. To test these

expectations, samples of A–Hauser crude oil combined with SDS and Al2O3 were placed in a 25°C water bath for 24 hours. The 1:9 ratio of water to oil (oil continuous) had a stable emulsion after 4 hours as pictured in Figure 3-20 a. The remaining samples exhibited rapid separation, as pictured in Figure 3-20 b, c, d, and e.

Figure 3-20. Al_2O_3/SDS and A-Hauser crude oil emulsions with different ratios at 25°C.

Samples of 2.5:7.5, 5:5, 7.5:2.5, and 9:1 water to oil ratios were completely separated into two phases in Figure 3-21 b, c, d, and e after 24 hours. The emulsion with water to oil ratio of 1:9 did not exhibit a phase separation as pictured in Figure 3-21 a.

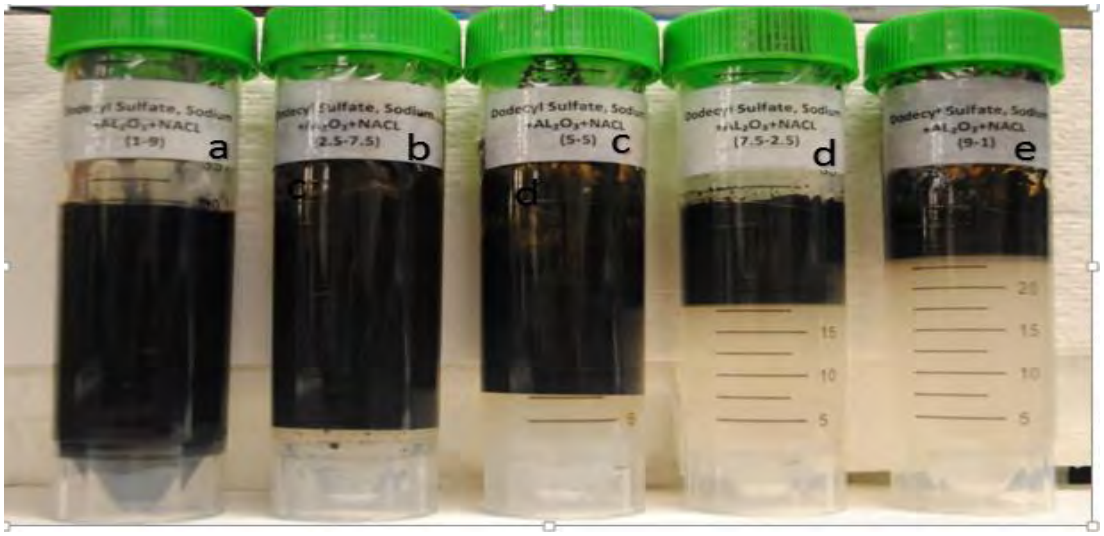

Figure 3-21. Al_2O_3/SDS and A-Hauser crude oil emulsions with different ratio at 25°C after 24 hours.

3.2.2.6 Emulsion Stability by A-Hauser Crude Oil, CTAB, and AL_2O_3

Theoretically, CTAB adsorbs on alumina. Water continuous emulsions are expected to be as stable as those with CTAB alone. The samples prepared with CTAB, Al_2O_3, and crude oil emulsions were placed in a 25°C water bath for 24 hours. The results are pictured in Figure 3-22. The samples with the water to oil ratios of 1:9 and 2.5:7.5 formed a stable emulsion as shown in Figure 3-24 a and b. The samples with the water to oil ratios of 5:5, 7.5:2.5, and 9:1 formed unstable emulsions (Figure 3-22 c, d, and e). The sample with the water to oil ratio of 9:1 had one yellow phase and one black phase. The sample with the water to oil ratio of 7.5:2.5 had a light brown phase and a black phase. The sample with the water to oil ratio of 5:5 formed a dark brown phase and a black phase. The samples with the water to oil ratio of 1:9 and 2.5:7.5 formed one phase of emulsion without separation. The samples with the water to oil ratios of 1:9 and 2.5:7.5 were next placed in a 40°C water bath for an additional 24 hours. Both samples (1:9 and 2.5:7.5) remained stable at that temperature.

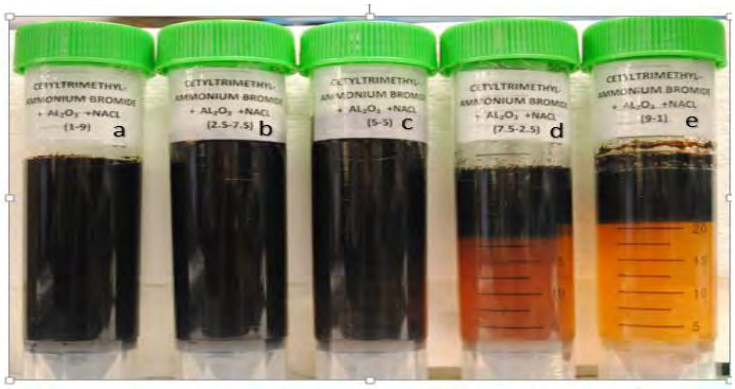

Figure 3-22. Al_2O_3/CTAB and A-Hauser crude oil emulsions with different ratios at 25°C after 24 hours.

3.2.2.7 Emulsion Stability by A-Hauser Crude Oil, IGEPAL CO-530, and SiO_2

If IGEPAL® CO-530 adsorbs significantly on silica, then both water continuous emulsions and oil continuous emulsions should be more stable than they are with IGEPAL® CO-530 alone. Only the water continuous emulsion should become unstable when the temperature is increased. To test this theory, the emulsion samples of A-Hauser, IGEPAL® CO-530, and SiO_2 were

placed in a 25°C water bath for 24 hours. All of the samples were stable, and no phase separation occurred (see Figure 3-23).

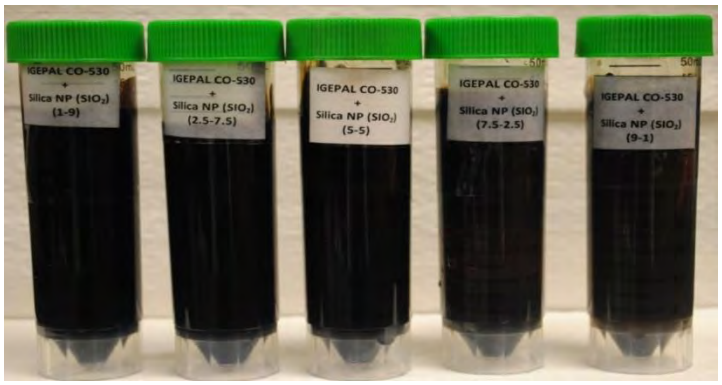

Figure 3-23. SiO_2/ IGEPAL® CO-530 and A-Hauser crude oil emulsions with different ratios at 25°C.

The temperature had to be increased every 24 hours to 40°C, 50°C, and 60°C to break the emulsion. Eventually, the temperature had no effect on the emulsion of IGEPAL® CO-530 and SiO_2 crude oil samples.

3.2.2.8 Emulsion Stability by A-Hauser Crude Oil, SDS, and SiO_2

SDS does not adsorb on silica. Water continuous emulsions are therefor expected to be as stable as those with SDS alone. Prepared samples that combined A-Hauser crude oil, SDS, and SiO2 were placed in a 25°C water bath for 24 hours. The 1:9 water to oil ratio (oil continuous) had a stable emulsion phase (Figure 3-24 a). The 2.5:7.5 water to oil ratios separated slightly with some drops of oil stuck on the surface (Figure 3-24 b). The 5:5, 7.5:2.5, and 9:1 water to oil ratios (water continuous) exhibited three phases: dark gray particles in the bottom, a milky solution in the middle, and black on the top (Figure 3-24 c, d, and e).

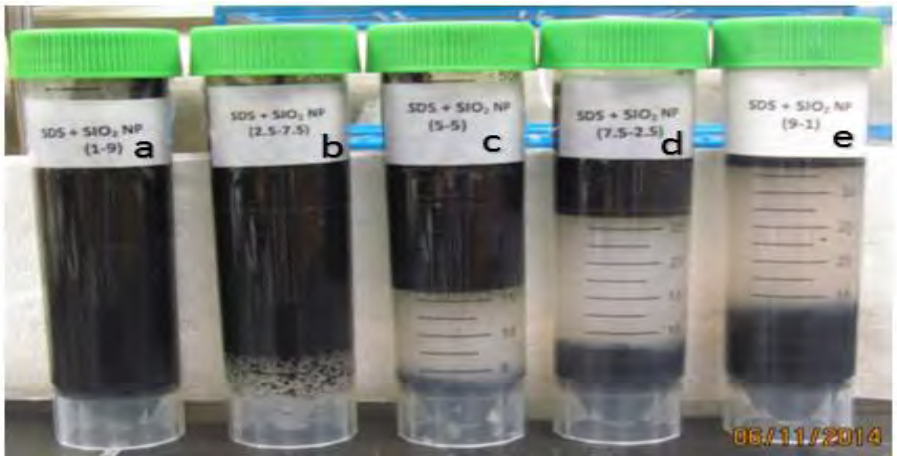

Figure 3-24. SiO_2/SDS and A-Hauser crude oil emulsions with different ratios at 25°C.

3.2.2.9 Emulsion Stability by A-Hauser Crude Oil, CTAB, and SiO_2.

CTAB adsorbs on silica. Such particles are partially hydrophobic and, hence, surface-active. Water continuous emulsions are expected to be more stable than those with CTAB alone. To examine these expectations, samples combining CTAB and SiO_2 were placed in a 25°C water bath for 24 hours. The samples with water to oil ratios of 1:9 and 2.5:7.5 had an oil continuous phase that formed a stable emulsion (Figure 3-25 a and b). The 9:1 water to oil ratio formed three phases: a yellow phase in the middle, a black phase on the top, and some gray particles at the bottom (Figure 3-25 e). The 7.5:2.5 and 5:5 water to oil ratios formed two phases: a milky brown phase at the bottom and a black phase on the top (Figure 3-25 c and d). There was no temperature effect on CTAB, SiO2, and crude oil emulsions after increasing temperature for the 1:9 and 2.5:7.5 water to oil ratios.

Figure 3-25. SiO_2/CTAB and A-Hauser crude oil emulsions with different ratios at 25°C.

3.2.3 Summary

This section described a study that was conducted to investigate the influence of surfactant on crude oil emulsion stability. It also described the influence of adding nanoparticles to surfactant solutions to achieve more emulsion stability. Both studies were performed using different ratios of water to oil, and under different temperatures. Nonionic surfactants might be affected by differences in temperature. Anionic and cationic surfactants, however, should not. A summary of the results of surfactants and crude oil emulsions is shown in Table 3-6.

Several of the samples exhibited a stable emulsion. Thus, some surfactants might have the ability to reduce the interfacial tension (IFT) that exists between the crude oil and the aqueous phase. The additional of nanoparticles should increase crude oil emulsion stability. A summary of the results of the emulsions with surfactants, Al2O3 nanoparticles, and crude oil is shown in Table 3-7. Different types of nanoparticles of varying sizes should lead to different results. A summary of the results of combining the surfactants with Si2O nanoparticles and crude oil in emulsions is shown in Table 3-8.

Table 3-6. Stability results of surfactants at 25°C and 40°C.

Water to Oil ratio	**Nonionic (IGEPAL® CO-530)**	**Anionic (SDS)**	**Cationic (CTAB)**
1-9	Unstable at 25°C Fig 3-16 a	Unstable at 25°C Fig 3-18	Stable at 25°C Fig 3-19 e
2.5 -7.5	Unstable at 25°C Fig 3-16 c	Unstable at 25°C Fig 3-18	Unstable at 25°C Fig 3-19d
5-5	Unstable at 25°C Fig 3-16 b	Unstable at 25°C Fig 3-18	Unstable at 25°C Fig 3-19c
7.5-2.5	Stable at 25°C, Fig 3-16 d Stable at 40°C, Fig 3-17 d	Unstable at 25°C Fig 3-18	Unstable at 25°C Fig 3-19b
9-1	Stable at 25°C, Fig 3-16 e Unstable at 40°C, Fig 3-17 e	Unstable at 25°C Fig 3-18	Unstable at 25°C Fig 3-19a

Table 3-7. Stability results of surfactants with Al_2O_3 at 25°C and 40°C.

Water to Oil ratio	Nonionic (IGEPAL CO-530)+Al_2O_3	Anionic (SDS)+Al_2O_3	Cationic (CTAB)+Al_2O_3
1-9	Stable at 25°C Stable at 40°C	Stable at 25°C	Stable at 25°C Stable at 40°C
2.5 -7.5	Stable at 25°C Stable at 40°C	Unstable at 25°C	Stable at 25°C Stable at 40°C
5-5	Unstable at 25°C	Unstable at 25°C	Unstable at 25°C
7.5-2.5	Unstable at 25°C	Unstable at 25°C	Unstable at 25°C
9-1	Slightly stable at 25°C	Unstable at 25°C	Unstable at 25°C

Table 3-8. Chemical additives system expectations and results.

System	Expectations	Results
IGEPAL® CO-530	o/w stable because of charge effect, temperature sensitive: becomes unstable at high temperature as it loses surface activity w/o unstable	o/w stable at 25°C w/o unstable o/w unstable at 40°C
SDS	o/w stable because of charge effect, but not temperature sensitive. w/o unstable	all unstable
CTAB	o/w stable because of charge effect, but not temperature sensitive w/o unstable	w/o stable no effect of higher temperatures
IGEPAL® CO-530 + Al_2O_3	adsorption on Al_2O_3 Stable than IGEPAL® CO-530 alone	w/o stable at 25°C o/w unstable
SDS + Al_2O_3	adsorption of SDS on Al_2O_3 Al2O3 is surface active.	w/o stable (1: 9 water: oil) o/w unstable
CTAB + Al_2O_3	no adsorption of CTAB on Al_2O_3	w/o stable o/w unstable
IGEPAL® CO-530 + SiO_2	no adsorption on SiO_2	all stable stable until temperature rises to 60°C
SDS + SiO_2	no adsorption of SDS on SiO_2, so SiO_2 is not surface active	w/o stable
CTAB + SiO_2	adsorption of CTAB on SiO_2, so SiO_2 is surface-active	w/o stable

3.3 Optical Experiments of Surfactants to Oil and Water Emulsion

Experiments were conducted using micro-models to visualize the emulsification process of the heavy oil and surfactants in porous media. A micromodel is the transparent networks of pores and constrictions that simulates the complexities of natural porous media. In our experiments, emulsion morphology was determined using decane and crude oil with different surfactants sorted by their HLB values. Quantitative measurement of the dispersed phase was conducted using software with a particular combination of surfactant, oil, and water. Flooding tests using water, surfactant and gas were observed under confocal and laser systems.

3.3.1 Introduction

Emulsions are dispersions of one liquid phase in the other which can be found in many fields of study, such as in the electronics, biomedical, aerospace, and pharmaceutical industries. In energy territory, oil and water emulsions are mostly discussed and mainly related to recovery improvement, especially for heavy oil recovery. Emulsion constitutions are caused by (1) water-oil ratio, (2) surfactant proportion, (3) surfactant characteristics, (4) environmental condition, which includes temperature and pressure, and (5) micro-scale interactions, such as mixing method and shearing strength. These factors can lead to different emulsion features that have effects on the recovery of heavy oil.

Ternary phase diagrams of an oil-surfactant water system are commonly used to describe the effect of the ratio of water, oil, and surfactant on emulsion. Emulsion constitution structure (Figure 3-26) and morphology (Figure 3-27) are discussed in the literatures [28, 29].

Besides ternary phase diagram, another important emulsion determination parameter is the HLB of a surfactant, which is a measure of the degree to which it is hydrophilic or lipophilic, determined by calculating values for the different regions of the molecule. Detailed HLB values and their application to emulsifiers are listed in Figure 3-28 [30]. In Davies' method, the effect of hydrophilic and lipophilic groups was used to calculate the HLB value using equation: $\mathrm{HLB} = 7 + \sum_{i=1}^{m} Hi - n * 0.475$, in which m represents the number of hydrophilic groups in the molecule, Hi represents the value of the ith hydrophilic group (Table 3-9), and n represents the number of lipophilic groups in the molecule. According to the HLB value, the polarity of surfactants can be determined, and emulsion solubility can be predicted.

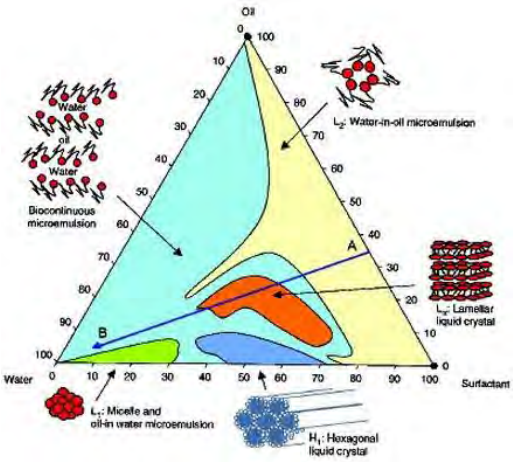

Figure 3-26. Ternary phase diagram of an oil-surfactant water system, based on a $C_{12}E_{10}$-oleic acid water system.

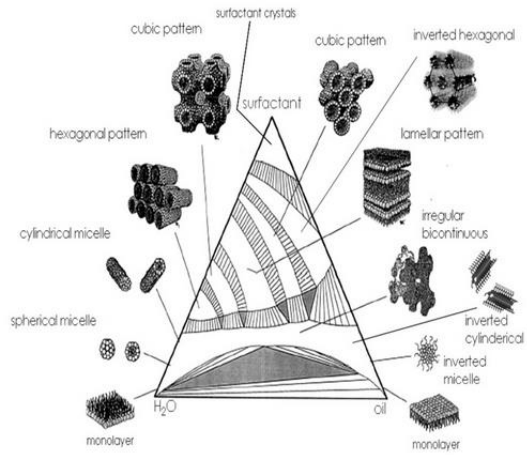

Figure 3-27. Phase diagram: Water (aqueous phase), oil, surfactant and the structure of microemulsion.

Range of HLB values	*Application*
3.5-6	*W/O emulsifier*
7-9	*Wetting agent*
8-18	*O/W emulsifier*
13-15	*Detergent*
15-18	*Solubilization*

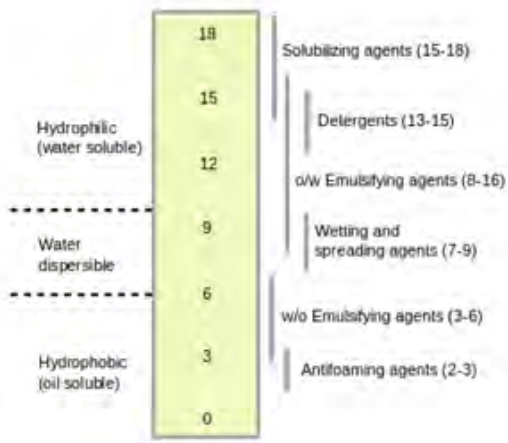

Figure 3-28. Classification of emulsifiers according to HLB values.

Depending on the surfactant selected and the aqueous phase chemistry, a Winsor Type I, Type II, or Type III system will result. The Winsor Type III system is associated with a middle-phase microemulsion and ultra-low interfacial tensions as shown in Figure 3-28 [31]. Oil in water emulsions will be formed in the lower layer of Winsor Type I system, and water in oil emulsions will be formed in the upper later of Winsor Type II system.

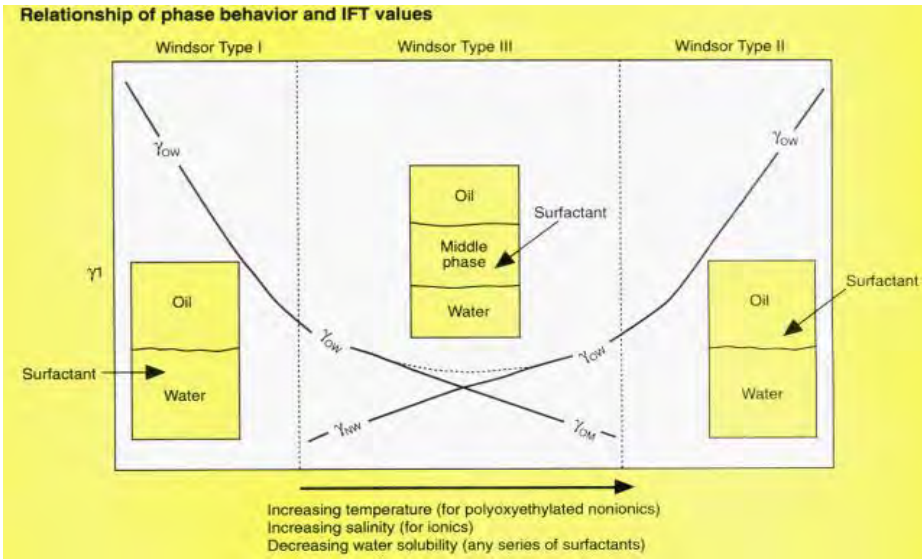

Figure 3-29. Relationship between phase behavior and IFT values.

Table 3-9. HLB group number.

Hydrophilic groups	*Group Number*
$-SO_4^-Na^+$	38.7
$-COO^-K^+$	21.1
$-COO^-Na^+$	19.1
N (tertiary amine)	9.4
Ester (sorbitan ring)	6.8
Ester (free)	2.4
-COOH	2.1
Hydroxyl (free)	1.9
-O-	1.3
Hydroxyl (sorbitan ring)	0.5
Lipophilic groups	
-CH-	
$-CH_2-$	
CH_3-	- 0.475
=CH-	
Derived groups	
$-(CH_2-CH_2-O)-$	+ 0,33
$-(CH_2-CH_2-CH_2-O)-$	- 0.15

One of the unique factors associated with microemulsions is the presence of different textures such as oil droplets in water, water droplets in oil, bicontinuous, and lamellar mixtures etc.,

which are formed by altering the curvature of the interface with the help of different factors, such as salinity, temperature, etc. Such a variety in the structure of microemulsion is a function of the composition of the system. Phase study greatly helps to elucidate different phases that exist in the region depending upon the composition ratios. One peculiarity of microemulsions is that their structures are interchangeable.

Construction of a phase diagram enables determination of aqueous dilutability and range of compositions that form a monophasic region, as showed in Figure 3-29 [32]. One of the unique factors associated with microemulsions is the presence of different structures, as classified by Winsor. Oil in water emulsion (Winsor I), water in oil emulsion (Winsor II), bicontinuous or middle phase microemulsion (Winsor III) and Winsor IV system are formed by altering the curvature of the interface with the help of different factors such as salinity, temperature, etc.

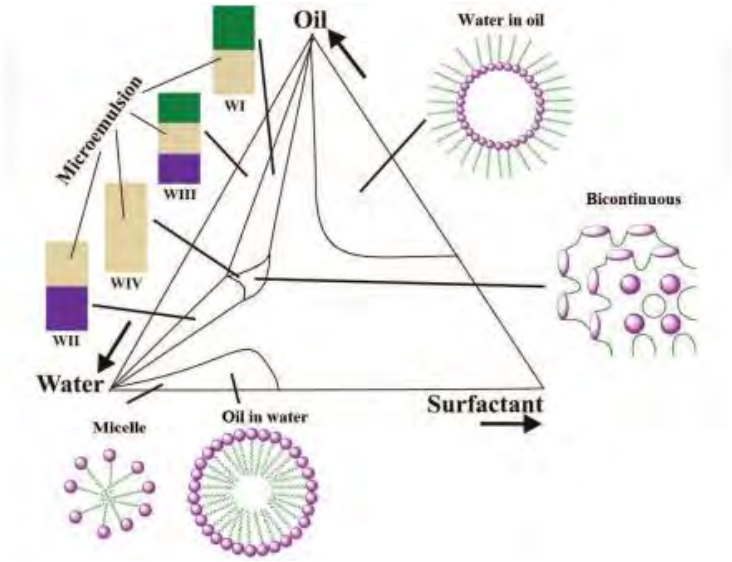

Figure 3-30. A hypothetical ternary phase diagram representing three components of the system.

As showed in Figure 3-30 [32], Winsor Type I indicates two layered immiscible phases, with a lower phase of a surfactant-rich water phase and an upper phase of a surfactant-poor oil phase; Winsor Type II consists an upper phase of a surfactant-rich oil phase and a lower phase of a surfactant-poor water phase; Winsor Type III represents the surfactant-rich middle phase, which coexists with both water and oil surfactant-poor phases; and Winsor Type IV is a single phase homogeneous mixture.

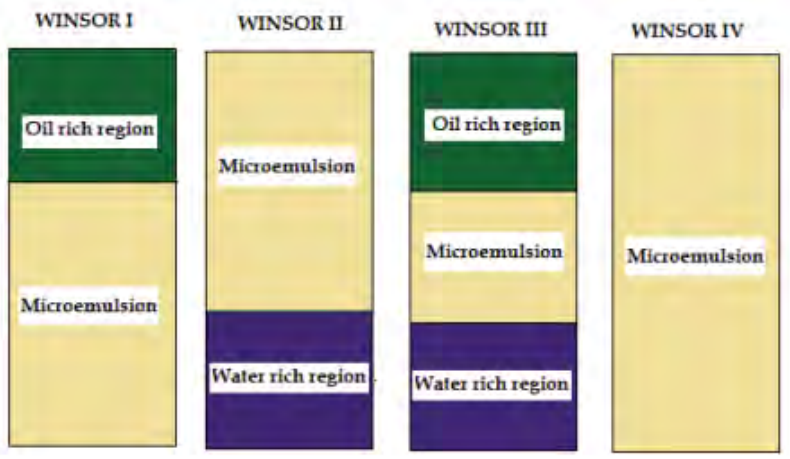

Figure 3-31. Schematic presentation of most frequently occurring surfactant associates.

3.3.2 Method and Materials

To better understand emulsion, an experiment using a certain water-oil-surfactant ratio was conducted and observed under laser microscope. To better simulate the emulsion active phase of reservoir recovery which usually is the tertiary phase, 85% water together with 10% oil and 5% surfactant were mixed. Deionized water was used to better understand the impact of surfactant itself. De-ionized water was obtained from the Milli-Q® Reference Ultra-pure Water Purification System. ACS grade (99.9%) decane was purchased from Fisher Scientific. All solutions were filtered by a 0.22 μm pore size nylon membrane prior to use. Decane with fluorescent dye Nile Red which has a lipophilic stain, and crude oil with a density of 0.929 g/ml and a viscosity of 656 cp were used as oil phase respectively. Nile Red was purchased from Invitrogen™ (Grand Island, NY) to serve as fluorescent dye at the final concentration of 100 mg/L in decane. Nile red has very low water solubility and no fluorescence in the aqueous solution. The emission spectra of Nile red in different solvents is shown in Figure 3-31. In non-polar solvents, such as hexane and decane, the emission is around 525 nm. According to Figure 3-32 [33], crude oil has natural fluorescence of visible in the range of wavelengths from 450 nm to 600 nm and is typically excited by ultraviolet wavelengths of 300 nm to 400 nm.

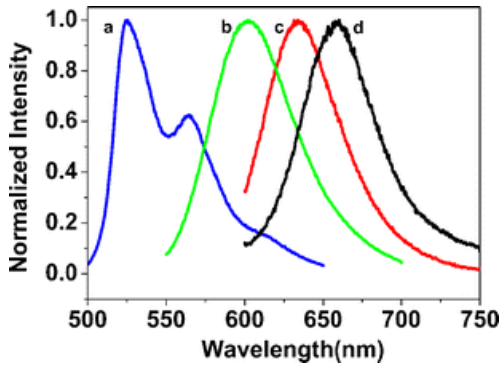

Figure 3-32. Emission spectrum of Nile Red in different solvents: (a) n-hexane; (b) ethyl acetate; (c) methanol; (d) water.

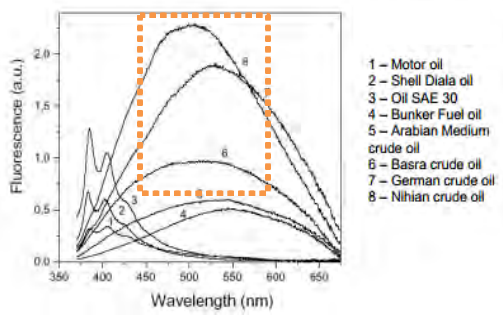

Figure 3-33. Natural florescence of crude oil 5-8.

Three surfactants were used for the emulsifier process and were chosen by HLB value as shown in Figure 3-33. The hydrophobic surfactant Span 80 with an HLB value of 4.3; wetting and spreading agents IGELPAL® CO-530, with an HLB value of 10.8; and the extreme hydrophilic surfactant sodium dodecyl sulfate (SDS) with an HLB value of 40, were added to water and oil including decane and crude oil solution, respectively.

A confocal microscope system was used to generate the 3-D reconstructions for residual phase distribution study. As mentioned above, epi-fluorescence microscopy method was used for images collection. The wavelength of the excitation light is at 488 nm and the wavelength of the emission light is at 525 nm. FITC dichroic mirror was used to filter out the excitation light (incident light) to reduce the background noise. All images were captured by a Nikon TiE motorized microscope equipped with a Yokogawa X1 confocal scan head and 4 lasers with AOTF control. The exposure time was set at 500 ms and data were acquired through the NIS-Elements software by Nikon. Confocal system provided a very sharp focus of a specific layer with resolution of 0.2 um. Multiple layers were scanned to construct the 3-D image. The experimental set-up is shown in Figure 3-34.

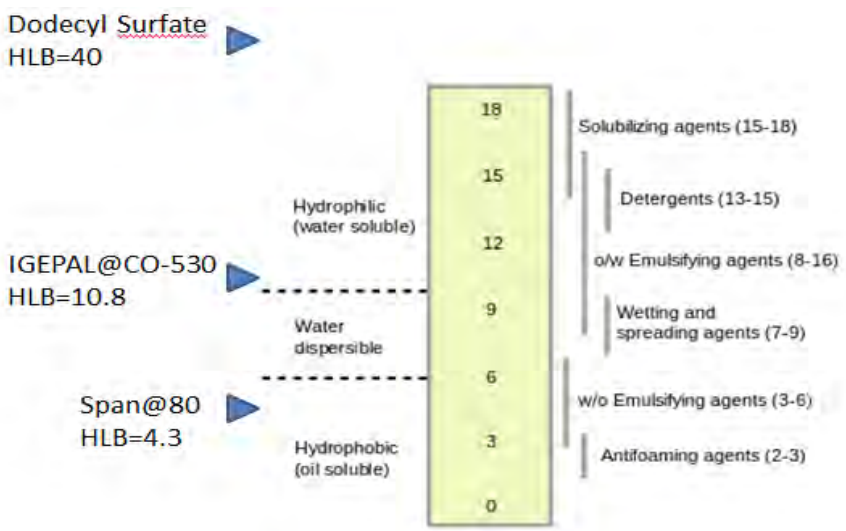

Figure 3-34. Surfactant selection and its HLB value.

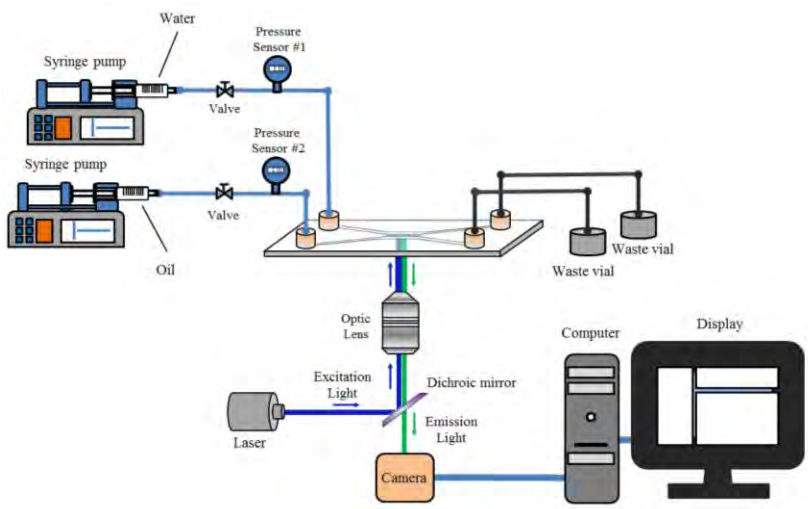

Figure 3-35. Schematic of the experimental apparatus.

3.3.3 Results and Discussion

3.3.3.1 Emulsion Preparation of Different Winsor Type

As previously noted, three surfactants were used for the emulsification process. Hydrophobic surfactant Span 80 with an HLB value of 4.3, wetting and spreading agents IGELPAL® CO-530 with an HLB value of 10.8 and extremely hydrophilic surfactant sodium dodecyl sulfate (SDS) with HLB value 40 were added to water and oil including decane and crude oil solutions,

respectively. After a 2 week period at room temperature, the emulsion types were showed in Figure 3-35 and Figure 3-36.

As shown in Figure 3-35, the water-oil ratio of 85:10 the hydrophilic surfactant Span 80 with an HLB value around 4, gave a Winsor Type III emulsion for both decane and crude oil. Phasing split was clear and a 3-layer emulsion system evident. The upper layer of oil and lower layer of water were relatively clear but turbid. The middle layer was a clear emulsion, which was sampled and observed under a laser microscope.

A new combination of water-oil ratio was evaluated with 75% oil and 20% water instead of 85% water and 10% oil. Deionized water was used to better understand the impact of surfactant itself. Deionized water was obtained from the Milli-Q® Reference Ultra-pure Water Purification System. ACS grade (99.9%) decane was purchased from Fisher Scientific. All solutions were filtered by a 0.22 μm pore size nylon membrane prior to use. Crude oil was used as oil phase with natural fluorescence visible in the range of wavelengths from 450 nm to 600 nm. Two surfactants were used for the emulsification process. Hydrophobic surfactant Span 80 with an HLB value of 4.3 and extreme hydrophilic surfactant sodium dodecyl sulfate (SDS), with an HLB value of 40, were added to water and crude oil solution, respectively. After a 2-week period sitting in room temperature, the emulsion types are showed in Figure 3-36.

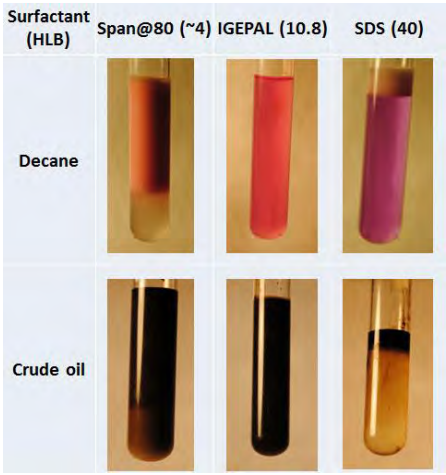

Figure 3-36. Emulsion types using decane and crude oil together with 3 different surfactants.

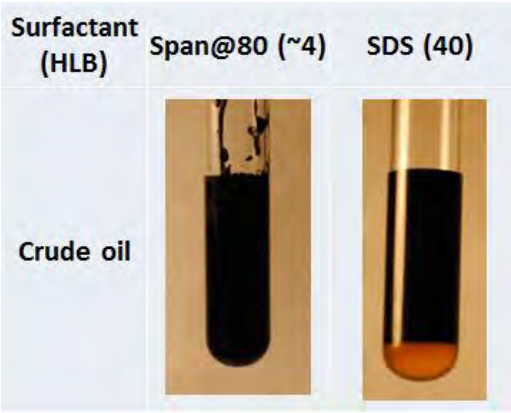

Figure 3-37. Emulsion types using water and crude oil together with 2 different surfactants.

3.3.3.2 Emulsion Morphology Observed Under Laser Microscope

For the emulsion mixture by Span 80 with both decane and crude oil, the results are shown in Figure 3-37. Because of the dyed decane and natural fluorescence of crude oil, oil phase was displayed as a colored phase in the results. On the other hand, water showed no fluorescence and stayed black. Figure 3-37 shows a poor distribution in both hydrocarbon mixtures. With the limitation of the resolution of the microscope and camera, the observed diameter of droplets varied from several micrometers to over a hundred micrometers. At the same time, a clear water in oil in water (W/O/W) emulsion was observed in decane mixture.

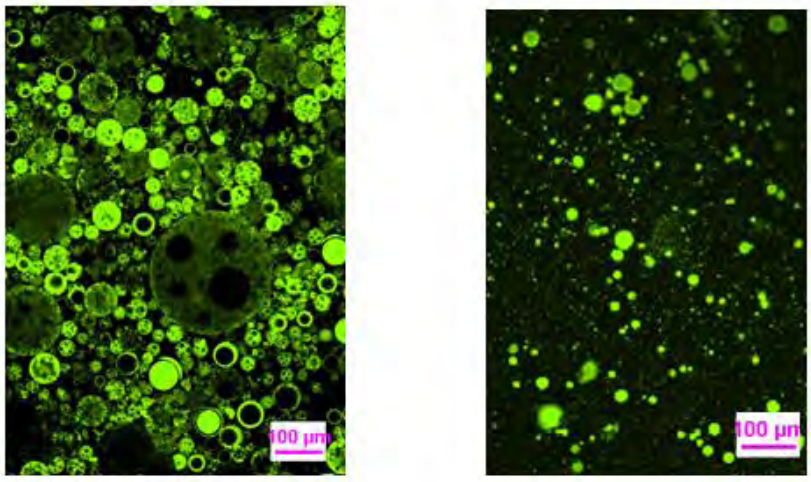

(a) (b)

Figure 3-38. Microscopic image of the middle layer using surfactant Span 80 with (a) decane and (b) crude oil.

IGELPAL® CO-530 is a wetting and spreading agents with an HLB value of 10.8 and is neutral in hydrophilic and hydrophobic performance. The emulsion was very stable using both decane and crude oil. The samples under the microscope then showed a typical bi-continuous phase of oil and water as Winsor Type IV emulsion (Figure 3-38).

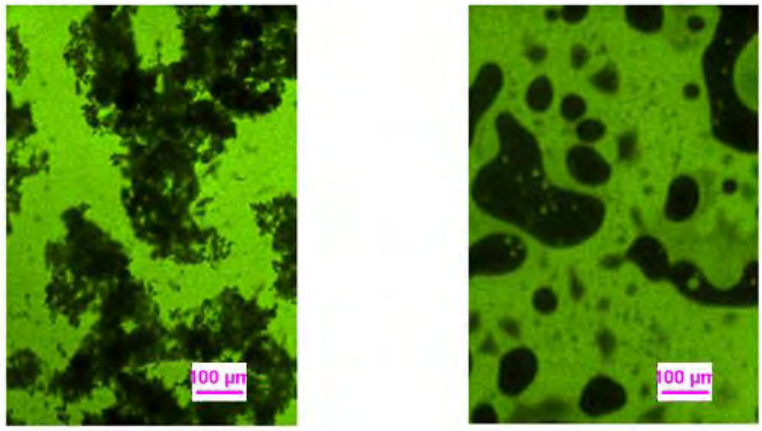

(a) (b)

Figure 3-39. Bicontinuous water and oil phase using IGEPAL® CO-530 and (a) decane and (b) crude oil.

Even though water to oil ratio was 85:10, the oil phase tended to be a continuous phase instead of dispersion. For Figure 3-38 a, the interface of water and oil was not very smooth with small dispersions in or under micro-scale.

For the extremely hydrophilic surfactant SDS, a Winsor Type I emulsion was formed with an upper layer of mostly hydrocarbon and a lower layer of oil in water emulsion. The lower layer was sampled and put under laser microscope as shown in Figure 3-39. Notice that the oil dropper size was smaller, and the droplets were more organized than the mixture of decane and Span 80.

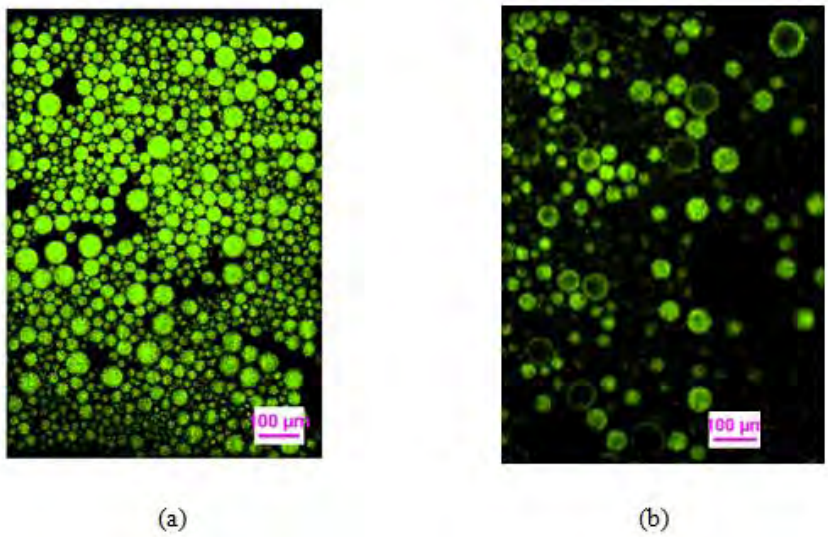

Figure 3-40. Oil in water emulsion with SDS and (a) decane and (b) crude oil.

As for 85:10 oil to water ratio emulsion, it was difficult to determine the Winsor Type because of the dimness of the majority of crude oil by using hydrophobic surfactant Span 80. Either Winsor Type I or Type IV was formed due to the colored lower phase that indicated either a surfactant-rich water phase (Winsor Type I) or a bicontinuous phase of oil or water (Winsor Type IV). However, hydrophilic surfactant SDS displayed a more lucid lower phase, still colored enough for the suspicious of surfactant-rich water phase. A test then was conducted by picking solvent sample from upper phase and imaging the sample by laser microscope as shown in Figure 3-40.

From Figure 3-36, notice that water dispersed phase, which is black, existed as the upper phase of emulsion. Therefore, a Winsor Type II seemed to be a better description of this emulsion. Another interesting part of this Winsor Type II emulsion was that some optical oil droplets were found within dispersed water drops which made it an oil in water in oil emulsion (O/W/O). Compare to the results shown in Figure 3-41, instead of an O/W/O emulsion, a W/O/W emulsion was formed using same surfactant, Span 80, but with a different water to oil ratio and oil type.

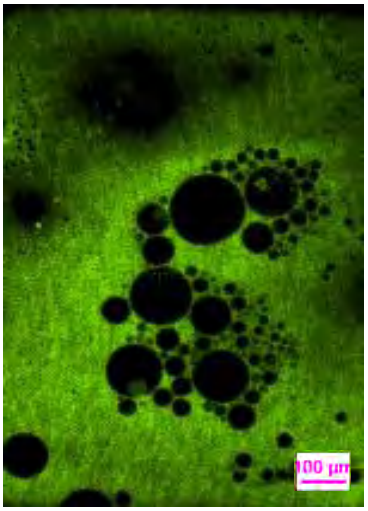

Figure 3-41. Microscopic image of the upper layer using Span 80 with crude oil.

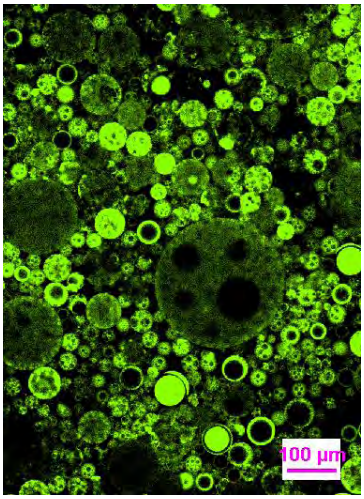

Figure 3-42. Microscopic image of the middle layer using Span 80 with decane.

3.3.3.3 Quantitative Measurement of Dispersed Phase under Laser Microscope

NIS-Elements AR software was used for image processing and numerical measurement. All information was included because the images were first transferred from the microscope and camera then captured by NIS-Elements AR so that there was no information lost due to the transformation of image format. An example is showed in Figure 3-42 using the laser microscope result from water-oil ratio 85:10 with decane and 5% SDS as surfactant.

Automated measurements were taken by software using thresholding method. Certain intensity of colored phase (oil) was chosen as region of interest (ROI), which was framed and labeled. Then the data acquisition was generated and could be exported into data file, including the information of objective ID, area and mean intensity of certain laser.

During the automated measurement procedure, some issues were revealed that related to intensity difference. Due to the intensity difference caused by the intensity binary effect and the diffraction effect of a single larger droplet or the area of high density of droplets, one standard of intensity threshold could not efficiently select all prospects. Thus a threshold partition method was developed to eliminate such error as showed in Figure 3-43 b and c.

Notice the intensity profile has a peak value at a low intensity area, which indicated the noise. Slightly right of the noise peak, there is a target intensity, with the peak value at about 160. By dividing the target intensity into two parts range from 142 to 172 and 172 to 215, two automated measurements were generated (Figure 3-43 b and c). Notice from Figure 3-43 b, after ruling out the noise intensity, relatively low intensity led to a broader ROI selection, which could be determined from the selection of the signal-weaker droplets from the lower part of the image; the framed part, however, exposed the limitation of the lower intensity threshold which was the indistinct of high intensity part. The reason for this would be that the intensity binary effect and diffraction effect of the larger droplets and denser distribution of that part introduced relatively high intensity noise between different droplets, which bonded the area into one large ROI. This problem could be easily solved by increasing the intensity threshold to 172-215 as shown in Figure 3-42 c. Higher minimum intensity diminished the noise mentioned above and high intensity area presented a good distinction among different droplets. However, as expected, there was an issue in that the framed low intensity area might be left out. After all the ROI area and intensity data were generated and exported to the data analysis software, a rule out was conducted using the maximum and minimum droplet size that could be observed, as shown in Figure 3-42 a. Any area data larger than the maximum limit and smaller than the minimum limit was then ruled out as a recording error.

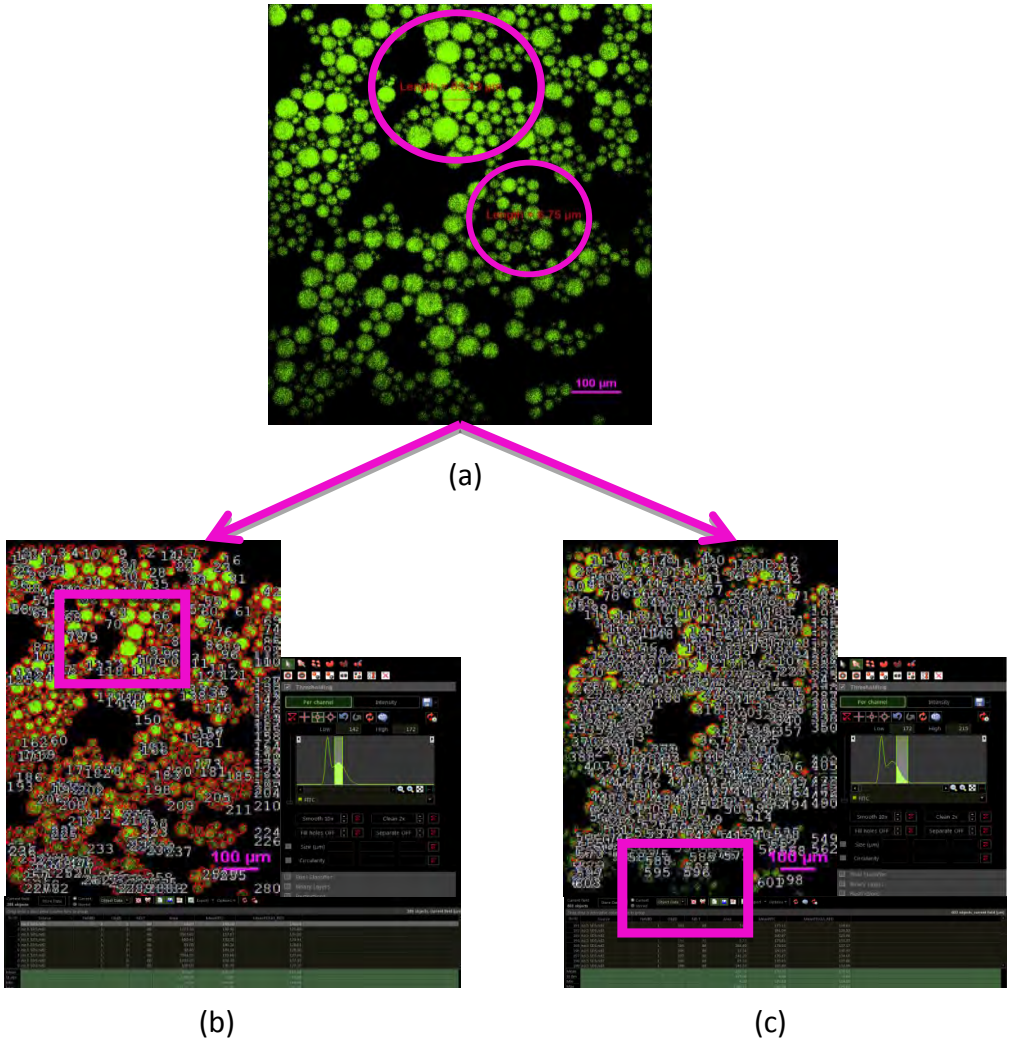

Figure 3-43. (a) Microscopic image of emulsion using SDS with decane and the measurement of droplets threshold, (b) Automated measurement of region of interest using an intensity threshold from 142 to 172, (c) Automated measurement of region of interest using an intensity threshold from 172 to 215.

The combination of the two intensity thresholds management would be appropriate for a relatively accurate evaluation of dispersed phase size distribution for two following reasons: 1) the intensity range could be manually set for the threshold partition method, so the double counting error could be eliminated without an overlap of the intensity range; 2) threshold partition method divided the intensity range into higher and lower parts which targeted high and low intensity zones, so the complementarity of the two sets of data would provide a more comprehensive result when put together after ruling out process.

Maximum and minimum droplet size thresholds were calculated using diameters of 55.43 um and 6.75 um, respectively (Figure 3-42 a). The screening criteria was from 47 um^2 to 2409 um^2. After applying the screening criteria there were 284 sets of ROI data remaining out of 603 sets of original data for an intensity range of 172 to 215, that was, the dispersed droplets with higher intensity while 85 out of 289 sets of data were used for further calculation in the intensity range from 142 to 172 (the lower intensity dispersed droplets). Combining the two parts gave a more convincible and reliable data set. Four different emulsions were measured numerically using the intensity threshold partition method, and the results are given in Figure 3-44 through Figure 3-47 represent results for 85% water, 10% decane, and 5% Span 80; 85%water, 10% decane, and 5% SDS; 85% water, 10% crude oil, and 5% Span 80; 85% water, 10% crude oil, and 5% SDS, respectively.

Figure 3-44. Dispersed phase size distribution for 85% water, 10% decane and 5% Span 80.

Figure 3-45. Dispersed phase size distribution for 85% water, 10% decane, and 5% SDS.

Figure 3-46. Dispersed phase size distribution for 85% water, 10% crude oil, and 5% Span 80.

Figure 3-47. Dispersed phase size distribution for 85% water, 10% crude oil, and 5% SDS.

All four emulsions had a dispersed phase size that fell within the normal distribution, with very good regression fit, and all four emulsions had only more than half of the complete wave profile due to the resolution of microscope, camera and computer graphics. The signal strength was also a limitation for observing tiny droplets of dispersed phase in different dye strength. Stability was the limitation for decane and the weak natural florescence material was the limitation for crude oil. By fitting Gauss bell curve regression whole normal distribution could be predicted and average and standard deviation are found in Table 3-10.

Based on the four different emulsion compositions, Table 3-10 displays the corresponding intensity control indicating the classification of the intensity threshold partition method, maximum and minimum size of the dispersed phase, average size of dispersed phase, and standard deviation of all size data after ruling out process.

Table 3-10. Statistical analysis of the size distribution in different emulsions.

Emulsion composition	Intensity control	Size, μm^2			Standard deviation
		Maximum	Minimum	Average	
Decane+Span	201-238-292	54781	109.3	732.3	1839
Decane+SDS	142-172-215	2409	47	404.9	421
Crude oil+Span	161-244-322	1065	2.26	16.8	34.3
Crude oil+SDS	114-130-177	5097	3.36	157.9	512

The intensity control range indicated the consistency of colored phase signal. From Table 3-10 we conclude that despite decane and crude oil having different fluorescent characteristics, with one due to the addition of fluorescent dye and the other consisting of materials that contained natural fluorescence, the hydrophilic surfactant Span 80 led to a much poorer organized signal strength, reflected by the significantly larger intensity control range. Two factors might be the case here: (1) the HLB value of 4 shows a very strong hydrophobic feature, which might lead to a weaker bonding effect with water phase; and (2) as mentioned above, W/O/W and O/W/O emulsions were formed using Span 80 surfactant, which would certainly have some influence on the color intensity controlled image processing method.

Average droplet size in the four emulsions showed the trend that decane could form some larger droplets, while crude oil droplets were smaller. Introducing the maximum and minimum droplet size difference and the standard deviation difference of four emulsions, a conclusion could be made that with exposure of extreme hydrophilic surfactant, emulsions with decane and crude oil displayed totally dissimilar performance. Decane formed a W/O/W emulsion with the greatest standard deviation, indicating the high diffusivity of light oil and the neutral surfactant Span 80, compared to the negatively charged surfactant SDS, which could constitute a more aggressive coalescence of dispersed phase.

3.3.3.4 Emulsion Forming and Its Recovery Improvement Using Confocal System

To better understand the structure or emulsion forming process under real reservoir conditions, with the fluid dynamic shear process, a set of experiments were conducted using micro-tubes with a diameter of 75 um. The procedures were shown in **Error! Reference source not found.**. First, two windows were opened by melting the surface material at the entrance and somewhere in the middle of the micro-tube. Transparent micro-tube glass was used so as to observe under

the confocal laser system. It helped us to monitor the residual oil in the entrance window and to monitor emulsion forming and flowing in the second window. Then, crude oil was injected into the micro-tube. Deionized water was first used to displace the crude oil, and images were taken over the second window along time, which are shown in Figure 3-48.

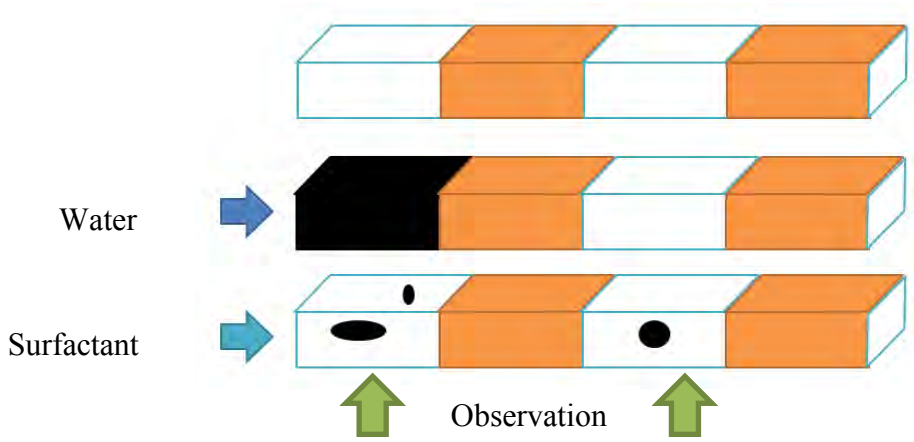

Figure 3-48. Procedures of surfactant flooding using a two-window micro-tube.

From the static residual oil configuration, the contact angle was 84°. For this intermediate-wet micro-tube, the tubular flow at first was observed with some oil film-like continuous phase flowing in the center. Later, residual oil drops appeared on the surface and did not change after a half-hour injection. After water flooding, the confocal images of the entrance window were taken, and a 3-D reconstruction of residual oil distribution was generated as Figure 3-49.

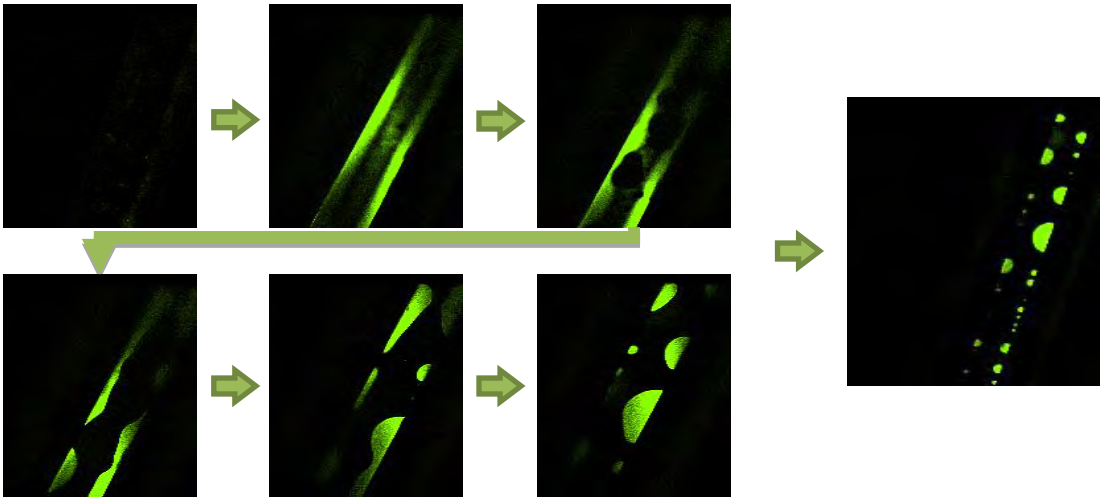

Figure 3-49. Crude oil water flooding process and the residual oil caused by high oil viscosity.

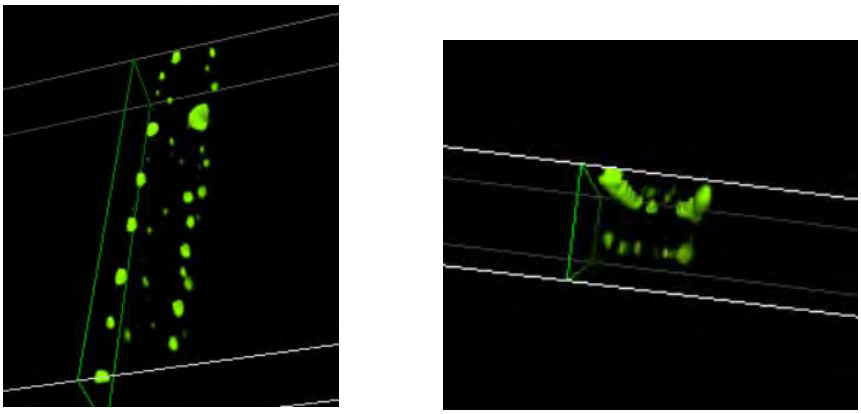

Figure 3-50. A 3-D reconstruction of residual oil distribution after water flooding.

Notice that most of the residual oil was attached to the corner of the square-shaped micro-tube due to the high viscosity of crude oil as well as interfacial tension difference caused by the shape of the micro-tube.

Surfactant flooding was conducted after water flooding. A 1% SDS surfactant solution was used in the displacing phase. Images were taken at the second window during the surfactant injection process, as shown in Figure 3-50. Clear dispersed oil drops were spotted flowing through the

tube. Residual oil at the inner wall surface formed an oil in water emulsion, and was reduced significantly.

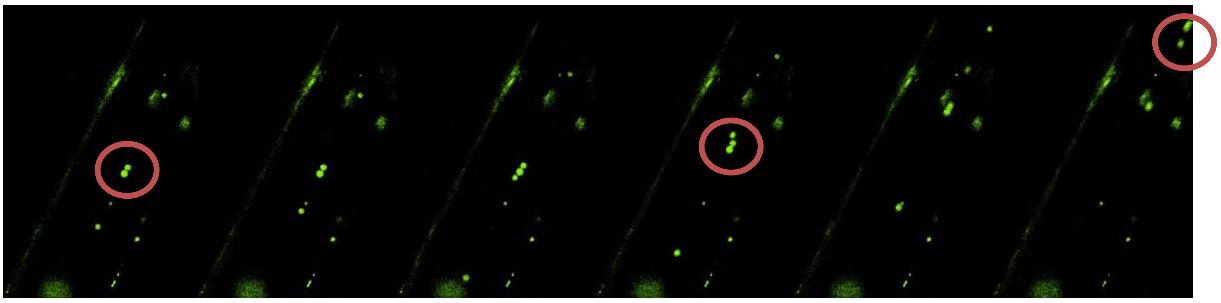

Figure 3-51. Oil emulsion forming and flowing within micro-tube using 1% SDS surfactant.

After the surfactant injection, entrance residual oil was captured, as shown in Figure 3-51. Notice that drops of residual oil disappeared; instead, a continuous phase with weak signal strength was formed. The colored signal strength indicated dispersed oil phase. The diameter of dispersed oil drop must be less than several micrometers to beat the limitation of resolution of confocal system. Nitrogen was injected after surfactant flooding. Figure 3-51 b shows the result after gas flooding. No signal and no oil phase was left at the entrance window, which indicated an almost 100% recovery of crude oil using surfactant followed by gas flooding. The reason for this result might be the simple and straight-forward structure of the micro-tube with tortuosity of 1.

(a) (b)

Figure 3-52. Entrance image after (a) surfactant flooding, and (b) gas flooding.

3.3.4 Summary

Emulsion morphology was determined using decane and crude oil with different surfactants sorted by HLB value. Different Winsor Types were identified using various water to oil ratios and surfactants with different HLB values. Results were also observed using a laser microscope. Water in oil, oil in water, water in oil in water, oil in water in oil emulsion morphologies were inspected. Quantitative measurements of dispersed phase were conducted using software with certain combination of surfactant, oil, and water. A threshold partition method was developed for more precise emulsion size and density distribution analysis. Optical flooding tests using water, surfactant, and gas were observed under confocal and laser system. Emulsion forming and transporting process was observed, and a significant improvement in heavy oil recovery was obtained using micro-tube.

3.4 Select the Best PPG Compatible with the Selected Surfactant(s) and Formation Water

One small producer serving as a partner on this project has leases in a reservoir in Kansas. Wells in this reservoir are being screened to provide the best candidate for the injection of PPG and surfactant. Pilot tests focused first on two injection wells in one lease; then, if the tests were satisfactory, more injections will be undertaken in additional nearby locations.

In addition to the heavy nature of the oil found in the focus areas of this study, it has been well established that most of the oil reservoirs in the Pennsylvanian Cherokee sandstone basin have limited ultimate recovery due to extreme heterogeneities within the sandstone body [34]. These heterogeneities vary from facies-type bedding boundaries and small-scale permeability barriers to channels and even fractures. A properly selected PPG could present a solution to these heterogeneities.

PPG recently has become the treatment of choice for many oilfield operators dealing with conformance problems because of its ability to block or partially block the water production zones and direct the injection solution into the low-permeability, oil-rich areas in the reservoir.

The properties of PPGs have been studied extensively by Bai et al. [35] and others in terms of its swelling ratio, rheological behavior, and ability to propagate through porous media.

To choose the PPG most compatible with the selected surfactant, a series of experiments was conducted to understand the behavior of PPG when it interacts with an aqueous surfactant solution.

The interaction between surfactant and gel has been studied extensively over the years, mainly for medical and pharmaceutical purposes. For example, Kokufuta et al. [36] reported that ionic surfactants affect the swelling equilibrium of nonionic hydrogels and that as the surfactant concentration increases, so does the volume of the gel. Gao et al [37] studied the interaction between surfactant and microgel, finding that the swelling and shrinking of microgel can be attributed partially to the micelle formation inside the microgel network.

The purpose of the experiment was to screen PPGs for their compatibility with surfactants by evaluating the former's swelling ratio and strength and the latter's phase behavior.

3.4.1 Materials and Methods

Preformed Particle Gel: Seven PPG samples from different companies were evaluated in terms of their swelling ratio, the strength of their swelling particles, and their interaction with the surfactants selected for their compatibility with the PPG. Table 3-11 describes these samples.

Table 3-11. Evaluated PPG Samples

PPG #	PPG Name	Physical Properties
PPG 1	DQ 3	Hard, millimeter size, brown color
PPG 2	DQ	Hard, millimeter size, gray color
PPG 3	Swelling controllable	Rubber-like, white color
PPG 4	-	Hard, millimeter size, white color
PPG 5	Nano-composite clay gel	Hard, millimeter size, light brown color
PPG 6	Cerogel™ PPG-746	Weak, sticky, brown color
PPG 7	40K super absorbent polymer	Hard, sugar like, white color

Surfactant: The following three types of surfactants were used: cationic surfactants {n-dodecylpyridinium chloride (98%), (1-hexadecyl) pyridinium bromide monohydrate (98%)}, anionic surfactants {sodium 4-n-octylbenzenesulfonate, sodium dodecyl benzene sulfonic acid}, and nonionic surfactants {IGEPAL® CO-530 and TERGITOL® NP-10}.

Measurement devices: A UVmini-1240V, UV–Vis spectrophotometer (from Shimadzu) was used to measure the change in surfactant concentration. A rheometer, the HAAKE RheoScope (from Thermo Scientific), was used to measure the storage (G') and loss (G'') moduli and the swollen PPG.

Test tubes (50 ml) were used to measure the swelling ratio of PPG in brine and surfactant solution, separately. First, 0.2 g of PPG was added to 20 grams of a brine or surfactant solution in a test tube. Then, the test tube was shaken vigorously by hand for 5 minutes before being left on a shaking device overnight. The final PPG swelling ratio, SW, was calculated using a weight method:

$$SW = \frac{m_t - m_0}{m_t}$$

where m_t represents the PPG weight after equilibrium time, and m_o represents the original weight of the dry PPG.

A HAAKE RheoScope was used to evaluate the strength of the swollen PPG samples. The oscillation time sweep curve model was selected for the measurement; it represents the storage and loss moduli logarithmically in Pascal (Pa) as a function of time in seconds. The frequency was set at 1.0 Hz. A controlled stress (CS) mode was chosen because the selected stress value had to be in the linear viscoelastic range. The stress applied to the PPG was 1.0 Pa to ensure that the gel strain and stress had a linear relationship during measurement. A PP35 Ti Po LO2 016 sensor, with a gap of 0.2 mm between the sensor and the plate holding the PPG sample was used. For each sample, storage and loss moduli readings were taken every 30 seconds for 5.0 minutes.

3.4.2 Results and Discussion

3.4.2.1 Screening of Different PPG

The swelling ratios of seven PPGs were measured at different brine concentrations, as shown in Figure 3-53 through Figure 3-59. PPG1 and PPG3 exhibited temperature sensitivity, so their swelling behavior at elevated temperatures (25, 45, 60, and 80°C) was tested. Dry gel particles were placed in varying surfactant solutions and then put in ovens at different temperatures. The PPGs were monitored for a few days until they reached equilibrium swelling. The other PPGs were tested at ambient temperature. Although they achieved swelling equilibrium in several hours, samples were left undisturbed for several days to ensure that all samples were fully swollen.

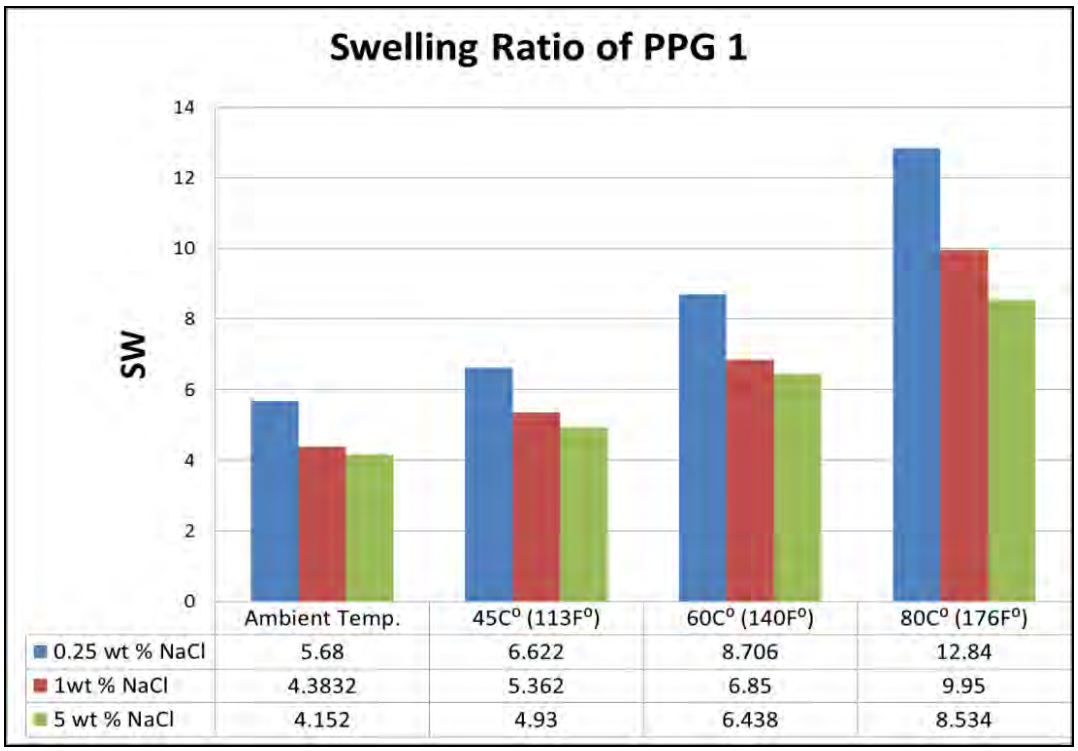

Figure 3-53. Effect of brine concentration and temperature on the swelling ratio of PPG1.

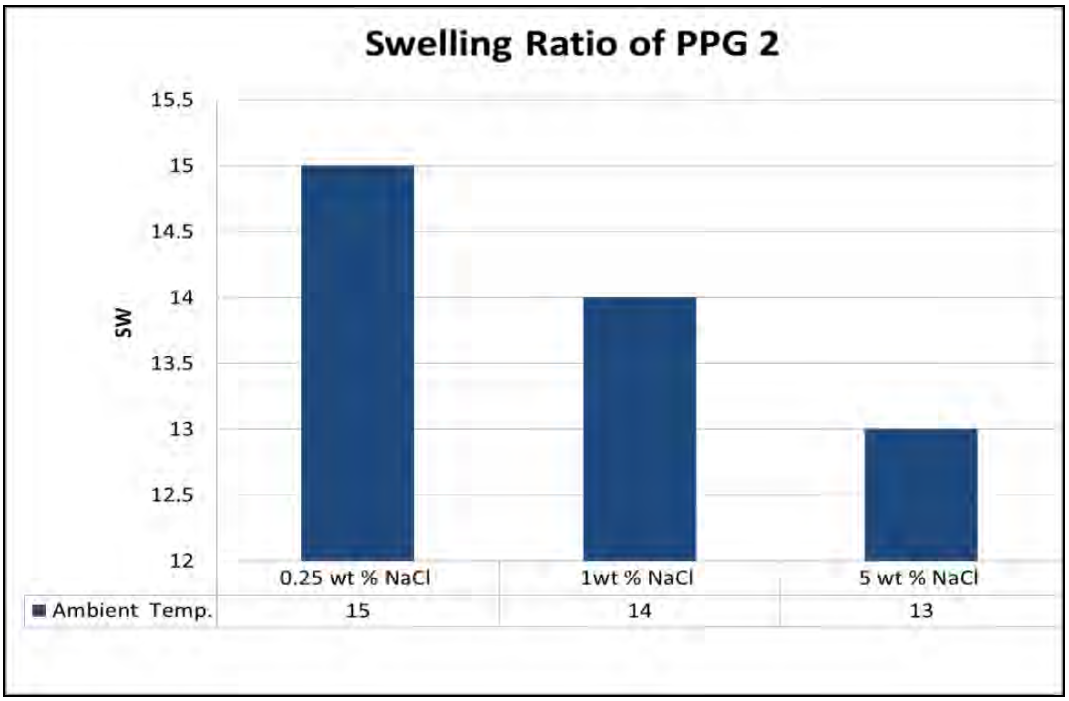

Figure 3-54. Effect of brine concentration on the swelling ratio of PPG2.

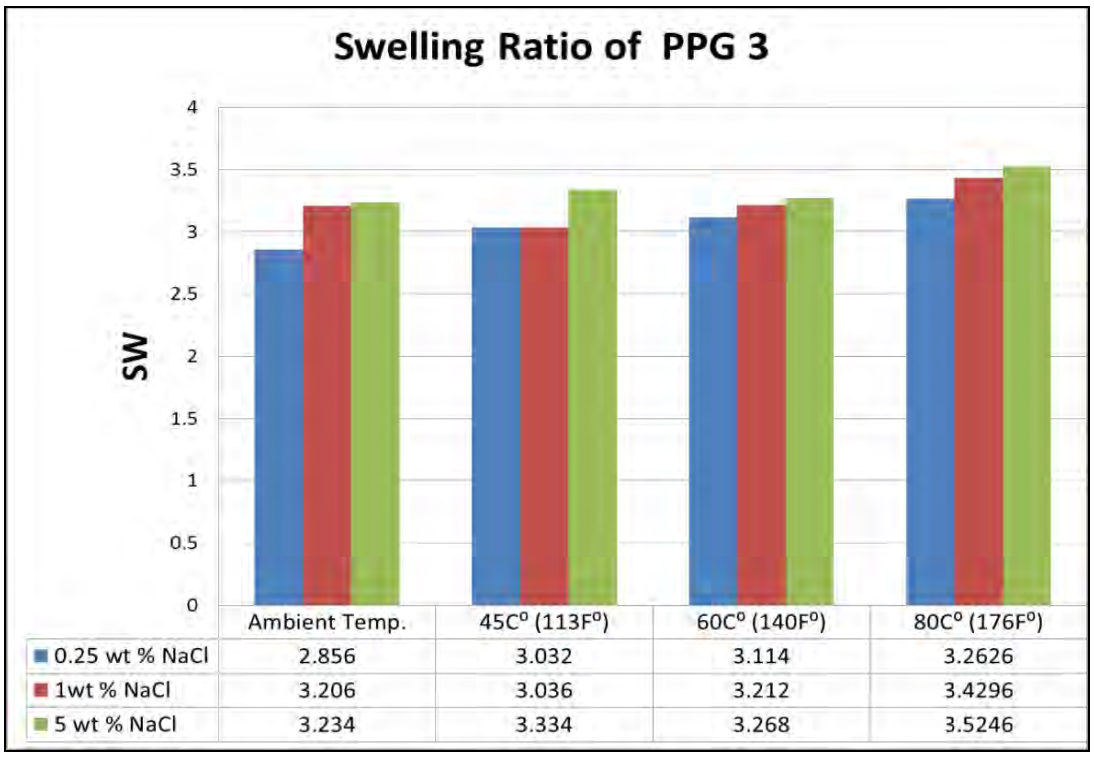

Figure 3-55. Effect of brine concentration and temperature on the swelling ratio of PPG3.

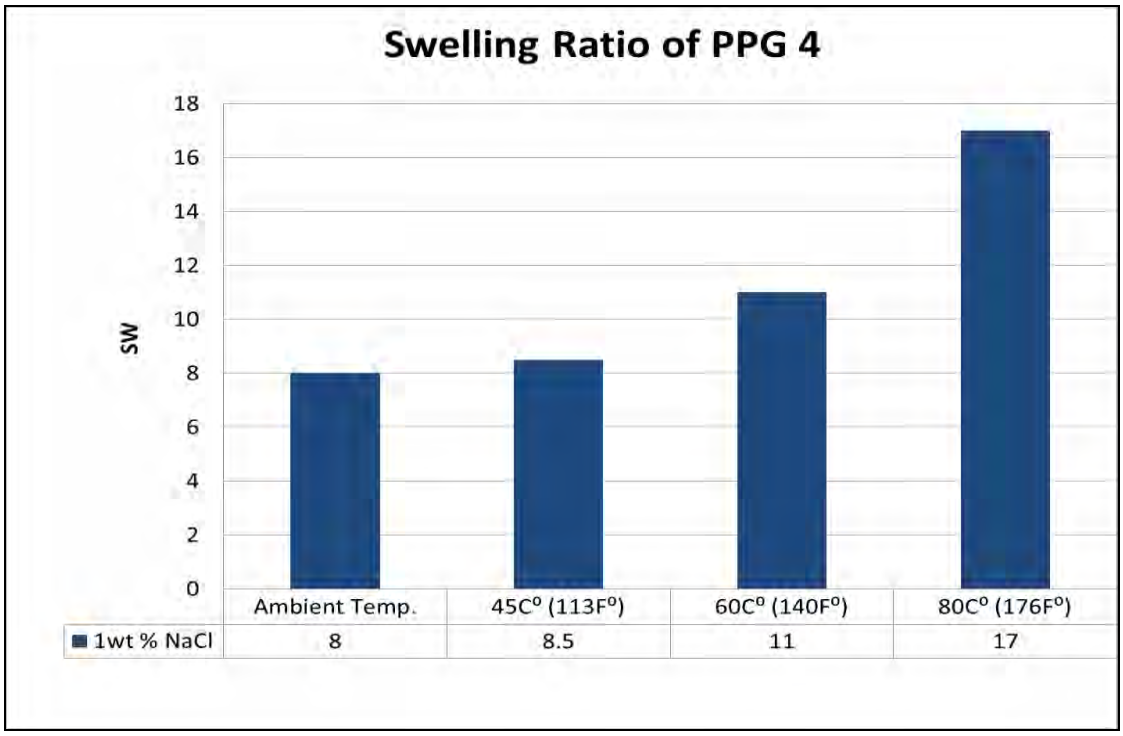

Figure 3-56. Effect of brine concentration on the swelling ratio of PPG4.

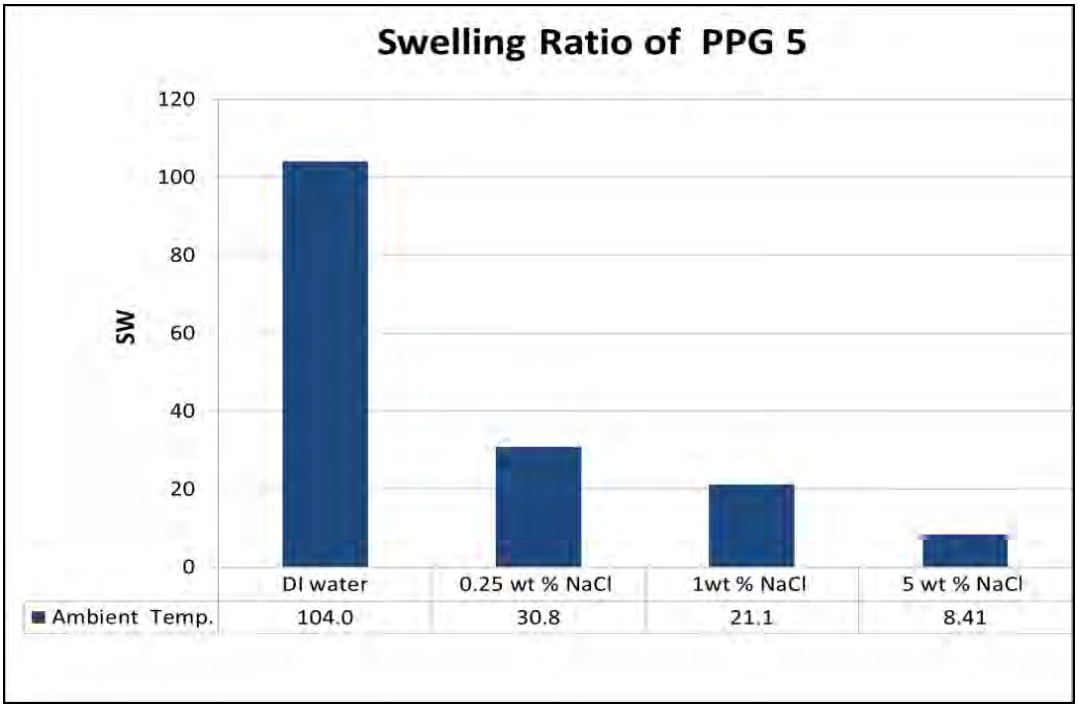

Figure 3-57. Effect of brine concentration on the swelling ratio of PPG5.

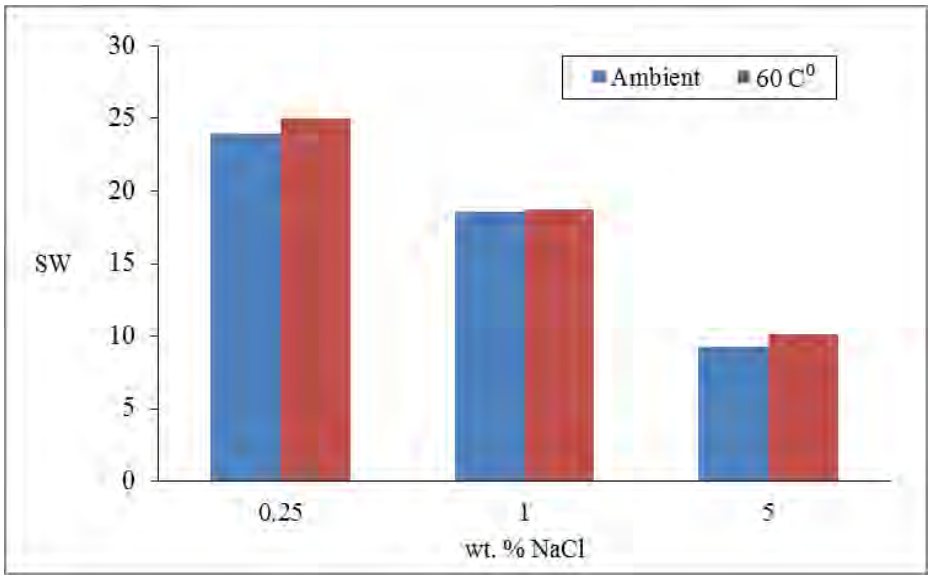

Figure 3-58. Effect of brine concentration on the swelling ratio of PPG6.

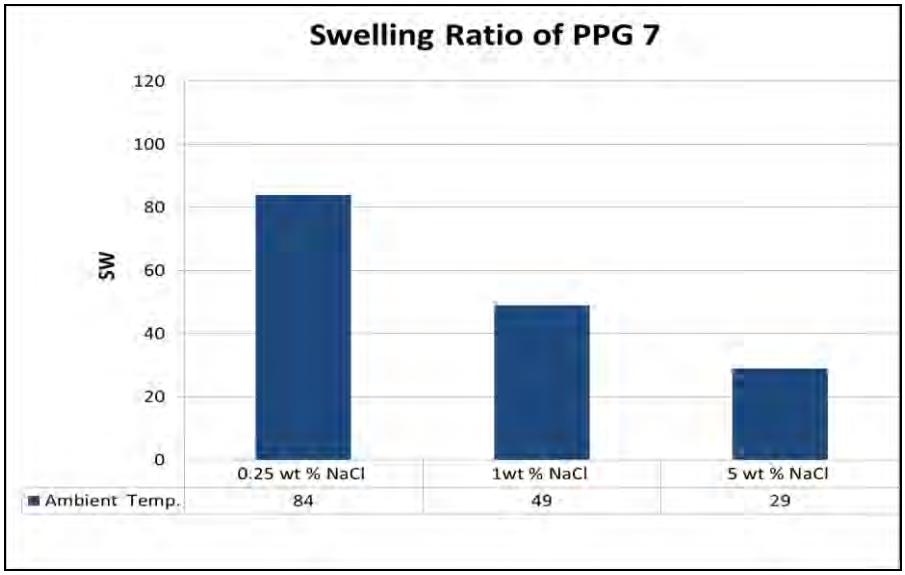

Figure 3-59. Effect of brine concentration on the swelling ratio of PPG7.

3.4.2.2 Swollen PPG Strength Measurement Results

Figure 3-60 shows the storage moduli (G') of the seven PPGs, which were categorized into three different classes. PPG2 and PPG3 were the strongest, with G' ranges from 3,900 to 4,250 Pa.

PPG1 and PPG4 were of medium strength, with G' ranges from 2,250 to 2,700 Pa. The third class consisted of the weak PPGs: PPG5, PPG6, and PPG7.

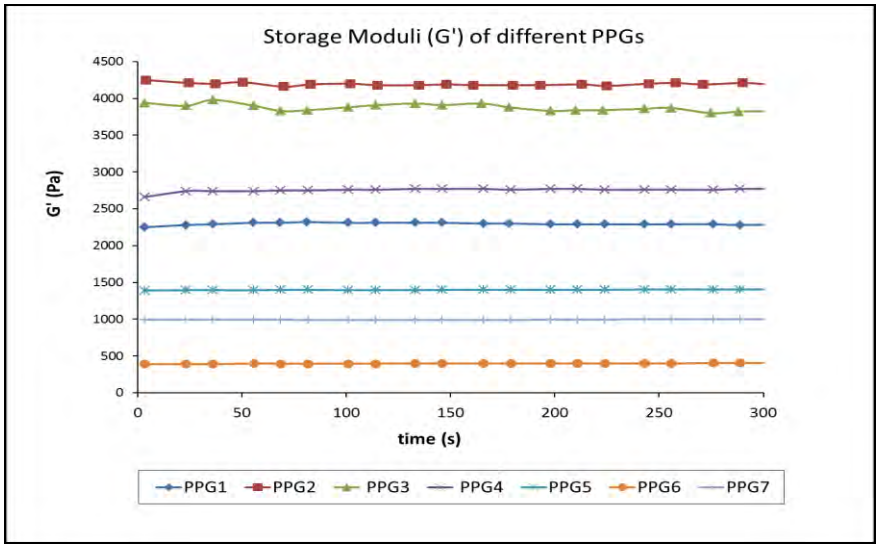

Figure 3-60. Strength (storage moduli, G') of seven PPGs swollen in 1.0 wt% NaCl.

3.4.2.3 Cerogel™ Characterization

Considering the swelling ratio, strength, uncertain parameters of the target reservoir, and injection well injectivity, it was decided to use Cerogel™ to treat target wells. Therefore, the interaction between this PPG and the surfactant was investigated.

Effect of salinity and temperature on Cerogel™ strength: Figure 3-61 depicts the strength of Cerogel™ at different brine concentrations. As the salinity increased, so did the strength of the Cerogel™.

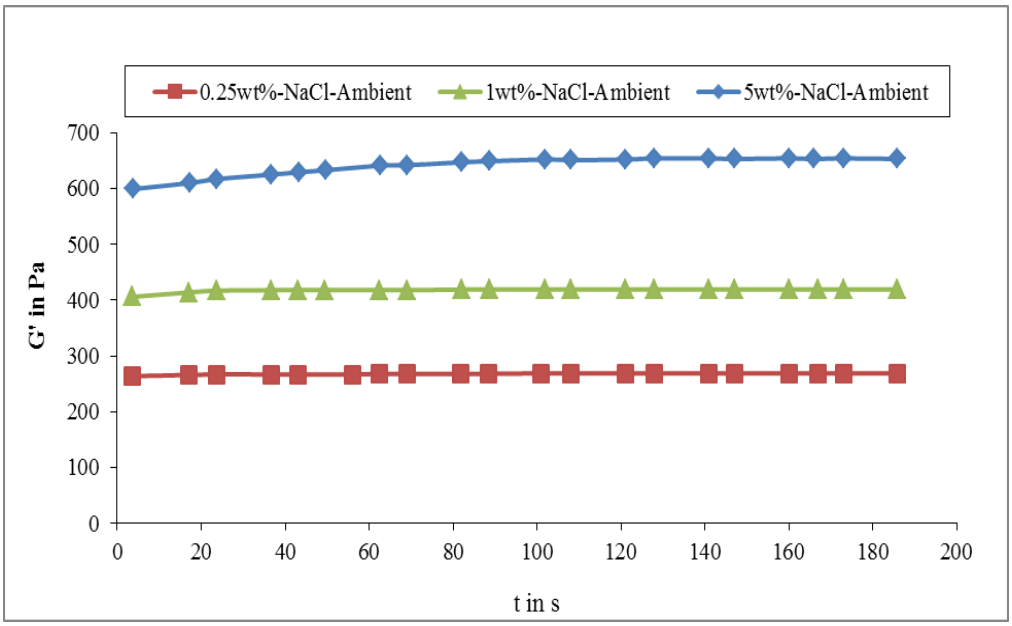

Figure 3-61. Effect of salinity on Cerogel™ strength at ambient temperature.

Effect of surfactant concentration on PPG swelling ratio at different temperatures: Figure 3-62 through Figure 3-64 compare the swelling ratio of Cerogel™ swollen in different concentrations of surfactant at ambient temperature, 60°C, and 80°C, separately. The results show that the surfactant concentration affected the PPG swelling ratio; however, it is unclear how each type of surfactant affected the strength of the swollen PPG. More work must be done to analyze how the surfactant type and concentration affect the PPG swelling ratio.

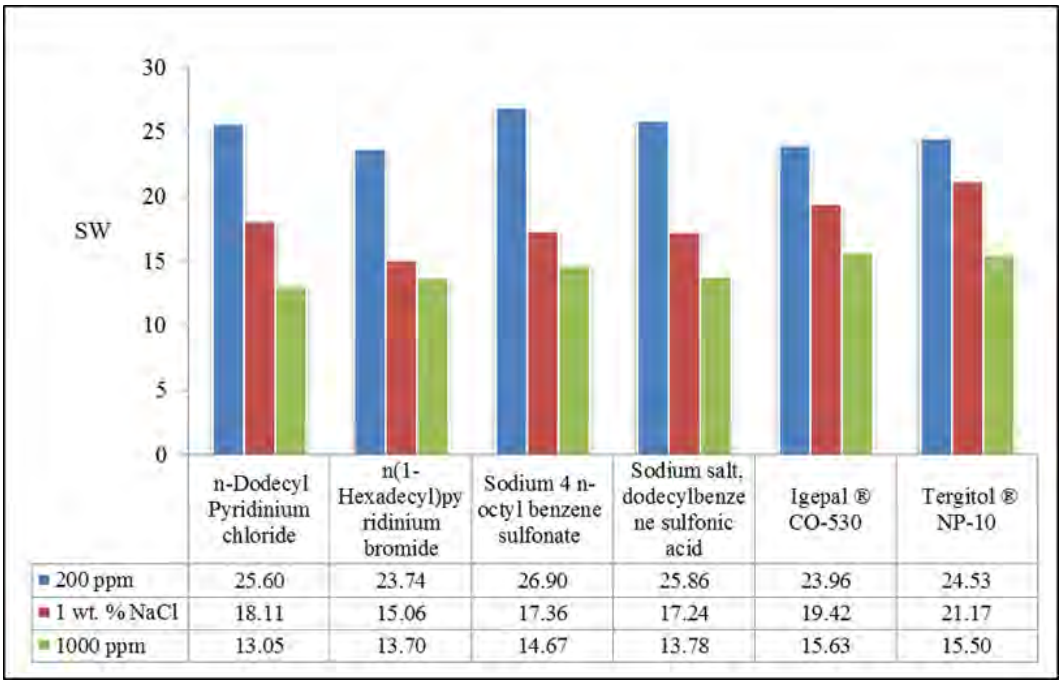

Figure 3-62. Swelling ratio of Cerogel™ at ambient temperature (25°C).

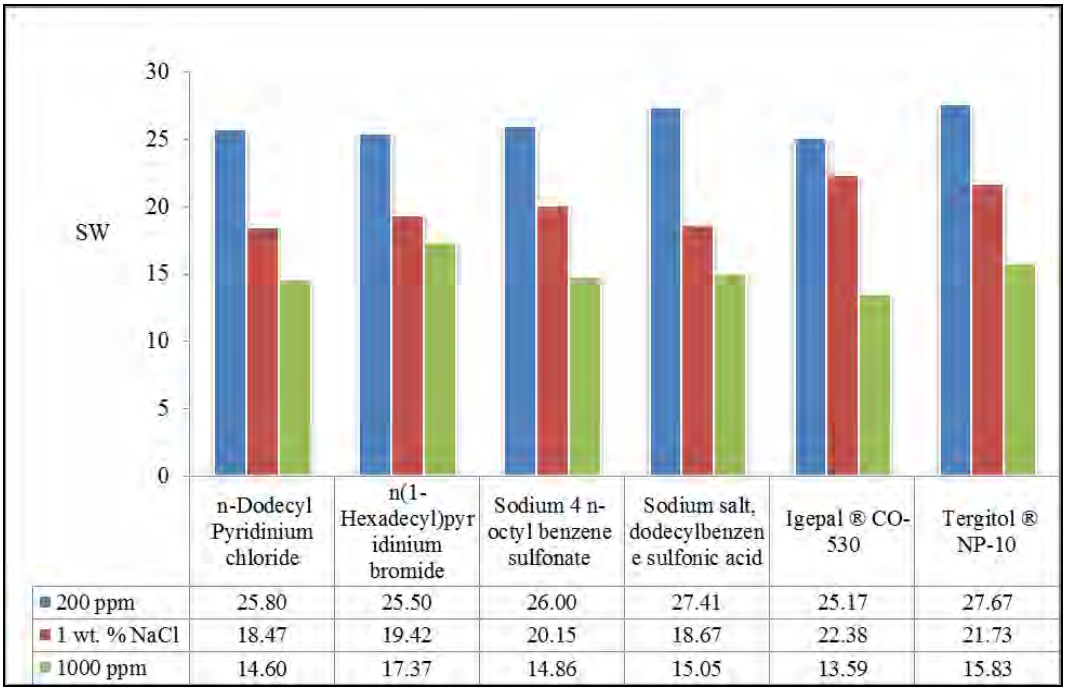

Figure 3-63. Swelling ratio of Cerogel™ at 60°C.

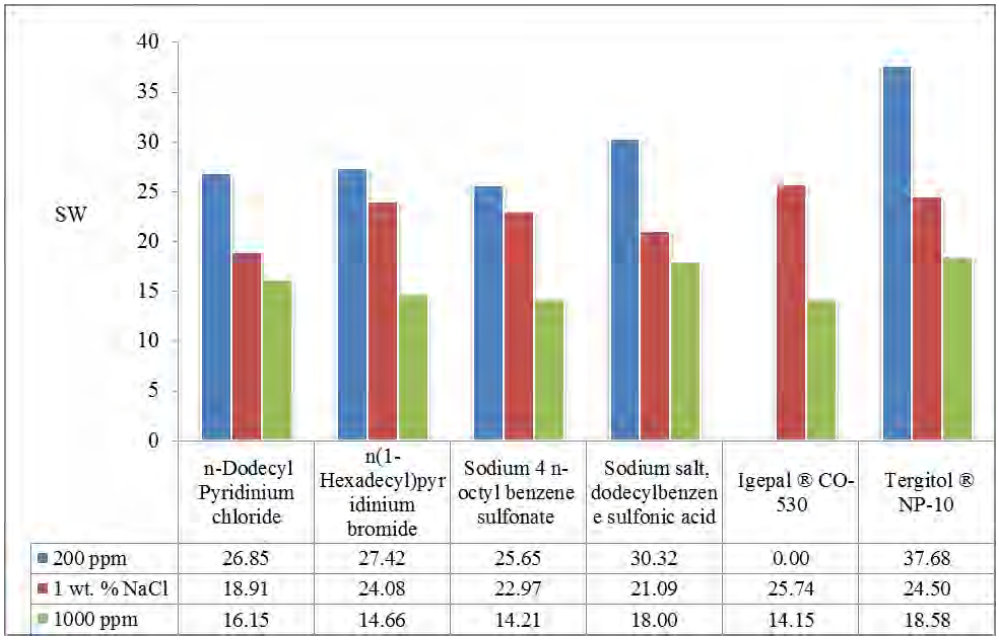

	n-Dodecyl Pyridinium chloride	n(1-Hexadecyl)pyridinium bromide	Sodium 4 n-octyl benzene sulfonate	Sodium salt, dodecylbenzene sulfonic acid	Igepal ® CO-530	Tergitol ® NP-10
200 ppm	26.85	27.42	25.65	30.32	0.00	37.68
1 wt. % NaCl	18.91	24.08	22.97	21.09	25.74	24.50
1000 ppm	16.15	14.66	14.21	18.00	14.15	18.58

Figure 3-64. Swelling ratio of Cerogel™ at 80°C.

Effect of surfactant concentration and temperature on PPG strength: Figure 3-65 through Figure 3-70 show how different surfactants affected the strength of the Cerogel™. As illustrated, all of the surfactants reduced the strength of the Cerogel™ as compared to the control test (1.0 wt.% NaCl).

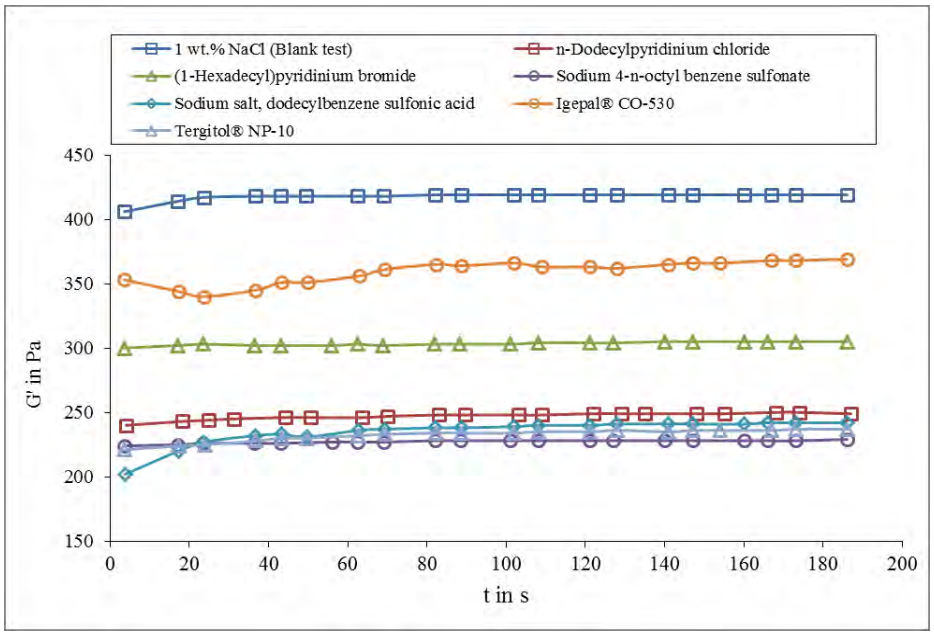

Figure 3-65. Effect of surfactant (200 ppm) on Cerogel™ strength at ambient temperature.

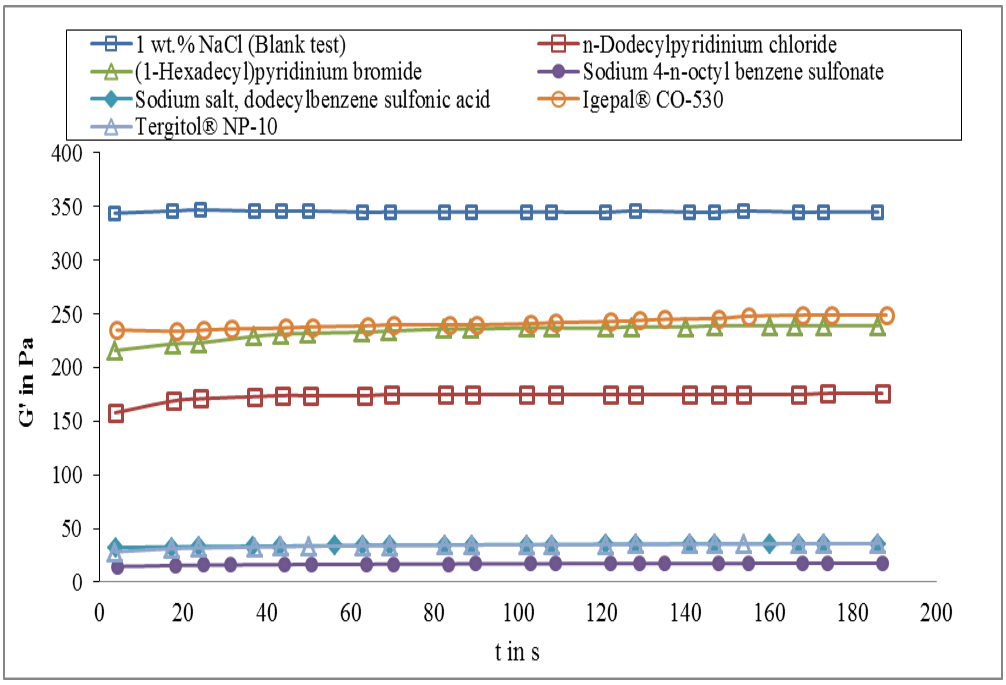

Figure 3-66. Effect of surfactant (200 ppm) on Cerogel™ strength at 80°C.

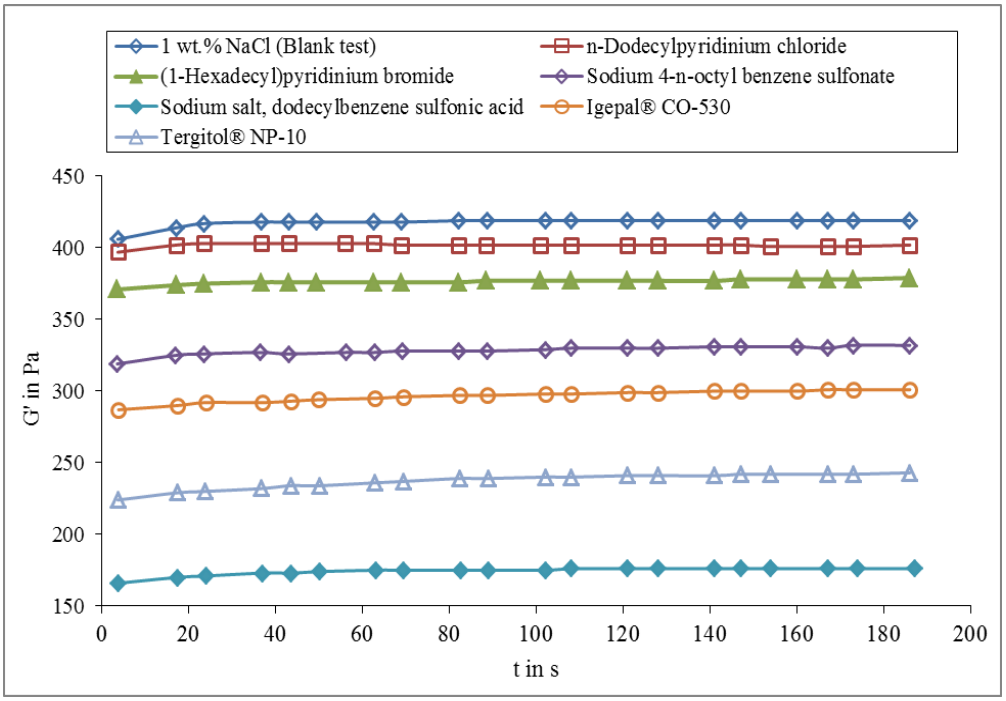

Figure 3-67. Effect of surfactant (500 ppm) on Cerogel™ strength at ambient temperature.

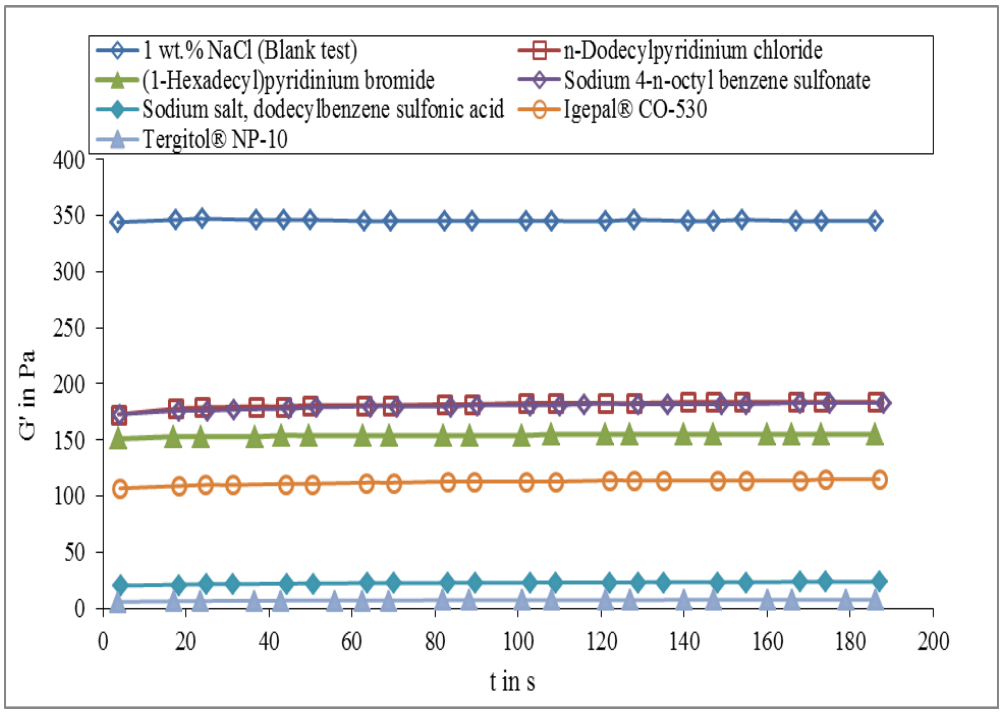

Figure 3-68. Effect of surfactant (500 ppm) on Cerogel™ strength at 80°C.

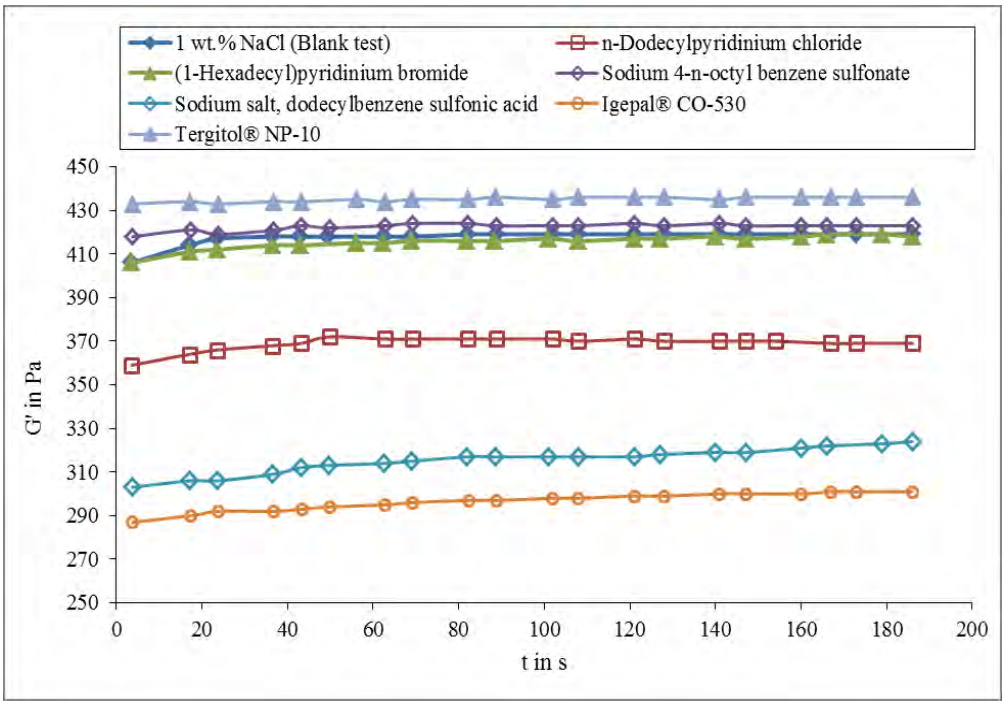

Figure 3-69. Effect of surfactant (1000 ppm) on Cerogel™ strength at ambient temperature.

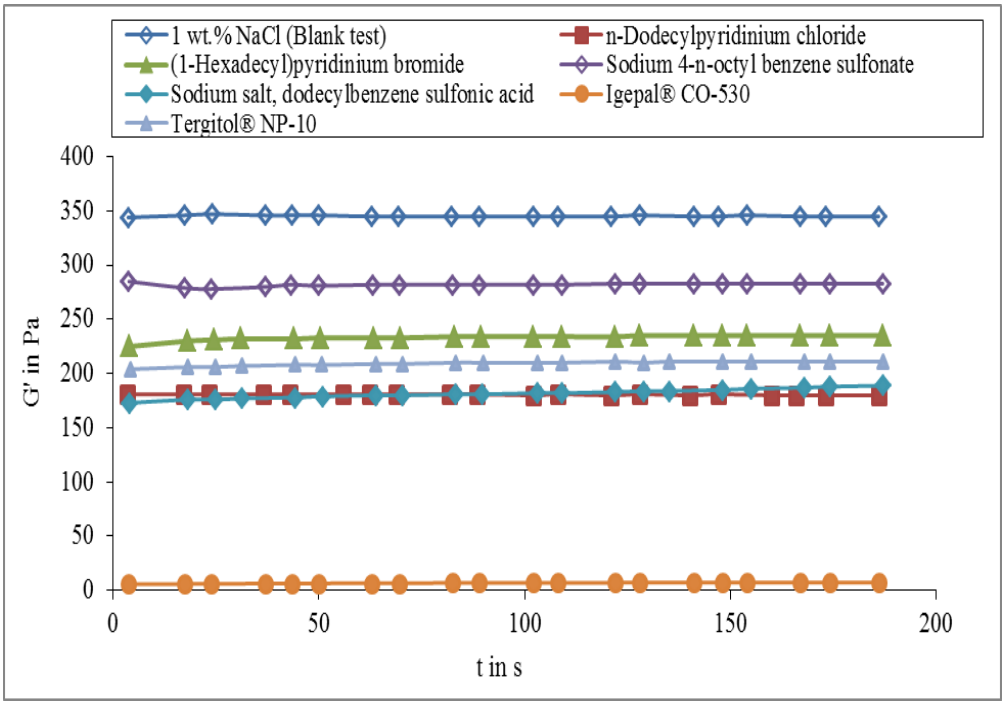

Figure 3-70. Effect of surfactant (1000 ppm) on Cerogel™ strength at 80°C.

3.4.3 Summary

The swelling ratios of seven PPGs were measured at different brine concentrations, where PPG1 and PPG3 exhibited temperature sensitivity so that swelling behavior was evaluated at elevated temperatures (25, 45, 60, and 80°C). The other PPGs were tested at ambient temperature. The strength of seven PPGs were measured and categorized into three different classes. PPG2 and PPG3 were the strongest, with G' ranges from 3,900 to 4,250 Pa. PPG1 and PPG4 were of medium strength, with G' ranges from 2,250 to 2,700 Pa. The third class consisted of the weak PPGs: PPG5, PPG6, and PPG7.

After the comparison among different PPGs, Cerogel™ was selected to be used to treat the target well, considering the swelling ratio, strength, uncertain parameters of the target reservoir, and injection well injectivity. The effect of salinity and temperature on Cerogel™ strength and the effect of surfactant concentration on PPG swelling ratio and strength at different temperatures were determined.

4. WELL CANDIDATE SELECTION

4.1 Introduction

Numerous methods are applied to select candidate wells for PPG treatment. Originally, the selection of wells for PPG treatment relied on experts' judgements and experience, which could not objectively reflect the situations in field applications. Zhao et al. [38] focused on the evaluation of single factor and introduced a pressure index (PI) decision-making method. The PI decision-making technique is based on the theory of transient well testing, and the value of the PI comes from the pressure drawdown test conducted from an injection well. An injection well is considered a candidate for treatment if the PI value of the well is low. However, the essential information about injection well and reservoir cannot be fully provided by the PI method by using only the wellhead pressure. Feng et al. [39] assessed several factors for both reservoir and injection well conditions, such as permeability, injection profile, injectivity, and pressure index (PI), in their fuzzy comprehensive evaluation method and assigned weights for each factors due to experts' perspectives. By comparing the potential values of each well with the average value of all the wells in the same area, the wells with higher potential values are selected as candidates. Liu et al. [40] improved this fuzzy comprehensive evaluation method by adding the analysis result of the offset production well conditions. Additionally, Bai et al. [41] reviewed and summarized characteristics of the reservoir and criteria of wells that were treated by using PPGs. However, no research has been found to apply a formal data analysis and assign objective weight for each evaluation factor for PPGs treatment and candidate well selection.

The goals of our research were to show the distribution of each factor that affects PPGs treatment and obtain objective weights for candidate well selection for this treatment. To generate a criteria and acquire weight factors for PPGs treatment and well selection and to conduct data analysis, we collected data of 874 successful PPGs treatments from papers and oil companies. Due to missing partial data in most treatments, only twelve treatments are selected to assess objective weights. Then, entropy method was integrated with analytic hierarchy process (AHP) to obtain

the objective weights. Eventually, a multiple criteria decision making method is proposed to rank the order of alternatives for candidate well selection.

4.2 Data Analysis

Factors affecting PPGs treatment and well selection are divided into three categories: reservoir conditions, injection well conditions, and corresponding production wells. First, reservoir conditions have a great influence on the PPGs thermal stability. PPGs could become unstable under high temperature and/or high salinity, which might reduce the efficiency of treatment. Second, PPGs are mostly applied to correct heterogeneity problems in a reservoir with high-permeability zones. High injectivity and low injection pressure index are good indicators of the existence of high-permeability zone. Third, excessive water production will cause serious environmental problems. Therefore, an injector with a high liquid production rate and water cut producers also needs to be treated. We also conducted an extensive survey and collected 874 treatments data from oil fields including Daqing, Zhongyuan, Shengli, Dagang, Xinjiang, Jiangsu, Changqing, Jilin, Qinghai, Liaohe and Qidong. On the basis of these data, distribution of each factor is illustrated using histograms and boxplots.

4.2.1 Reservoir Conditions

4.2.1.1 Temperature

Figure 4-1 depicts the distribution of reservoir temperatures. The histogram shows two peaks in the data set. The first peak contains temperature values from 120 to 140°F, involving Daqing and Changqing oil fields where most PPGs treatments were applied. The second peak includes values between 180 and 200°F. This result suggests that PPGs can also be used in relatively high temperature reservoirs. Since the PPGs become unstable at extremely high temperatures, boxplot indicates that the maximum temperature is 266°F.

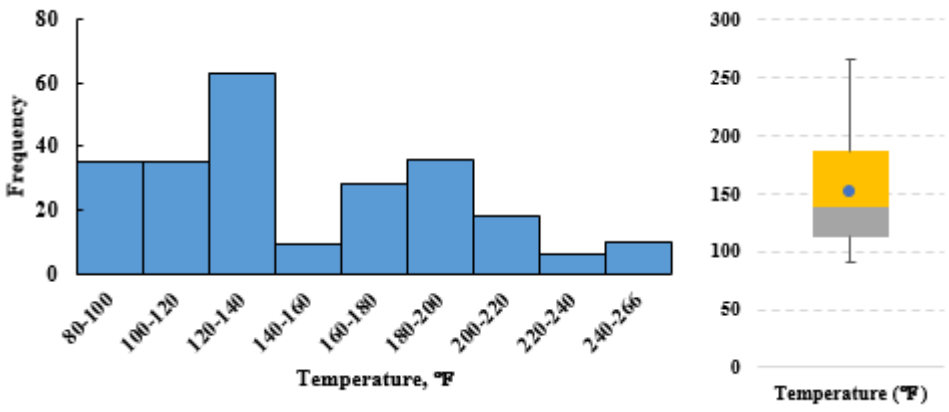

Figure 4-1. Distribution of reservoir temperatures.

4.2.1.2 Salinity

Error! Reference source not found. shows the distribution of the salinity of formation water. Most of the values fall between 5,000 and 55,000 ppm. The maximal salinity in our data set is 320,000 ppm.

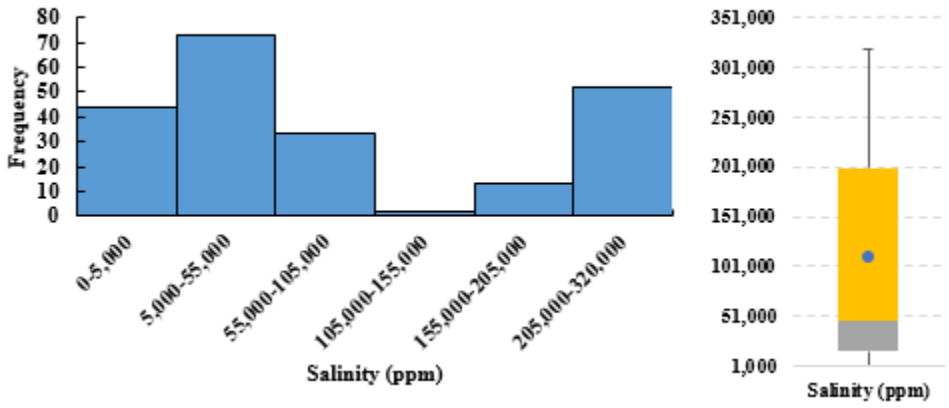

Figure 4-2. Distribution of reservoir salinity.

4.2.1.3 Permeability

Figure 4-3 summarizes the permeability distribution indicating that the majority range is from 200.5 to 400.5 md. The minimum permeability is only 0.5 md in that the low permeability reservoir has natural fractures leading to serious reservoir heterogeneous problems. However, the largest permeability was 6,000 md because the permeability was measured for the big channels.

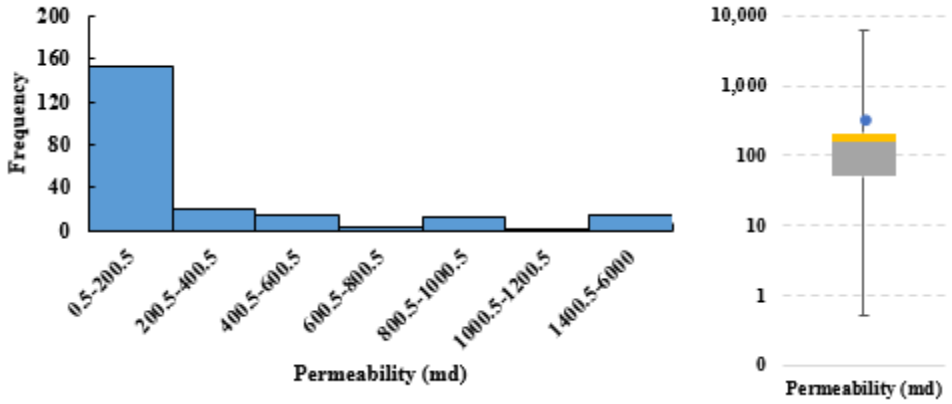

Figure 4-3. Distribution of reservoir permeability.

4.2.1.4 Reservoir Heterogeneity

Vertical permeability heterogeneity and vertical water injection profile heterogeneity were used to evaluate the reservoir heterogeneity. To make these two parameters comparable, Lorenz coefficient was used to calculate both the vertical heterogeneity of reservoir and vertical water injection profile heterogeneity. The Lorenz coefficient is defined as the area of ABCA divided by the area of ABDA (Figure 4-4).

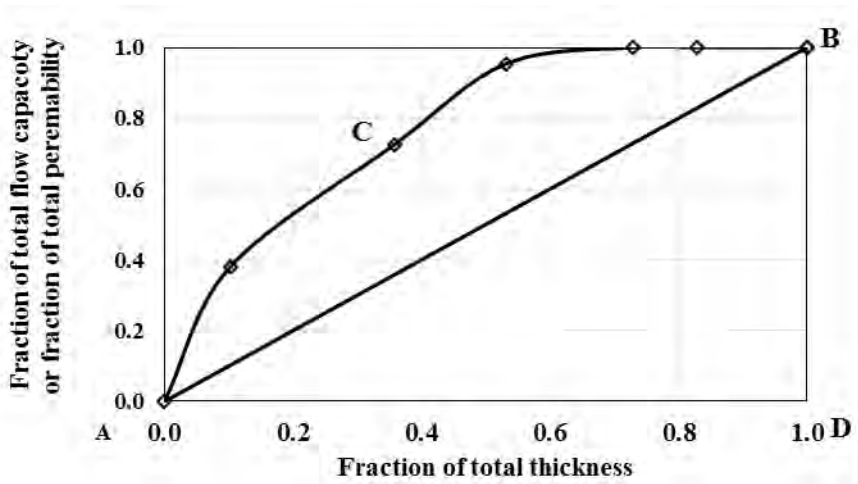

Figure 4-4. Lorenz coefficient for injection flow distribution.

Figure 4-5 indicates the distribution of permeability heterogeneity. Most PPGs treatments have been applied in the reservoir with severe heterogeneity because the majority of the values fall

between 0.75 and 0.8. Figure 4-6 illustrates the distribution of injection profile heterogeneity. Although this parameter is critical for well selection, only 12 treatments reported this value.

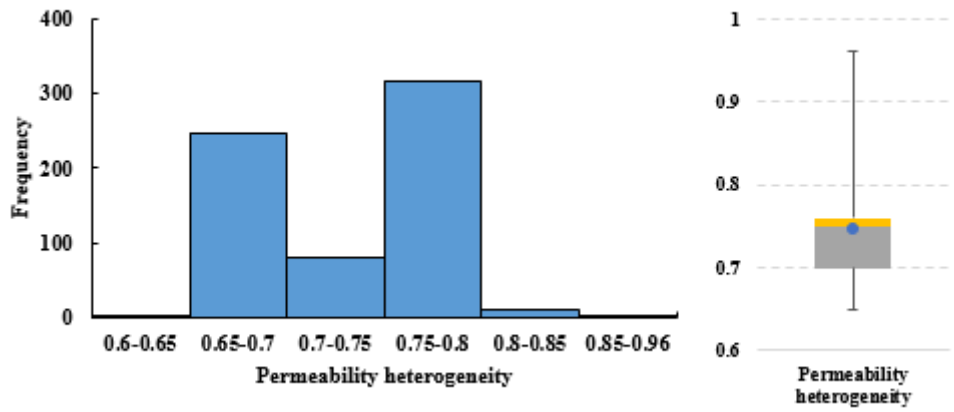

Figure 4-5. Distribution of reservoir permeability heterogeneity.

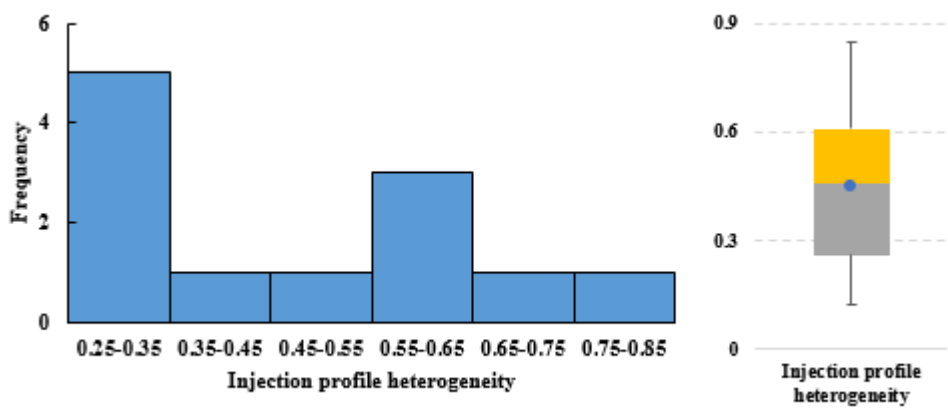

Figure 4-6. Distribution of injection profile heterogeneity.

4.2.2 Injection Well Conditions

4.2.2.1 Injectivity

Water injectivity index (Inj) is defined as

$$Inj = \frac{q}{p_{wh} h} \tag{4-1}$$

where q is the injection rate, P_{wh} is the well head pressure, and h is the thickness of water absorption layers.

Low injection pressure with a high injection rate is a good sign for PPGs treatment. Figure 4-7 and Figure 4-8 illustrate the distribution of the injectivity of the injection wells. The majority of the pressure varies from 800 to 1,200 psi, and the largest injection pressure was 3,552.5 psi. Most of the injection rates fall into a range from 200 to 300 bbl/day with a maximum value of 1,660.4 bbl/day.

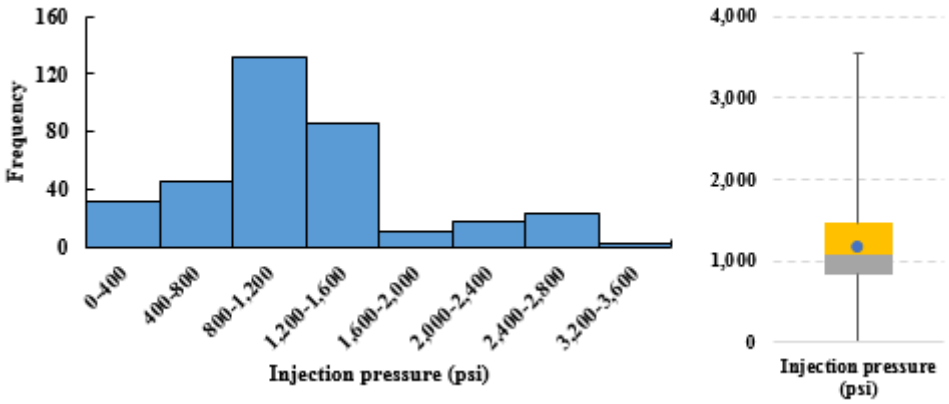

Figure 4-7. Distribution of injection pressure.

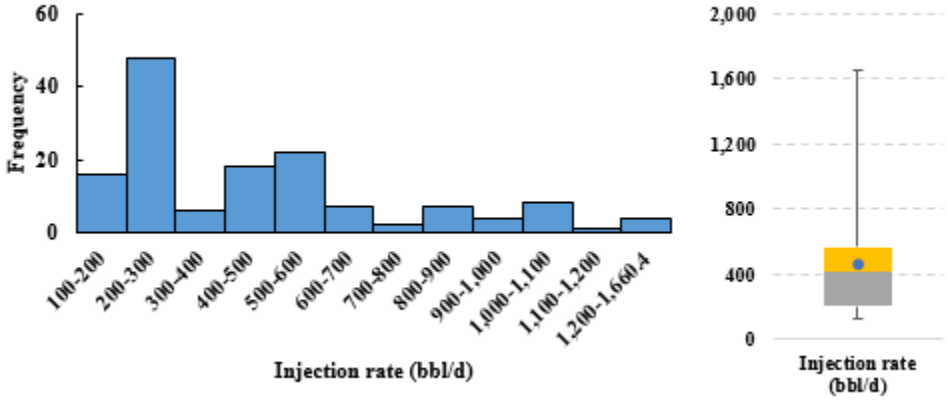

Figure 4-8. Distribution of injection rate.

4.2.2.2 Pressure Index (PI)

The PI value comes from the pressure drawdown test (Figure 4-9), which is based on the transient well test. It can be calculated from the wellhead pressure decline, which is conducted 90 minutes after an injection well is shut down. The PI (90) is calculated using the following equation:

$$PI(t) = \frac{\int_0^T p(t)dt}{T} \tag{4-2}$$

where PI(t) = Pressure Index, psi; P(t) = Pressure at time t after a well is shut in, psi; T = shut-in time, in minutes, usually 90 minutes.

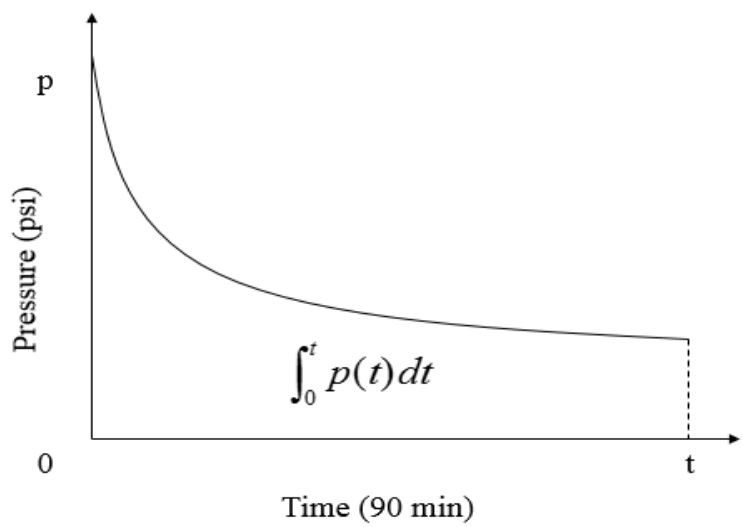

Figure 4-9. Pressure draw-down curve.

For the pressure index, the histogram in Figure 4-10 appears with two peaks. One is from 400 to 800 psi, and the other is from 1,200 to 1,600 psi. The highest PI was 1,770.5 psi.

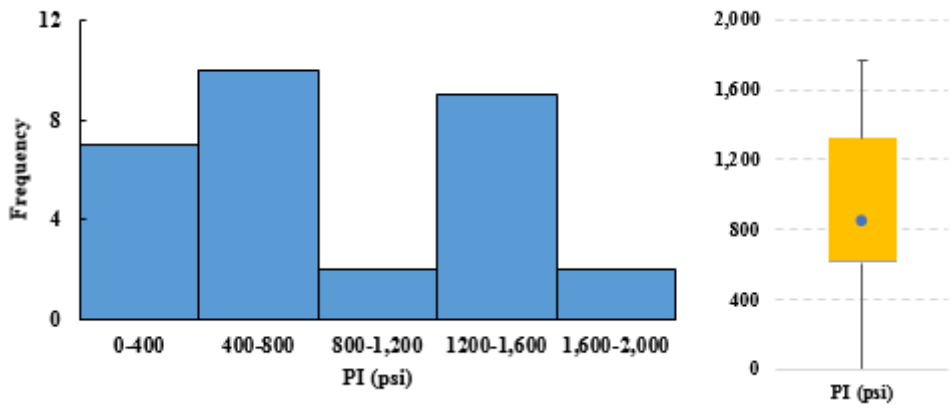

Figure 4-10. Distribution of pressure index (PI).

4.2.3 Corresponding Production Wells Conditions

4.2.3.1 Liquid Production

Figure 4-11 illustrates that most of the liquid production rates for the corresponding producer were less than 500 bbl/day. The maximum liquid production rate was 9,059 bbl/day.

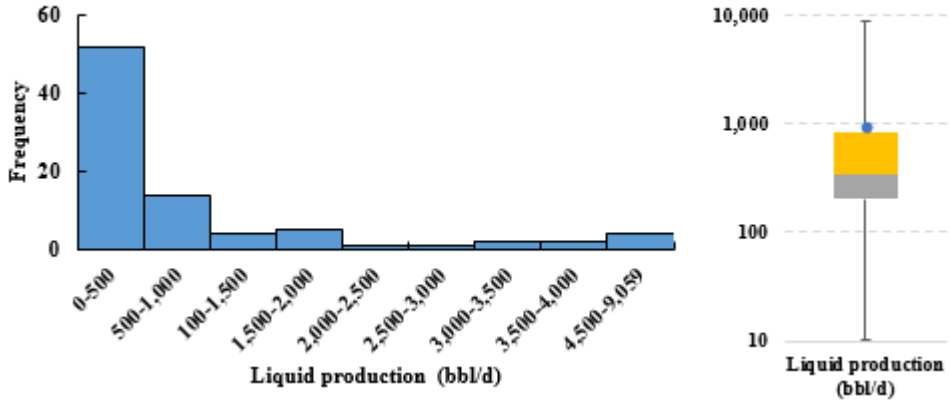

Figure 4-11. Distribution of liquid production.

For the distribution of water cut shown in Figure 4-12, most PPGs treatments were used to control the excess water production from the production wells when their water cut were higher than 85%.

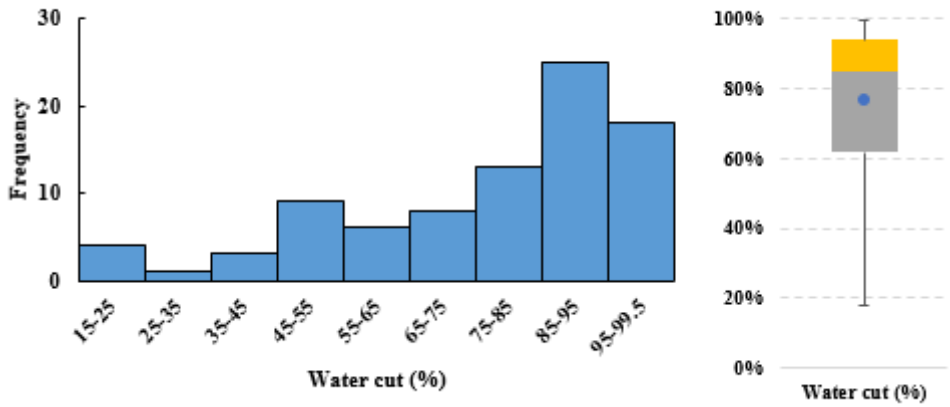

Figure 4-12. Distribution of water cut.

Finally, the injection well selection criteria can be summarized as follows in Table 4-1: permeability > 0.5 md; permeability variation > 0.65; injection profile variation > 0.12; temperature < 266°F; salinity < 320,000 ppm; injection pressure < 3,552.5 psi; injection rate > 125.8 bbl/day; pressure index < 1,770.45 psi; production rate > 10.29 bbl/day; and water cut > 18%.

Table 4-1. Criteria for well selection.

	Mean	Median	Standard Deviation	Minimum	Maximum	Count
Permeability (md)	337.27	153.2	698.2	0.5	6,000	220
Permeability variation	0.74	0.75	0.04	0.65	0.96	663
Injection profile variation	0.45	0.46	0.24	0.12	0.85	12
Temperature (°F)	151.37	138.56	46.1	91.4	266	240
Salinity (ppm)	108,972	46,000	118,255	1,700	320,000	217
Injection pressure (psi)	1,165.58	1,087.5	624.9	0	3,552.5	349
Injection rate (bbl/day)	468.88	419.3	314.3	125.79	1,660.43	143
PI (psi)	856.76	623.5	547.7	0	1,770.45	30
Production rate (bbl/day)	974.89	340.47	1,639.3	10.29	9,058.98	85
Water cut (%)	77	85	22	18	100	87

4.3 Methodology

4.3.1 Determining the Weight Factors of Each Index

Determining rational weights of each index is a critical and challenging task for the candidate well selection for PPG treatment. Entropy weight method is an objective approach to determine the importance of indices, which is introduced from thermodynamics to information systems. Entropy refers to disorder or uncertainty of the source of information and entropy weight is derived from the intrinsic information that contains among the statistical physics. The lower the entropy, the higher the weight. Entropy method highly relies on the quality and quantity of test samples. In field applications, missing data is a common issue during the evaluation of candidate wells, which probably limit the accuracy of entropy weight. In this case, expert's judgments should also be taken into consideration as a complement to do necessary adjustments of entropy weight. The analytic hierarchy process (AHP) process is widely used to quantify experts' opinions and judgments by systematically prioritizing alternative options on the basis of the hierarchical structure analysis. To get a better candidate well evaluation result for PPG treatment, we integrated entropy weight with AHP method to get the combination weights.

4.3.1.1 Determining the Weight Factors by Using Entropy Method

The initial decision matrix of the evaluation issue is $R = (X_{ij})_{m\times n}$, where m is the number of objects to evaluate and n is the number of evaluation indices. To reduce the impact of the differences among data with various dimensions for the evaluation indices, the initial matrix needs to be normalized to obtain $R' = (\mu_{ij})_{m\times n}$. Parameters for candidate well selection are categorized into two subclasses: "benefit type" and "cost type". A "benefit-type" parameter characterized as high value reflecting a good candidate such as water injectivity index, permeability heterogeneity coefficient, water injection profile heterogeneity coefficient, and water-cut. The remaining indicator, pressure decline index, represents a good candidate with a low value. To make the two subclasses parameters comparable, all of them are converted to a range between 0 and 1.

For "benefit-type" parameters:

$$\mu_{ij} = \frac{x_{ij} - \min x_j}{\max x_j - \min x_j} \tag{4-3}$$

For "cost-type" parameters:

$$\mu_{ij} = \frac{\max x_j - x_{ij}}{\max x_j - \min x_j} \tag{4-4}$$

where i (I = 1,2,…,m) is the number of injectors and j (j = 1,2,…,n) is the number of parameters for one injector.

Then the information entropy for each index is defined as:

$$E_j = -(\ln m)^{-1} \sum_{i=1}^{m} p_{ij} \ln p_{ij} \tag{4-5}$$

where $p_{ij} = (1+\mu_{ij}) / (\sum_{i=1}^{m} (1+\mu_{ij}))$ (4-6)

The weight is expressed as follows:

$$\omega = (1 - p_j) / (n - \sum_{j=1}^{n} p_j) \tag{4-7}$$

4.3.1.2 Determining the Weight of Each Index Using AHP Process

i. Constructing the pair-wise comparison matrix

In AHP method, a 9-point scale (Table 4-2) is frequently applied to represent the pair-wise comparison. The importance of each index was acquired according to experts' opinions. A matrix X was established as follows:

$$A = \begin{bmatrix} a_{11} & a_{12} & \cdots & a_{1n} \\ a_{21} & a_{22} & \cdots & a_{2n} \\ \vdots & \vdots & \cdots & \vdots \\ a_{n1} & a_{n2} & \cdots & a_{nn} \end{bmatrix}, a_{ii} = 1, a_{ji} = \frac{1}{a_{ij}}, a_{ij} \neq 0 \tag{4-8}$$

Table 4-2. The relative importance values of pair-wise comparisons.

Scale	Definition
1	Equally important between i and j
3	i is slightly more important than j
5	i is obviously more important than j
7	i is very strongly more important than j
9	i is extremely more important than j
2,4,6,8	Intermediate values between 1~3, 3~5, 5~7, 7~9
Reciprocals	For inverse comparison

ii. Calculate the weight

The weight of an index was calculated by the square-root method as

$$M_i = \prod_{j=1}^{n} a_{ij} \tag{4-9}$$

$$\overline{W_i} = \sqrt[n]{M_i} \tag{4-10}$$

$$W_i = \frac{\overline{W_i}}{\sum_{j=1}^{n} \overline{W_i}} \tag{4-11}$$

iii. Consistency check

The consistency ratio or CR is used to judge the consistency of the judgmental matrix. The upper limit value of CR is 0.1. If CR < 0.1, the consistency of the matrix is considered relatively satisfactory; otherwise, the single-factor value in the matrix A should be adjusted.

$$CR = \frac{CI}{RI} \tag{4-12}$$

RI is the random index, which is in shown in Table 4-3

$$CI = \frac{\lambda_{\max} - n}{n-1} \tag{4-13}$$

where $\lambda_{\max}$ is the largest eigenvalue of matrix A.

Table 4-3. The value of the random index (RI).

Scale	1	2	3	4	5	6	7	8
RI	0	0	0.52	0.89	1.11	1.25	1.35	1.4

4.3.1.3 Determining the Weight by the Combination of Entropy and AHP Method

$W = (w_1, w_2, \ldots w_n)$ represents the weight matrix obtained from entropy method and $W' = (w_1', w_2', \ldots, w_n')$ denotes the weight matrix calculated from AHP method. And combination weight is $W_c = ww' / \sum_{i=1}^{n} ww'$.

4.3.2 The Comprehensive Evaluation Method

After evaluation matrix and weight factors are obtained, the final results can be calculated by using comprehensive evaluation method, as follows:

$$P_w = (w_{c1} w_{c2} w_{c3} w_{c4} w_{c5} w_{c6}) \begin{pmatrix} \mu_{11} & \mu_{21} & \cdots & \mu_{m1} \\ \mu_{12} & \mu_{22} & \cdots & \mu_{m2} \\ \mu_{13} & \mu_{23} & \cdots & \mu_{m3} \\ \mu_{14} & \mu_{24} & \cdots & \mu_{m4} \\ \mu_{15} & \mu_{25} & \cdots & \mu_{m5} \\ \mu_{16} & \mu_{26} & \cdots & \mu_{m6} \end{pmatrix} = (\sum_{k=1}^{6} w_{ck} \mu_{k1}, \sum_{k=1}^{6} w_{ck} \mu_{k2}, \ldots, \sum_{k=1}^{6} w_{ck} \mu_{km})$$

where w_c is the combined weight factor; m is the number of injectors; k is the number of evaluation factors and μ is the normalized value from Eqs. 4-3 and 4-4.

The potentials of each well for PPG treatment is ranked by the potential value P_w.

4.4 Illustrated Case

This section presents an application of the proposed methodology, including 12 cases with six evaluated factors in Table 4-4, which were collected from an oil service company located in Daqing Oilfield in China. The objective here is to determine the weights of indicators and then rank the alternatives for decision-making.

In these 12 cases, reservoir heterogeneity for each individual well was replaced by the original reservoir heterogeneity because the oil service company did not test the permeability before they did the PPGs treatment. For the first four injection wells, we only have the average liquid production and water cut values. Owing to the quality of the sample data, a hybrid weight factor determining method needed to be employed to mitigate the potential derivation resulting from the data. The process of evaluation method are summarized as follows.

Table 4-4. Water injection well raw data.

	Reservoir heterogeneity	Profile heterogeneity	Injectivity (bbl/d·psi·ft)	PI (psi)	Liquid production (bbl/day)	Water cut (%)
Well 1	0.730	0.750	0.024	1,322.400	7,916.400	0.957
Well 2	0.725	0.620	0.028	1,007.750	7,916.400	0.957
Well 3	0.710	0.260	0.020	1,592.100	7,916.400	0.957
Well 4	0.734	0.850	0.023	1,612.400	7,916.400	0.957
Well 5	0.710	0.560	0.066	652.500	3,027.290	0.976
Well 6	0.707	0.440	0.085	551.000	3,701.650	0.975
Well 7	0.690	0.140	0.047	754.000	3,511.070	0.979
Well 8	0.710	0.260	0.067	739.500	2,734.090	0.993
Well 9	0.700	0.350	0.080	768.500	4,588.580	0.987
Well 10	0.670	0.280	0.015	1,290.500	869.778	0.833
Well 11	0.660	0.120	0.019	826.500	3,313.453	0.915
Well 12	0.680	0.600	0.010	145.000	5,033.145	0.896

4.4.1 Determining the Weight Factors of Each Index

4.4.1.1 Determining the Weight Factors by Using Entropy Method

Based on Eqs. 4-3 and 4-4, we obtained the normalized the data in Table 4-5. Then through Eqs. 4-5 to 4-7, we calculated the entropy and weight of each factors as tabulated in Table 4-5. According to this objective method, the most significant factors for candidate well selection are injectivity, followed by profile heterogeneity, liquid production, PI, reservoir heterogeneity and water cut. This trend is generally consistent with the idea that the primary task for PPG treatments is to minimize the heterogeneity problems and enhance injection pressure. However, the missing data of reservoir heterogeneity and liquid production resulted in a little bias in their weights. Hence, the subsequent AHP method was employed to appropriately fix the derivation.

Table 4-5. Normalized index matrix and entropy-based weights of factors.

	Reservoir heterogeneity	Profile heterogeneity	Injectivity	PI	Liquid production	Water cut
Well 1	0.946	0.863	0.181	0.198	1.000	0.773
Well 2	0.875	0.685	0.235	0.412	1.000	0.773
Well 3	0.680	0.192	0.132	0.014	1.000	0.773
Well 4	1.000	1.000	0.163	0.000	1.000	0.773
Well 5	0.673	0.603	0.741	0.654	0.306	0.893
Well 6	0.632	0.438	1.000	0.723	0.402	0.885
Well 7	0.404	0.027	0.494	0.585	0.375	0.913
Well 8	0.673	0.192	0.761	0.595	0.265	1.000
Well 9	0.539	0.315	0.931	0.575	0.528	0.962
Well 10	0.135	0.219	0.067	0.219	0.000	0.000
Well 11	0.000	0.000	0.111	0.536	0.347	0.513
Well 12	0.269	0.658	0.000	1.000	0.591	0.391
Entropy	0.992	0.990	0.988	0.992	0.991	0.994
Weight	0.148	0.183	0.231	0.153	0.176	0.109

4.4.1.2 Determining the Weight of Each Index Using AHP Process

Pairwise comparison matrix and weigh factors are tabulated in Table 4-6. Square-root method was adopted to derive these weights and the consistency was checked by using Eqs. 4-12 and 4-13. The results according to the consistency test concluded as the following: the maximum eigenvector was 6.44, consistency index was 0.089 and the consistency ratio was 0.07, which satisfied the criteria of consistency by being less than 0.1.

Table 4-6. Pairwise comparison matrix and AHP-based weight factors.

	Reservoir heterogeneity	Profile heterogeneity	Injectivity	PI	Liquid production	Water cut	Weight
Reservoir heterogeneity	1	1/5	1/5	1/3	2	3	0.064
Profile heterogeneity	5	1	2	3	7	9	0.337
Injectivity	5	1	2	3	7	9	0.337
PI	3	1/2	1/2	1	6	8	0.196
Liquid production	12	1/7	1/7	1/6	1	2	0.040
Water cut	1/3	1/9	1/9	1/8	1/2	1	0.026

4.4.1.3 Determining the Weight by the Combination of Entropy and AHP Method

The final combination weight matrix was $w_c = (0.05, 0.327, 0.412, 0.158, 0.037, 0.015)$.

4.4.2 Evaluation Results by Comprehensive Evaluation Method

The final rank results are shown in Table 4-7. The average potential value of all 12 wells was 0.44, and the wells that had greater potential values than the average were wells: 1, 2, 4, 5, 6, 8 and 9. Among them, Well 6 was selected as the best candidate because it had the highest potential value.

Table 4-7. Final well ranking.

Well Number	Potential	Rank
Well 1	0.484	6
Well 2	0.479	7
Well 3	0.202	10
Well 4	0.493	5
Well 5	0.665	2
Well 6	0.730	1
Well 7	0.353	9
Well 8	0.529	4
Well 9	0.639	3
Well 10	0.141	12
Well 11	0.151	11
Well 12	0.415	8

4.5 Summary

- The single injection well selection criteria can be summarized as follows: permeability > 0.5 md; permeability variation > 0.65; injection profile variation > 0.12; temperature < 266°F; salinity < 320,000 ppm; injection pressure < 3,552.5 psi; injection rate > 125.8 bbl/day; pressure index < 1,770.45 psi; production rate > 10.29 bbl/day; and water cut > 18%.

- A comprehensive evaluation method was proposed by combining entropy method with AHP method.

- An illustrated example was presented to demonstrate how to conduct the comprehensive evaluation.

5. PILOT TESTS IN SMALL PRODUCER LEASES

The pilot tests took place in four leases in southeast Kansas. The leases are operated by Blue Top Energy LLC and Colt Energy, Inc., which are small production companies that collaborated with Missouri University of Science and Technology on this research project. Wells in these leases were screened to provide the best candidate for the injection of PPG or PPG combined with a surfactant.

The objective of the pilot tests was to determine whether the PPGs could be injected into the target reservoirs and the extent to which the treatments could increase water injection pressure, decrease water production, and increase oil production. The lessons learned from the pilot tests can help producers and service companies to better apply PPG treatments and the coupled technology.

5.1 Background on the Pilot Areas

The pilot tests were conducted in four leases in Kansas. In 2011, Kansas was ranked 9th among the 50 states in crude oil production. The state produced 43.7 million barrels of oil in 2012. Oil is produced in Kansas from rocks ranging in age from Proterozoic to Permian. Table 5-1 presents subdivisions of the stratigraphic systems, stages, and groups that are productive and also highlights the intervals for these pilot tests. The information in this section was acquired from public data in the Kansas Geological Survey (KGS) website: http://www.kgs.ku.edu/.

We conducted the pilot tests initially in Humboldt-Chanute field in Allen and Coffey counties, southeastern Kansas, where Blue Top Energy LLC (small producer collaborator) operates several leases. Oil has been produced in Allen and Coffey counties as far back as 1895. The main producing formation of this field is Bartlesville sandstone formation with a depth of 650 ft. to 850 ft. The well candidates of Blue Top Energy are located in E. Larsen and L.L. Baker leases. Then we conducted more pilot tests in the Crotts lease which is located in Neosho Falls-Leroy field and operated by another small producer, Colt Energy. The first wells of cross lease date back to 1970; since then, seven wells have been drilled. The main producing formations are Squirrel sandstone bed and Mississippian system.

Table 5-1. Stratigraphic chart of oil-producing formations in Kansas.

(Pilot test area formations are highlighted in green.)

Era	System	Stage	Group	Producing Rock Units
Mesozic	Cretaceous		Colorado	Niobrara
Paleozoic	Permian	Guadalupian		
		Leonardian	Nippewalla	
			Sumner	Red Cave
		Wolfcampian	Chase	Herington, Krider, Winfield, Towanda, Fort Riley
			Council Grove	Neva, Cottonwood
		Virgilian	Admire	Indian Cave
			Wabaunsee	Langdon, Tarkio, Willard, White Cloud, Howard
	Pennsylvanian		Shawnee	Topeka, Elgin, Hoover, Toronto
			Douglas	Ireland, Stalnaker
		Missourian	Lansing	
			Kansas City	Layton, Perry Gas
			Pleasanton	Cleveland, Knobtown, Hepler
			Marmaton	New Albany, Wayside, Bandera, Weiser, Pawnee, Peru, Fort Scott, Oswego
			Cherokee	Mulky Coal, Prue, Bevier Coal, **Squirrel**, Cattleman, **Bartlesville**, Weir-Pittsburg, McLouth, Riverton Coal, Burgess
		Atokan		
		Morrowan	Morrow	
				Basal Pennsylvanian Conglomerate, Gorham
	Mississippian	Chesteran	Chester	
		Meramecian		Saint Genevieve, Saint Louis, Spergen, Warsaw
		Osagian		
		Kinderhookian		
	Devonian			Misener
	Silurian		Hunton	
	Ordovician			Maquoketa
				Viola
			Simpson	
			Arbuckle	
	Cambrian			
				Reagan
				Granite Wash

5.1.1 Cherokee Group Basin

Cherokee Group "shoestring" sandstones in eastern Kansas and northern Oklahoma (Figure 5-1) are known by a variety of names, including Bartlesville (Bluejacket), Squirrel, Warner, Burgess, Lagonda, Cattleman, Burbank, Cabanis, Riverton, Upper Cherokee, Krebs, and Penn-Basal conglomerate. These sandstones produce from stratigraphic, structural, and structural-stratigraphic traps. These reservoirs typically range from up to 55 ft. thick to 1,000-2,000 ft. wide and as long as 14 miles. Desmoinesian sandstones have been the most productive reservoirs in the Midcontinent. Cherokee Group sandstones are the oldest oil exploration and exploitation plays in the midcontinent, dating from the 1860s.

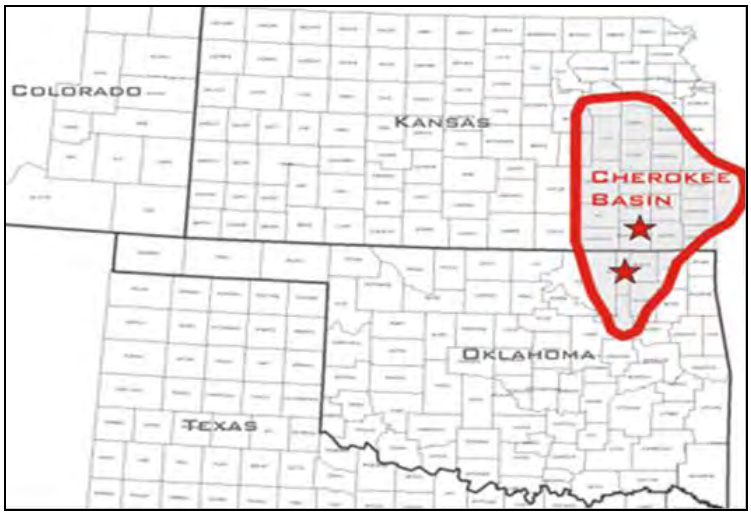

Figure 5-1. Map showing the Cherokee Group basin.

The ultimate recovery of oil from reservoirs in the Cherokee Group sandstones is affected by facies-type, small-scale, sedimentary structures; bedding boundaries; intergranular, small-scale permeability barriers; and diagenetic changes (internal architecture), commonly identified as heterogeneities within the sandstone body [34]. These heterogeneous bodies restrict the recovery of oil from hydrocarbon-rich matrices because the flooded water will bypass these matrices and travel along the easier paths towards the producer well.

5.1.2 The Humboldt-Chanute Field

Humboldt area of Allen County was discovered in 1901, and later, it was found that the two areas were part of one reasonably continuous producing area covering parts of Allen and Neosho counties in Kansas, now called the Humboldt-Chanute field. Figure 5-2 shows the location of the field. Oil in the Humboldt-Chanute field is produced from the Bartlesville sand of the lower Pennsylvanian age, which is found at depths of 650 to 850 ft. and ranges in thickness from 12 to 40 ft. Average values taken from core analyses indicate that the sand has a porosity of 20%, a permeability of 177 md, and an oil saturation of 43%. Oil saturation in the Bartlesville sand vanes widely throughout the field. The crude oil has an average gravity of 23 API° and an average viscosity of 750 cp at bottom hole temperature. The primary oil production has occurred via dissolved-gas drive. The field has a total productive area of 15,300 acres, and it accounts for approximately 65% of the oil-producing area of the counties where it is located. The reservoir in this field was generated in the Cherokee Group "shoestring" sandstones in eastern Kansas. Table 5-2 summaries the production history of Humboldt-Chanute Oilfield. Table 5-3 shows the decline curves and annual production of this field from 1970 to 2011.

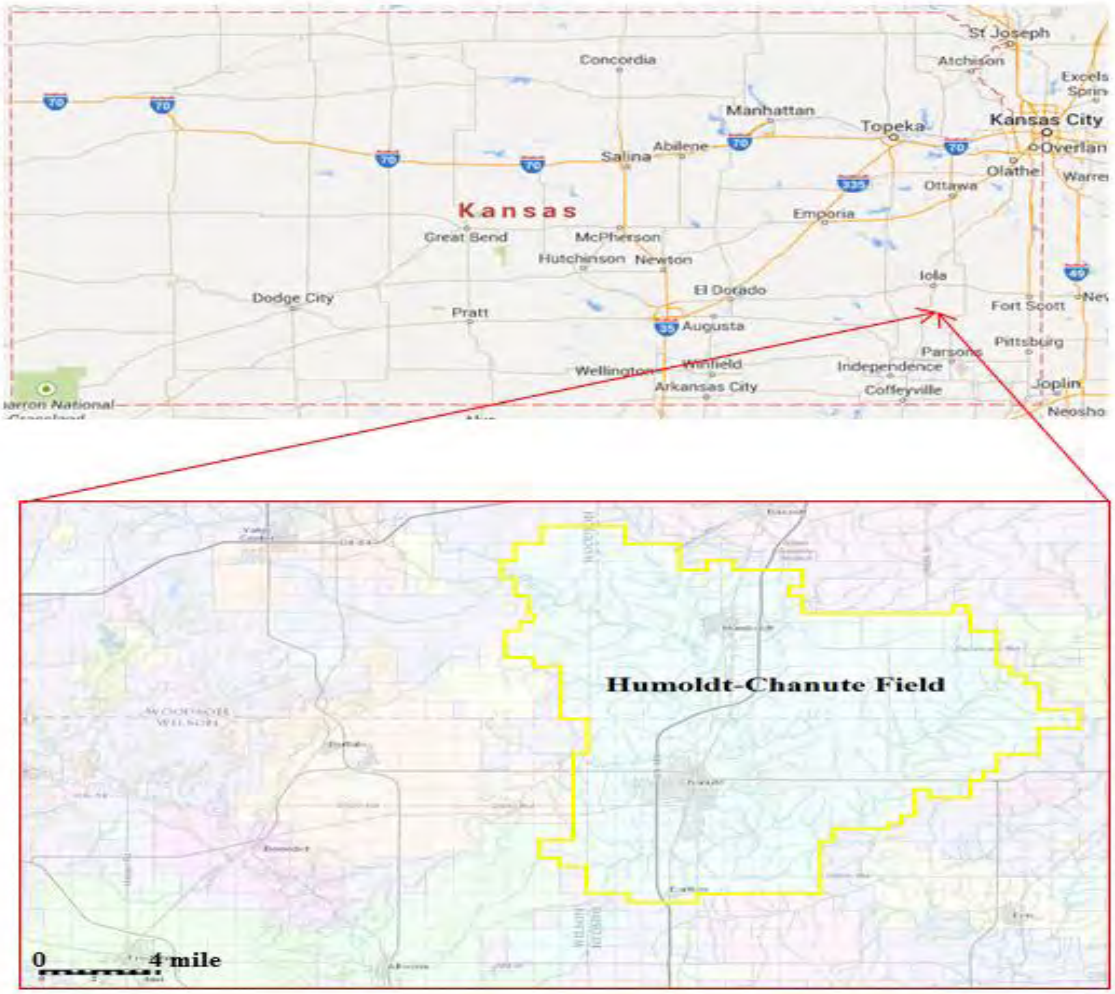

Figure 5-2. Location of Humboldt-Chanute field.

Table 5-2. Summary of the production history of Humboldt-Chanute field.

Field Size	172,160 acres
Total Wells	2,238
Productive Oil Wells	1,344 as of May 2013
Productive Gas Wells	42 as of May 2013
Cumulative Oil	23 MMSTB as of May 2013

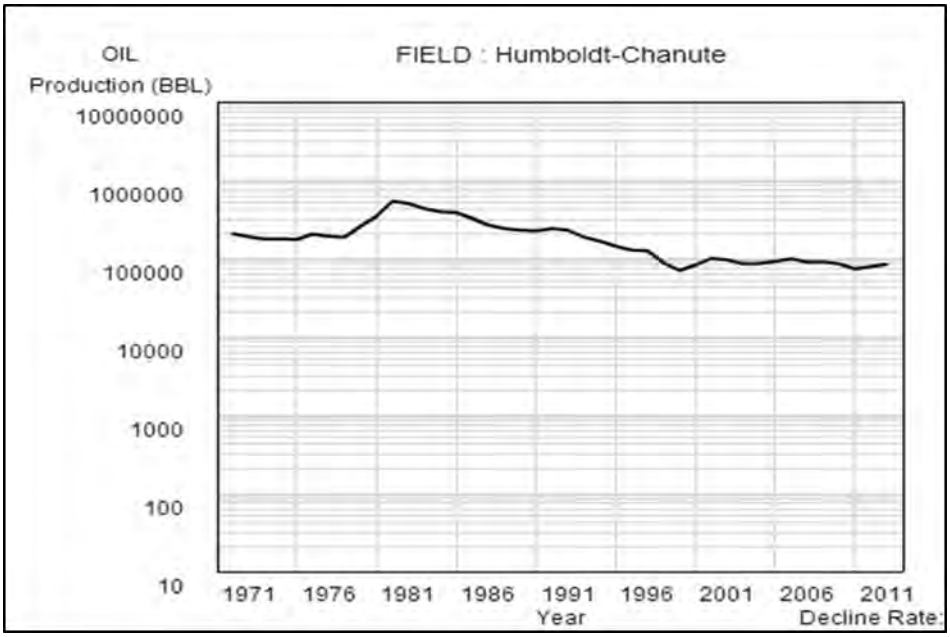

Figure 5-3. Annual oil production from Humboldt-Chanute field.

Blue Top Energy conducted the pilot tests in the southeastern end of the Humboldt-Chanute oilfield, focusing on Bartlesville sandstone formation reservoir. Table 5-3 shows the average characteristics of the reservoir. The reservoir is approximately 400 ft. wide and 2,500 ft. long, with a maximum net productive sand thickness of 21 ft. The reservoir has no appreciable dip and is closed on the sides by the degradation of sand into shale. The main body of sand is heavily laminated with shale stringers that, are not continuous between wells. The main reservoir is overlain by 30 to 40 ft. of laminated, low-permeability sand and shale streaks. Core analyses indicated that no gas cap exists. The low primary production indicates that the crude oil was under-saturated.

Table 5-3. Reservoir characteristics of Bartlesville sandstone formation.

Average Depth	889 ft.
Production Area	68.6 acres
Average Sand Thickness	8.8 ft.
Maximum Net Productive Sand Thickness	21 ft.
Reservoir Volume	664 acre-ft.
Porosity	20.3%
Permeability	177 md
Reservoir Temperature	78°F
Gravity of Produced Crude	23 API°
Average Oil Viscosity	750 cP at 70°F
Connate-water Saturation	23%
Estimated Formation Volume Factor	1.05
Primary Production	61 bbl/acre-ft.
Estimated Original Oil in Place	1,150 bbl/acre-ft.
Pattern Area	1.25 acres
Distance Between Injection and Production Wells	165 ft.
Production-well Bottom-hole Pressure	14 psia
Oil Saturation	43%
Water Saturation	35%
Specific Gravity of Oil	0.966

5.1.3 The Neosho Falls-Leroy Field

The Neosho Falls-Leroy Field is located near Leroy City in Coffey County, Kansas. It was discovered in January 1905. The field is producing oil from the Squirrel sandstone formation of lower Pennsylvanian age, which is found at depths of 965 to 974 ft. and ranges in thickness from 5 to 10 ft. The average values taken from core analyses indicate that the sand has an average porosity of 17 to 20%, a permeability of 60 to 80 md, and an oil saturation of 43%. The crude oil has an average gravity of 27.9 API° and an average viscosity of 150 cp at bottom hole temperature. The field has a total productive area of 160 acres. The reservoir in this field was generated in the Cherokee Group shoestring sandstones in eastern Kansas. Colt Company conducted the pilot tests in the north end of the Neosho Falls-Leroy Field where Crotts lease is located. Figure 5-4. Production history and decline curve analysis of Neosho Falls-Leroy Field

(Source: KGS website)shows the production history of Neosho Falls-Leroy field. Figure 5-5 shows the location of Neosho Falls-Leroy field. The field covers most of Coffey County.

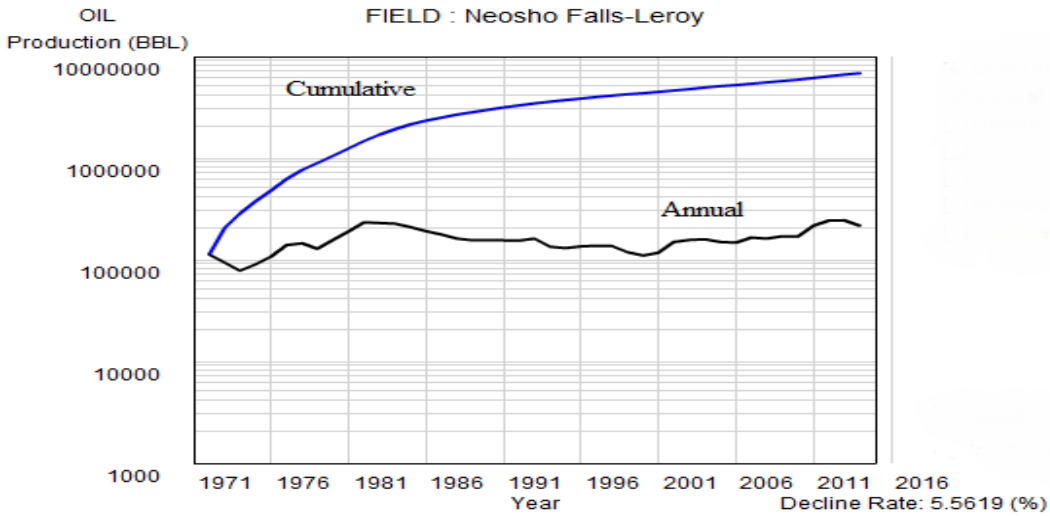

Figure 5-4. Production history and decline curve analysis of Neosho Falls-Leroy Field (Source: KGS website).

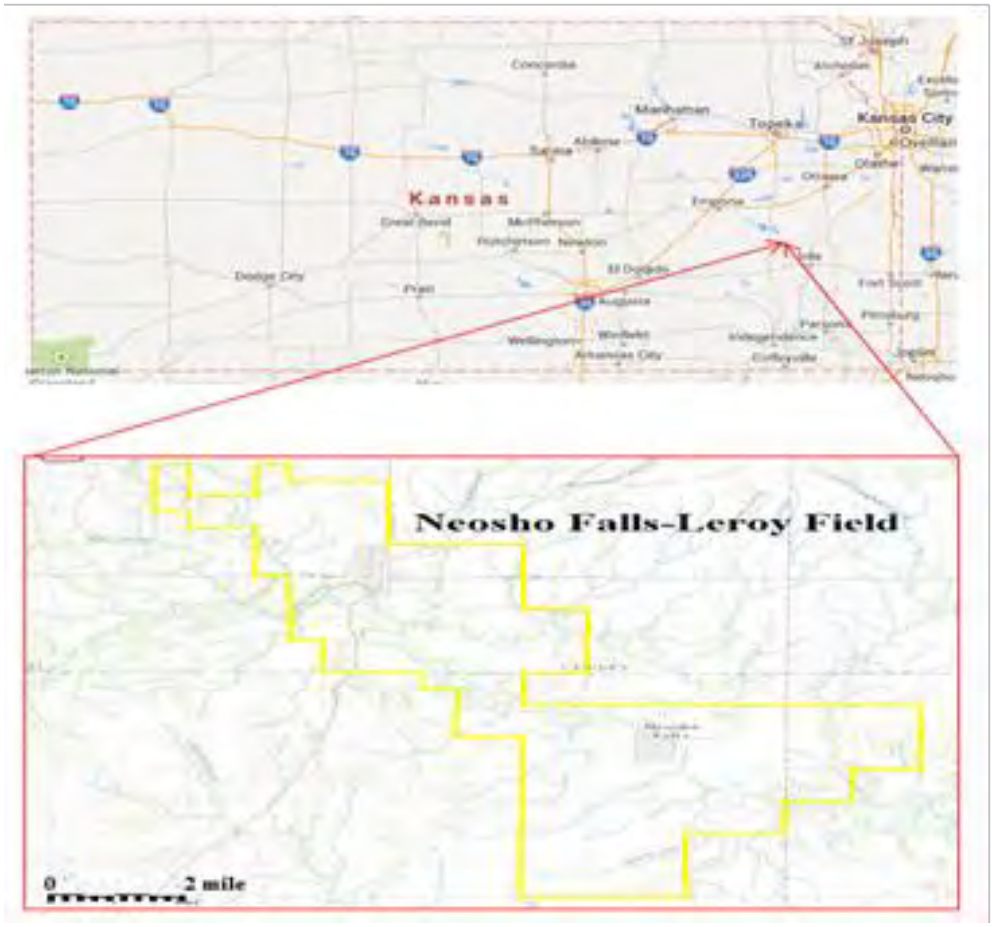

Figure 5-5. Location of Humboldt-Chanute Field.

5.2 Pilot Tests Preparation, Operation, and Results Evaluation

Four leases were selected for investigating the novel combined EOR method in Kansas. Information about the leases and the oil company operating the lease are given in Table 5-4. The E. Larsen and L. L. Baker are operated by Blue Top Energy, LLC, and the Crotts and Murray B are operated by Colt Energy. The leases are under water flood and represent most of the oil-producing horizons in Kansas. Selecting these leases for PPG combined with surfactant treatment was an easy task because of the clear evidence of water rapid breakthrough and the huge excess of water return to the storage tanks.

Table 5-4. Leases selected for the oilfield pilot tests.

Lease name	E. Larsen	L.L. Baker	Crotts	Murray B
County	Allen	Allen	Coffey	Coffey
Operator	Blue Top Energy	Blue Top Energy	Colt Energy	Colt Energy
Oil gravity (API°)	19.9	30	27.9	
Producing wells	4	3	4	28
Injection wells	2	2	3	11
Net area (acre)	664	664	160	
Avg. thickness (ft)	20	20	5	40
Producing Zone	Bartlesville	Bartlesville	Squirrel	Squirrel
Rock type	Sandstone	Sandstone	Sandstone	Sandstone
Total depth (ft)	889	889	974	983

The chemical systems used in the pilot tests include PPGs and surfactant. The commercial PPGs called Cerogel™ was acquired from ChemEOR, Inc. Two particle sizes of Cerogel™ were selected: PPG-746, with a particle size range of 60-70 mesh sizes, and PPG-780, with a particle size range of 100-120 mesh sizes. The properties of these two PPGs are presented in Table 5-5. A non-ionic surfactant, IGEPAL® CO-530, was selected to be used in this pilot tests. The same injection water used by the leases operation was used in mixing the PPG and the surfactant.

Table 5-5. Properties of PPGs used in the pilot test.

Cerogel™	Mesh Size	Swelling Ratio, g/g in injection water	G′, Pa
PPG-780	60-70	32.33	391
PPG-746	100-120	40.33	406

One of the advantages of PPG treatment is that it does not require a complex workover operation and it also requires a very small footprint. The surface facility used in this treatment was quite simple and is mainly comprised of a mixing tank to blend the PPG and surfactant with the injection water and a pump to inject the mixture into a target well. Figure 5-6 shows a typical layout of the surface equipment used for the combined technique.

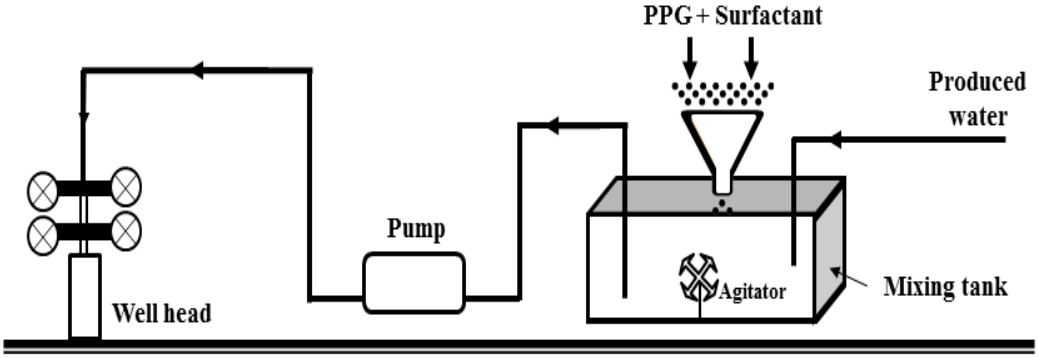

Figure 5-6. Flow chart of typical surface equipment for the novel EOR methods.

5.2.1 Pilot Tests in E. Larsen Lease

5.2.1.1 Introduction of Lease Reservoir and Production Conditions before Treatment

The first candidate wells for the PPG and surfactant treatment are located in the E. Larsen lease in southeastern Kansas. The wells in this lease were first drilled in 1981. Since then, the lease has produced a total of approximately 55 MSTB. Figure 5-7 presents the production history of the lease. Based on direct conversation with a veteran operator in the eastern Kansas area, this lease had been aggressively water flooded by the first operator because of the heavy nature of the oil in this lease and the low initial primary production. This might have contributed to the conformance problems by enlarging the natural fractures or introducing new ones.

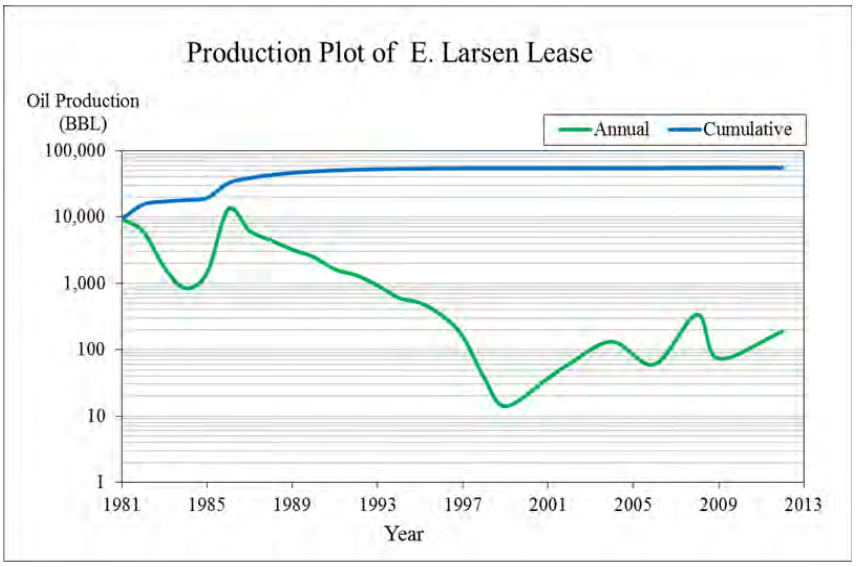

Figure 5-7. Production plot for E. Larsen lease (Source: KGS website).

The well distribution in the E. Larsen lease is presented in a map in Figure 5-8. The lease initially had a total of 16 wells, six injectors, and six producers. By the time of the treatment in 2013, the active wells consisted of only two injectors and four producers.

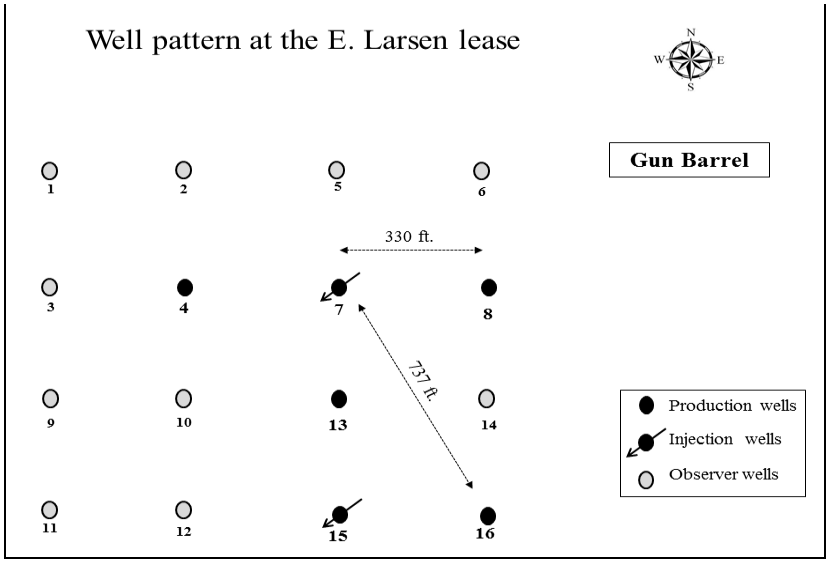

Figure 5-8. Well distribution at E. Larson lease.

Table 5-6 presents the properties of the injection water. Figure 5-9 shows the API and viscosity of the crude oil in the lease as a function of temperature. At the reservoir temperature of around 25°C (75°F), its viscosity is approximately 1,000 cp and gravity is about 19.8 API°. The average oil production from the lease is 0.25 bpd before treatment.

Table 5-6. Properties of injection water.

TDS (mg/l)	Conductivity (S/m)
2,525	3.96

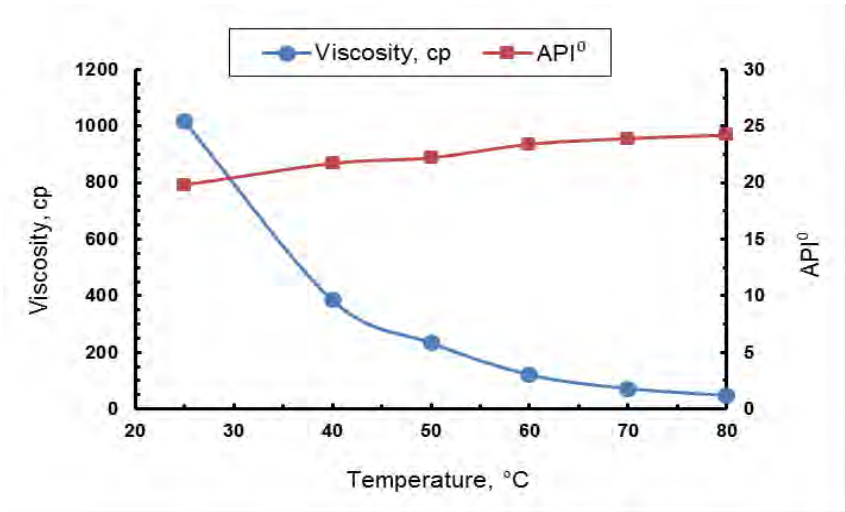

Figure 5-9. Crude oil viscosity and API° of E. Larsen lease.

5.2.1.2 Problem Identification

From direct conversation with the lease operator, it was indicated that for many years, the rapid breakthrough and excessive cycling of injecting water was recognized as a severe problem that hindered the oil production and added costs to the lease operation. Adding the heavy nature of the oil to this conformance problem led to several wells being shut in due to limited production. According to the lease operator, the most severe case was the direct communication between injection Well 7 and production Wells 13 and 16. Therefore, Well 7 was selected for the initial well testing to confirm the above mentioned problems and to better understand the severity of the fractures or channels between these wells.

Tracer Tests were conducted on both injection wells in E. Larsen lease. In the first tracer test, urea was used as a tracer agent because it was readily available, inexpensive, less toxic, and had

a high nitrogen content that could be detected easily. A color disc method was used for this tracer testing. The nitrogen content at the producing wells was detected using a test kit called the Nitrate Test, manufactured by HACH Company. This test kit could detect up to 50 mg/L of nitrogen in water. Figure 5-10 shows a photo of the device used to measure the urea concentration in water.

Figure 5-10. Nitrate test kit, 0-50 mg/L NO_3-N.

Figure 5-11 shows the lease map with tracer test results over time. Nitrogen was first detected after three hours from Wells 13 and 16, with a concentration of 33 and 25 mg/l, respectively. After four hours, 5 mg/l of nitrogen was detected in Well 8. No nitrogen was detected in Well 4 within 24 hours.

These results indicated that the fracture/channel was oriented towards the south to the southeast of the lease, and its size could be in the order of several mm because of the short time it took the nitrogen to migrate to Wells 13 and 16; this could be also true in Well 8, but to a lesser degree. In contrast, from the observation in Well 4, one can conclude that there is no easy path for the water to follow.

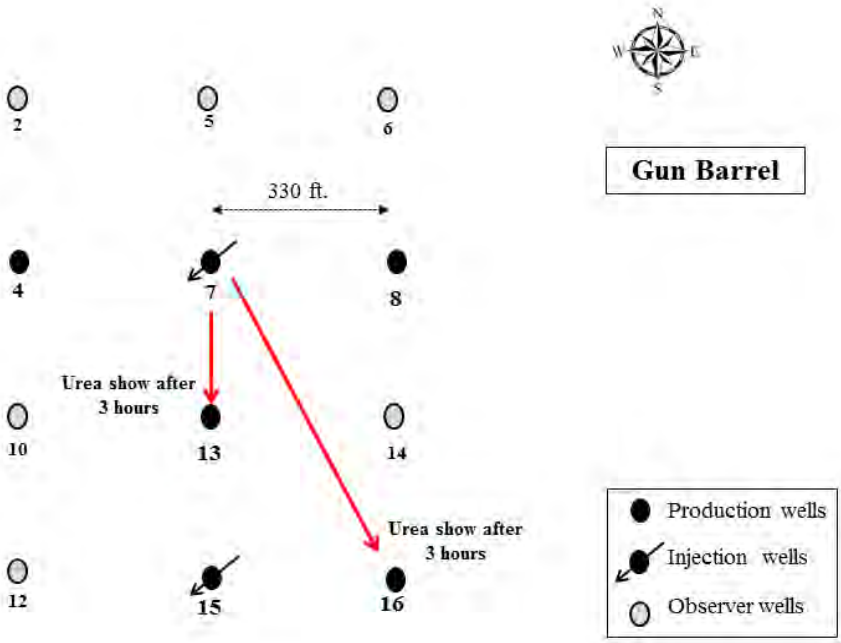

Figure 5-11. Tracer test results from four production wells.

To confirm the urea tracer results and to better understand the heterogeneity of the formation in the E. Larsen lease, a second tracer test was conducted. A green dye was mixed with the injected water in injection Well 7. The results showed that the dye tracer was apparent in Wells 13 and 16 after two and half hours, and in Well 8 after four hours. The dye tracer was not detected in Well 4. These results confirmed the findings from the chemical tracer.

Step Rate Test (SRT) was performed on injector Well 7 to understand the injectivity response of the formation. Figure 5-12 shows the SRT results in terms of the relationship between the flow rate on the x-axis and the wellhead pressure on the y-axis. The results showed that the injection pressure only increased slightly rather than increasing linearly with the flow rate, indicating the well had a satisfactory injectivity.

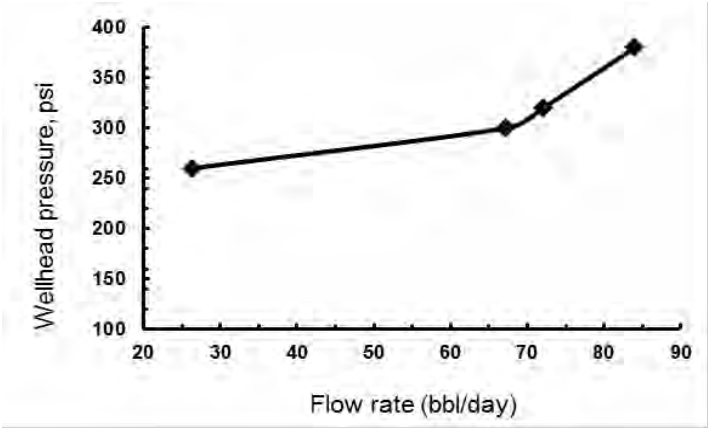

Figure 5-12. Step rate test on injector Well 7.

In March 2014, Well 7 was treated again along with Well 15. Also the two injection wells in L. L. Baker lease were treated on that day. The following is the description of the treatment design and the initial results.

5.2.1.3 Treatment Design

Considering the lack of information on the reservoir history of the pilot area and the limited capacity of the leases' surface facilities, the pilot tests were designed to be small scale batches of PPGs and surfactant mixtures. A local pumping operator was contracted for PPGs and surfactant injection. A cement pump unit, which could inject up to 700 psi, and a small batch mixing tank with a 3 bbl capacity were used. A water truck with a capacity of 30 bbl was also used to bring injection water to the well site. Figure 5-13 shows a picture of the cement unit used to inject the PPG and surfactant mixture.

Figure 5-13. Cement unit used for the PPG and surfactant treatment in E. Larsen lease.

Cerogel™ PPG-780 was selected for the treatment. These PPGs come in 55 lb. bags. Figure 5-14 shows the bags of PPG-780 at the location on the day of the treatment. We used a 5000 ppm concentration of PPG for the field treatment, which means we added 1.75 lb. of PPG for each barrel of water to prepare the PPG dispersion. The concentration of surfactants was designed as 8,000 ppm. A total of 125 bbl of PPG and surfactant blend was injected into Well 7. At the end of the treatment, 10 bbl of produced water was injected to flush the PPG and surfactant out of the wellbore.

One of the advantages of the PPG treatment is that PPGs can be changed quickly. If the pressure does not increase as expected, the PPG concentration or particle size can be increased or another PPG with higher strength can be used. If the pressure increases rapidly, the PPG concentration can be reduced or smaller sizes of particles or more deformable particles can be used.

Figure 5-14. Bags of Cerogel™.

5.2.1.4 Field Operations

The first field test was performed in October 2013. Well 7 in E. Larsen lease was treated. The treatment was implemented using the following procedures:

- Normal injection in the lease was seized and the shut-in pressure in Well 7 was recorded. The shut-in pressure at the wellhead was 200 psi.

- Small batches of the suspension were mixed in the mixing tank and bullheaded into the Well 7. Figure 5-15 shows the suspension mixture of PPG and surfactant in the mixing tank. It is important to keep the PPG suspended in the aqueous solution by agitating it so it will not settle in the bottom of the mixing tank.

Figure 5-15. PPG and surfactant were mixed before injection into Well 7.

- The injection pressure and rate were monitored and recorded. Injection rate of 0.4 bbl/min was maintained throughout the treatment. The injection rate was kept as low as possible to avoid exceeding the formation parting pressure.

- Once the treatment was completed, the well was shut-in, and the pressure was recorded.

- After 24 hours shut-in, normal operation in the lease was resumed and a draw-down pressure test was conducted to test whether PPG reduced the permeability of the channels.

- The production wells were monitored for any possible PPG breakthrough and the changes of oil and water production rates.

5.2.1.5 Evaluation of Treatment Results

Injection pressure response during PPG injection: A positive pressure response was observed during the treatment. Figure 5-16 shows the monitored real-time injection pressure during the combined PPG and surfactant treatment. The pressure increased steadily during the treatment, indicating that PPG was successfully injected into the reservoir. There was a noticeable pressure drop after 80 minutes of the injection, which might be caused by the release of previous formation damage. Figure 5-17 shows the wellhead pressure gauge reading right before the treatment and immediately after the treatment.

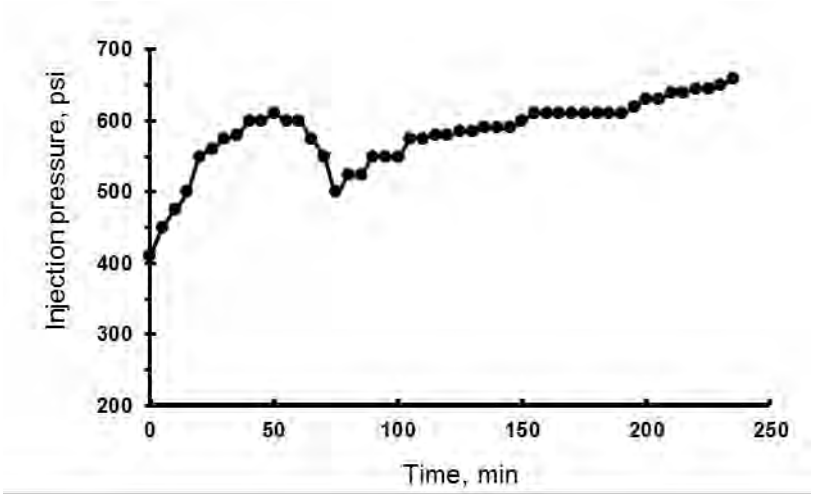

Figure 5-16. Real time injection pressure during PPG and surfactant treatment in Well 7.

Before the treatment After the treatment

Figure 5-17. Wellhead pressure gage reading of Well 7 before and after the treatment.

Comparison of draw-down test results before and after treatment: Figure 5-18 shows the draw-down pressure test results before and one day after the treatment. The results showed that the flowing capacity of the preferential flow channels were obviously reduced. After 24 hours of shut in, the well was put back into production and the injection pressure was increased to 340 psi.

Oil and Water Production Change: The water and oil production were monitored and recorded to assist in designing the next PPG treatments. The lease operated by Blue Top Energy LLC initially did not see an obvious oil and water production rate change. However, the lease technician told us that the west adjacent lease operated by another small producer observed an obvious increase in oil production after the treatment, but no detailed information was released. In addition, when the production resumed after winter shut-down, the lease reported oil production of 0.62 bpd, compared to 0.25 bpd before treatment.

Other information: The pressure in the observer Wells 5 and 6 increased moderately, and the two wells produced some extra oil. No particles were produced from producers.

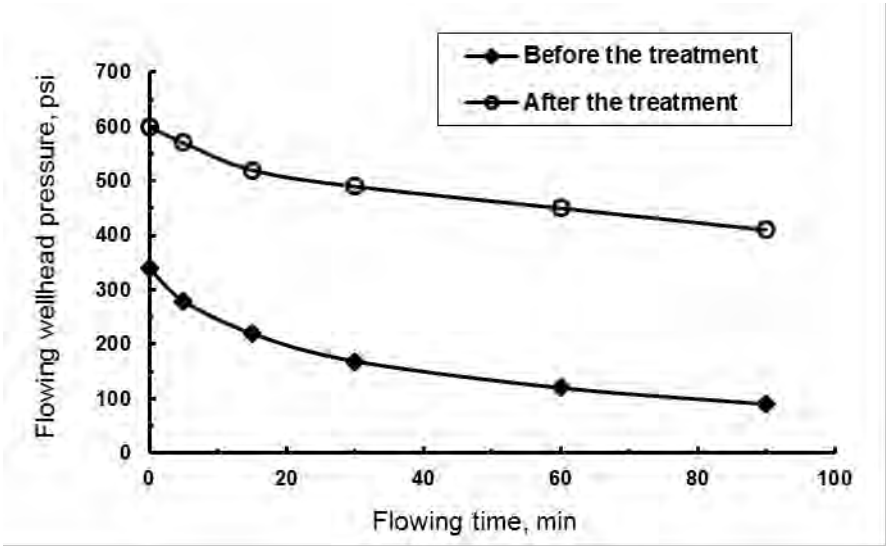

Figure 5-18. Draw down pressure before and after PPG treatment.

5.2.1.6 Brief Description of Other Pilot Tests in E. Larsen

In March 2014, Wells 7 and 15 were treated at the same time to better control the water performance in the lease.

Well 7 treatment: A high concentration of PPGs, approximately, 10,000 ppm were designed to better plug the formation. However, immediately after PPGs injection, the pressure quickly rose to 700-800 psi. The injection rate was reduced, and only 5 gallons of suspension was injected in

1.5 hours. To resolve this issue, the well was flew back, some scales of black emulsion-like materials were seen, which could be attributed to the fact that the lease was shut-in during the winter. As a result of the flow back and well bore cleaning, the treatment resumed again, and no injectivity problem was found though the injecting pressure remained high at 800 psi. Approximately 75 lbs. of PPGs and three gallons of surfactant were injected during this treatment.

Well 15. The wellhead pressure was reading 0 psi, and the well was in vacuum condition before PPG injection, indicating that the well could have had a severe channeling problem and should be a good candidate for the treatment. The PPG concentration was designed to be 10,000 ppm. The pressure started to increase gradually and was stabilized at 550 psi. A total of 110 lbs. of PPG was injected, and the shut-in pressure was 550 psi.

It was reported by the technician of the lease that the water injection pressures was increased as expected after the treatment. After two months Well 7 was still holding 150 psi, which indicates that the PPG treatment was successful in partially plugging the channeling problem. There was much more oil in storage tanks than before, which was evidenced by the following email.

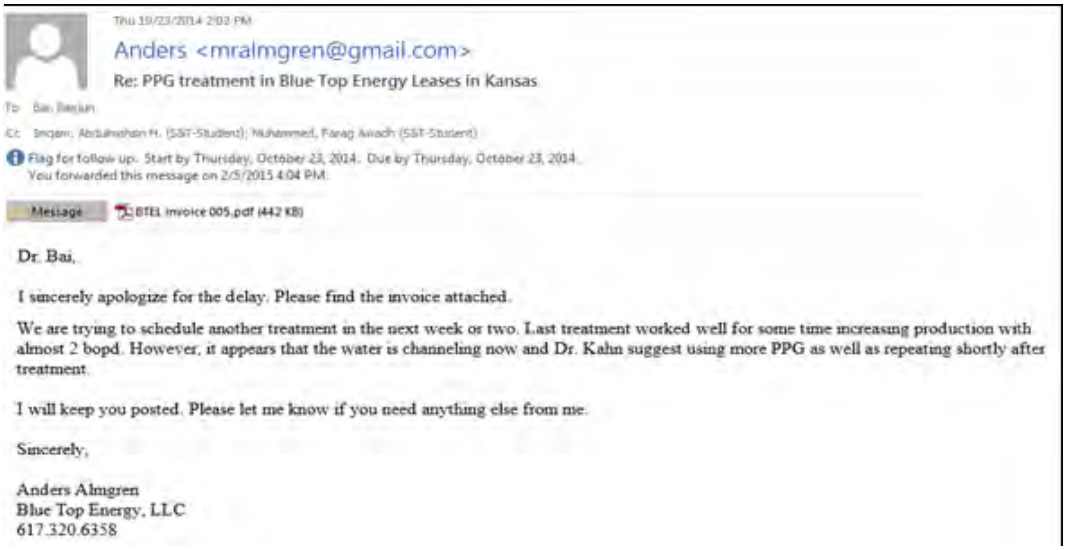

Thu 10/23/2014 2:02 PM

Anders <mralmgren@gmail.com>

Re: PPG treatment in Blue Top Energy Leases in Kansas

To: Bai, Baojun

Cc: Imqam, Abdulmohsen H. (SAT-Student); Muhammed, Farag Awadh (SAT-Student)

Flag for follow up. Start by Thursday, October 23, 2014. Due by Thursday, October 23, 2014.
You forwarded this message on 2/5/2015 4:04 PM.

Message | BTEL Invoice 005.pdf (442 KB)

Dr. Bai,

I sincerely apologize for the delay. Please find the invoice attached.

We are trying to schedule another treatment in the next week or two. Last treatment worked well for some time increasing production with almost 2 bopd. However, it appears that the water is channeling now and Dr. Kahn suggest using more PPG as well as repeating shortly after treatment.

I will keep you posted. Please let me know if you need anything else from me.

Sincerely,

Anders Almgren
Blue Top Energy, LLC
617.320.6358

5.2.2 L. L. Baker Lease

This lease is located approximately two miles east of E. Larsen lease and is also operated by Blue Top Energy LLC. The oil in this lease has a gravity API of 30° and a viscosity of 11 cp at

reservoir temperature. The first well in this lease was drilled in 1980. Since then, a total of four wells have been drilled. From 1980 to 2014, the lease had a cumulative oil production of approximately 5 MSTB. Figure 5-19 presents the production history of the lease.

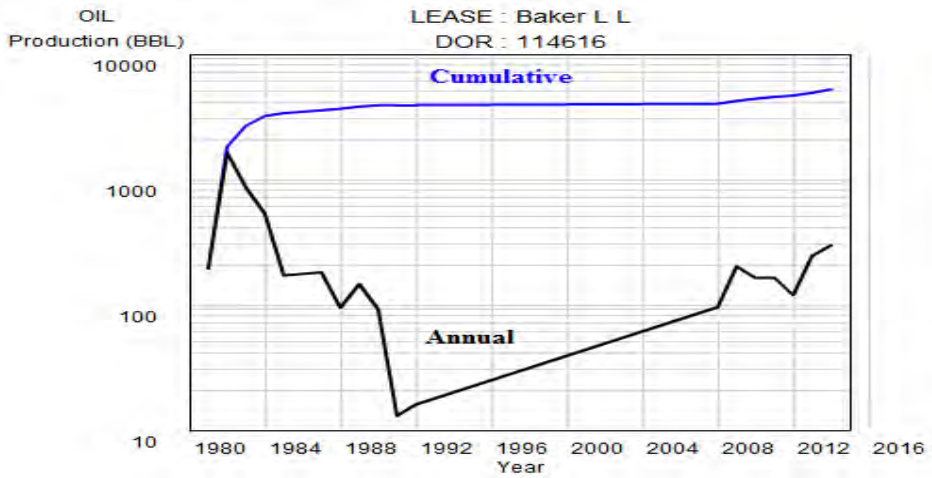

Figure 5-19. Production history for L. L. Baker lease (Source: KGS website).

The well distribution in the L. L. Baker lease is presented in a map in Figure 5-20. The lease has five active wells consisting of two injectors and three producers. The distance between wells is approximately 330 ft.

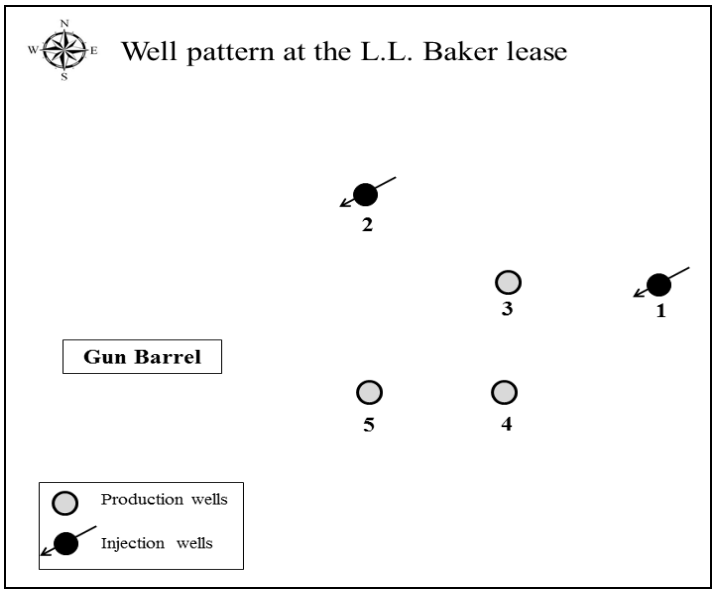

Figure 5-20. Well distribution in L. L. Baker lease.

According to the technicians in the lease, there are severe channeling problems between injection Well 1 and production Well 3. The well head pressure in the injector was 0 psi and the well was in vacuum condition. A dye tracer test was run to define the channeling problems. After one hour of injection, the dye was found in Well 3.

The treatment in L. L. Baker lease was performed in injection Wells 1 and 2. The PPG concentration used in this treatment was 10,000 ppm. In Well 1, the pressure increased gradually to 800 psi which was close to the parting pressure after 4.5 bbls of PPG suspension (28 lbs dry PPG) were injected, so the treatment had to be ceased. Although treating Well 2 was not initially planned, the technicians in the lease requested that a small batch of PPG for treatment be applied because some oil was witnessed at the surface next to a nearby abandoned well. We injected the same amount of PPG and water mixture in this well (28 lbs. of PPG mixed in 4.5 bbl water), and the pressure quickly rose so fast to 850 psi.

Treatment results: After the treatment, the technician in the lease informed us that the wellhead pressure for both wells increased to more than 200 psi, but no further information was provided.

5.2.3 Field Testing in Crotts Lease

The lease is owned and operated by Colt Energy LLC. It is located southeast of LeRoy City, Coffey County, Kansas. The oil in this lease has a gravity API of 27.8° and viscosity of 37 cp at

room temperature. The first well in this lease was drilled in 1970. Since then, a total of seven wells have been drilled. From 1970 to 2014, the lease had an accumulative oil production of approximately 40 MSTB. Figure 5-21 presents the production history of the lease.

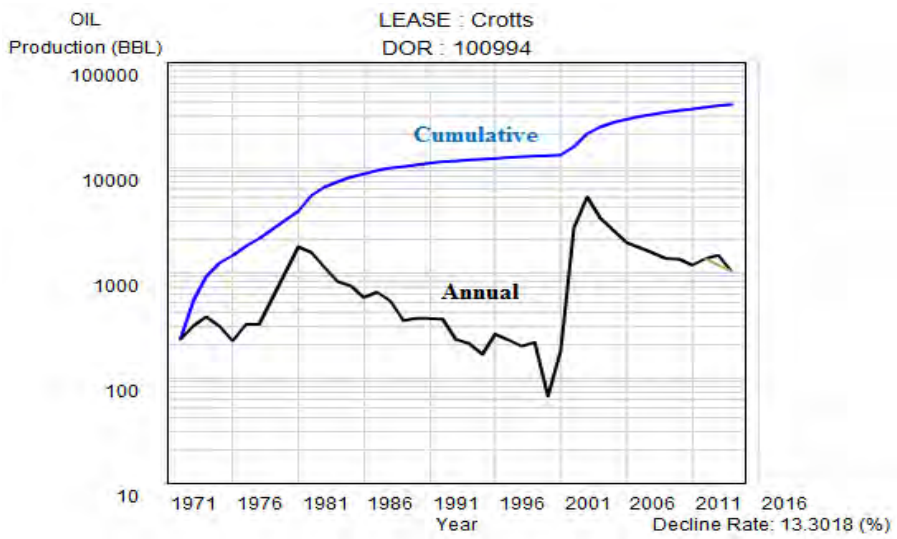

Figure 5-21. Production history for Crotts lease (Source: KGS website).

The well distribution in the Crotts lease is presented in a map in Figure 5-22. The lease has seven active wells consisting of three injectors and four producers. The distance between wells is approximately 330 ft.

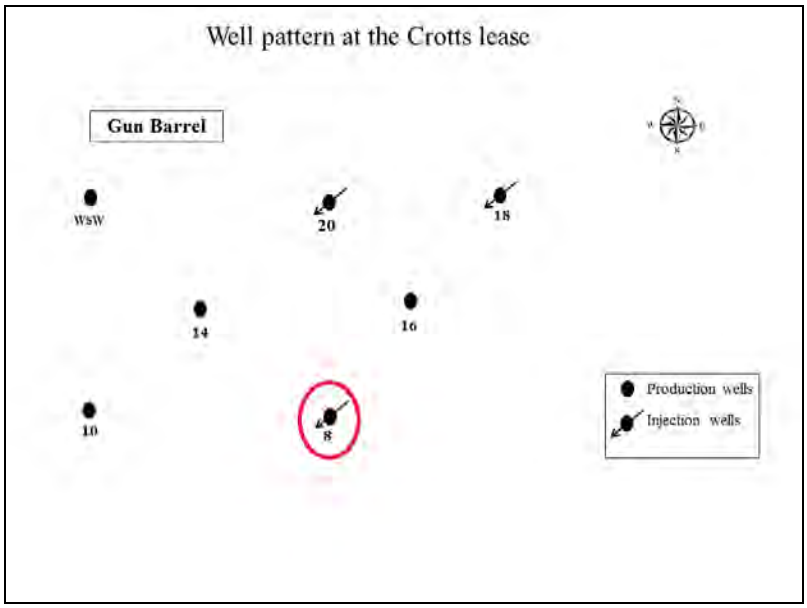

Figure 5-22. Well distribution in Crotts lease.

The lease operators verified that there exists a direct communication between Well 8 and Well 16. Well 8 is a candidate for treatment. The Well 8 is a slim hole completion (2 7/8 in. casing). It was perforated from 962 ft. to 970 ft. with 17 perforations.

Well 8 was originally completed in the Squirrel sand as an oil producer in August 2001. It was converted to an injection well in August 2005. Several wells were converted at this time because reservoir pressure was low. The initial injection rate into Well 8 was 5 bpd, and it was gradually increased to 20 bpd by July 2008. The well head pressure increased and peaked at 380 psi by August 2008. From September 2008 to June 2009, the pressure dropped from 380 psi to 0 psi while the water production increased at Well 16. By the time the pressure decreased to 0 psi in June 2009, 19,078 bbl of water had been injected into Well 8.

The treatment was conducted in Well 8 in the Crotts lease in July 2014. We used a regular cement pump (Figure 5-23) to injection PPG dispersion, which was much more reliable than the one used in Blue Top Energy pilots.

Figure 5-23. The cement pump to inject PPG dispersion.

The well was treated with 110 lbs. of PPG mixed in 70 bbl of produced water. Initially, Cerogel™ PPG-746 was used in the treatment, with a concentration of 8,000 ppm, but a surfactant was not used because (1) the oil in this lease is light and it does not need surfactant to create emulsion to assist in viscous fingering mitigation, and (2) the lease operators are using bacteria to treat the produced water; thus, using surfactant could complicate the produced water treatment. The injection rate was maintained at 0.5 bbl/min throughout the treatment. The treatment was conducted for two days. The first day, we injected 70 bbls (110 lbs.) of PPG dispersion, and the injection pressure was increased to 210 psi. The second day, we resumed injecting water, and the pressure was 0 psi, so we decided to use large particle sizes of PPG and also increase the PPG concentration to 16,000 ppm. When the dispersion of 50 bbls of PPG (110 lbs. dry particle) was injected into the well, the shut in pressure rose up to 310 psi. Figure 5-24 shows the real time injection pressure at the well head of Well 8 during the PPG treatment.

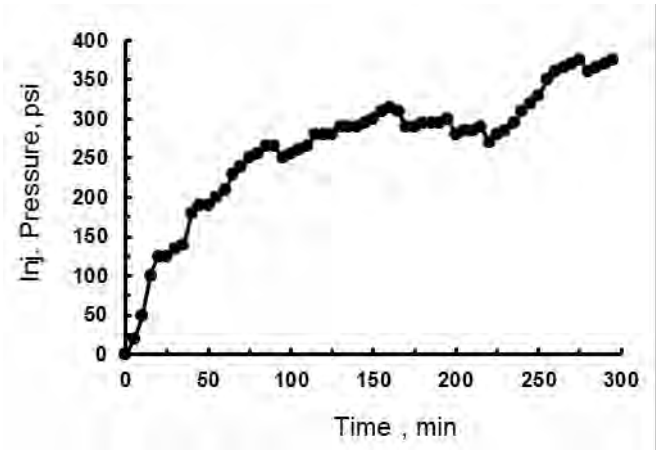

Figure 5-24. Monitored real-time injection pressure of PPG injection.

5.2.4 Murray B Lease

This lease is operated by Colt Energy LLC. It is located southeast of LeRoy City, Coffey County, Kansas. The first well in this lease was drilled in 1970. Since then, a total of 39 wells have been drilled. From 1970 to 2014, the lease has an accumulative oil production of approximately 229 MSTB. Figure 5-25 presents the production history of the lease.

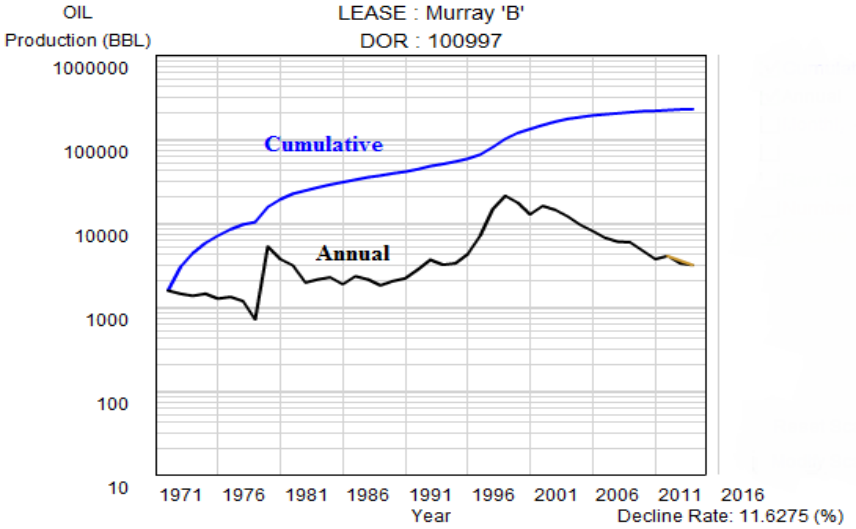

Figure 5-25. Production history for Murray B lease (Source: KGS website).

The well distribution in the Murray B lease is presented in a map in Figure 5-26. The lease has seven active wells consisting of three injectors and four producers. The distance between wells is approximately 330 ft.

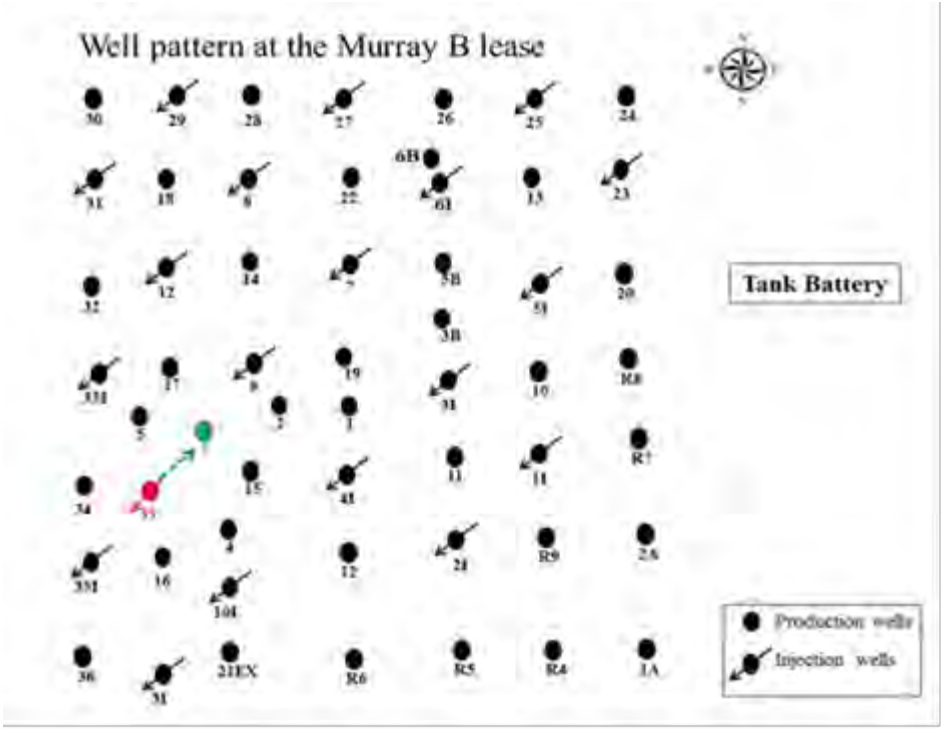

Figure 5-26. Well distribution in Murray B lease.

The lease operators identified severe channeling between the injecting well Murray 11 and the producer Murray 3. The Murray 11 is a slim hole completion (2 7/8 in. casing).

On July 29, Well 11 in Murray lease was treated with PPG (Cerogel™ 780 and Cerogel™ 746). Before the treatment, 20 bpd of water was injected, and the injection pressure was 120 psi. PPG injection procedures are listed as follows:

First, we mixed a bag (55 lbs) of Cerogel™ PPG-746 with 20 bbls of injection water and then injected the mixture into the well. We also added fluorescent yellow/green dye as a tracer into the last 5 bbls of PPG suspension to determine the efficiency of PPG treatment. During the injection, the pressure increased from 225 to 340 psi.

Second, we injected the mixture of another bag (55 lbs.) of Cerogel™ PPG-746 and 20 bbls of injection water. The pressure initially was 380 psi but dropped to 340 psi at the end of the batch, so we decided to use a larger size of PPG.

Third, we injected another 40 bbls of PPG suspension, which was prepared by two bags (55 lbs.) of the Cerogel™ PPG-780, the injection pressure was stable at 325 psi.

All production wells surrounding Well 11 were checked, and no trace of the dye injected in the treatment was found.

A total of 110 lbs. of Cerogel™ PPG-780 and 110 lbs. of Cerogel™ PPG-746 were injected into the well. Figure 5-27 shows the real time injection pressure at the well head of Murray B lease during the PPG treatment.

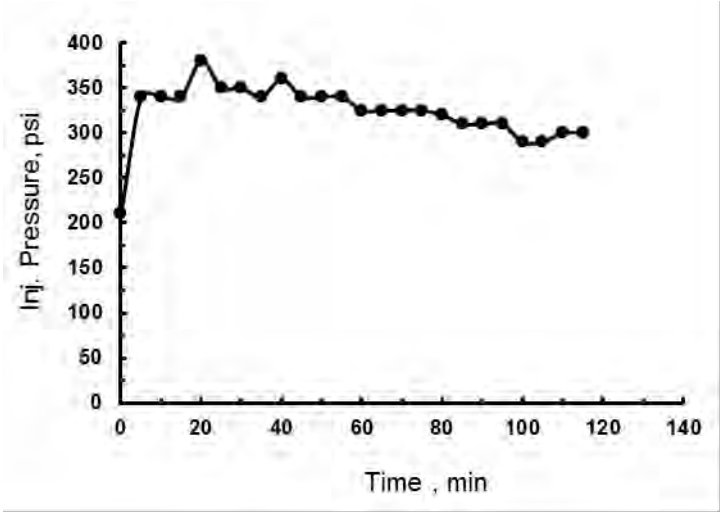

Figure 5-27. Real time injection pressure during PPG treatment of Well 11 in Murray lease.

After resuming water injection, the injection pressure was stable at 290 psi, compared to the initial water injection pressure of 120 psi.

The following email indicates an increase in oil production in their lease, but no updated information was provided, which might be caused by the shut-in of some wells due to the current low oil price (~40 dollars/bbl).

From: John Amerman [mailto:johnamerman@hotmail.com]
Sent: Friday, February 13, 2015 5:47 PM
To: Bai, Baojun <baib@mst.edu>
Cc: Dunn-Norman, Shari <caolila@mst.edu>
Subject: RE: production response from well treatments

Baojun,

Sorry of the delay in getting back to you, I was at NAPE in Houston this week. We plan on re-treating the wells that started channeling again and treating other wells that are channeling. We hope to improve our technique of injecting the polymer based on what we learned during the initial treatments. We were not planning on seeing anything significant for 6 months to a year but the average production from the leases of the wells treated has increased approximately 1 bopd.

I will be out of the office next week but plan on additional review once I am back in the office.

John

5.3 Summary and Lessons

We have carried out six pilot tests in four leases owned by two small producers. The results are summarized below.

In E. Larsen lease, the PPG and surfactant were injected successfully, and the injection pressure was increased as expected. The adjacent lease to the west of E. Larsen reported an increase in oil production after the treatment. The pressure in observer Wells 5 and 6 increased moderately, and the two wells produced some extra oil. No particles were produced from producers. The increase in oil production was observed in the lease.

In L. L. Baker lease, the treatment was relatively small due to low injectivity of the wells, but the communication between the injector and producer was effectively blocked. However, no information was provided about whether the treatment reduced water production and increased oil production.

In Crott lease and Murray B, PPGs were injected successfully into the selected wells, and the injection pressure increased as expected during PPG injection. The water injection pressure increased after the PPG treatment. The treatment mitigated the rapid water breakthrough problem between two wells. It was reported that there was about a 1 bpd increased in this area after the treatment.

Lessons learned from the pilots tests can be summarized as follows:

1. PPGs can be successfully injected into more mature oilfields even though the particle sizes are relatively large for those formation without channels, indicating the channels are prevalent in mature oilfields.

2. PPG treatment is a simple process that requires a minimum of surface facilities or equipment for injecting practices.

3. Too few PPGs were injected into each well, which caused no obvious oil production increase in most treatments except for the treatment in E. Larsen.

6. TECHNICAL TRANSFER

6.1 Research Website

http://www.ppgeor.org/

6.2 Publications

1. Elsharafi, M., Bai, B. Minimizing Formation Damage for Preformed Particle Gels in Mature Reservoirs. Paper SPE 174645 presented in SPE Asia Pacific Enhanced Oil Recovery Conference, August 11-13, Kuala Lumpur, Malaysia.

2. Imqam, A., and Bai, B. 2015. Optimizing the strength and size of preformed particle gels for better conformance control treatment. *Fuel* 148, 178–185.

3. Imqam, A., Bai, B., Wei, M. 2015. Combining Conformance Treatment with Mobility Control Improve Oil Sweep Efficiency in Non-Cross Flow Heterogeneous Reservoirs. Paper SPE 176728 accepted to present at SPE Russian Petroleum Technology Conference, October 26-28, Moscow, Russia.

4. Muhammed, F.A., and Bai, B. 2014. Heavy Oil Recovery from Sandstone Reservoirs in the Mid-Continent Region Using Preformed Particle Gel Enhanced Surfactant. Presented at AAPG Annual Conference & Exhibition, April 6-9, Houston, Texas.

5. Muhammed, F.A., Bai, B., and Al-Ibrahim, A. 2014. A Simple Technique to Determine Gel Strength of Millimeter-sized Particle Gel. Paper SPE 169106 presented at 19th SPE Improved Oil Recovery Symposium, April 12-16, Tulsa, Oklahoma.

6. Muhammed, F.A., and Bai, B. 2014. Preformed Particle Gel – Enhanced Surfactant Flooding for Improving Heavy Oil Recovery. Paper SPE 170067 presented at SPE Heavy Oil Conference, June10-12, Calgary, Alberta, Canada.

7. Imqam, A., Elue, H., Muhammed, F., Bai, B. 2014. Hydrochloric Acid Applications to Improve Particle Gel Conformance Control Treatment. Paper SPE- 172352 presented at the SPE Nigeria Annual International Conference and Exhibition, August 5-7, Lagos, Nigeria.

8. Bai, B, Wei, M., Liu, Y. 2013. Field and Lab Experience with a Successful Preformed Particle Gel Conformance Control Technology. Paper SPE 164511 presented at SPE Production and Operations Symposium, March 23 - 26, Oklahoma City, Oklahoma, USA.

9. Bai, B., Wei, M., Liu, Y. 2013. Injecting Large Volumes of Preformed Particle Gel for Water Conformance Control. *Oil & Gas Science and Technology*,–Revue d'IFP Energies nouvelles 67 (6), 941-952.

10. Tongwa, T, Nygaard, R., Bai, B. 2013. Evaluation of a Nanocomposite Hydrogel for Water Shut-off in Enhanced Oil Recovery Applications: Design, Synthesis, and Characterization. *Journal of Applied Polymer Science*, 128 (1), 787-794.

11. Elsharafi, M., Bai, B. 2013. Effect of Strong Preformed Particle Gel on Unswept Oil Zones/Areas during Conformance Control Treatments. Paper SPE 164879 presented at 75th EAGE Conference & Exhibition incorporating SPE EUROPEC, June 10 -13, London, United Kingdom.

12. Bai, B., Zhou, J., and Liu, Y. 2013. Thermo-Dissoluble Polymer for In-Depth Mobility Control. Paper IPTC 16991 presented at 6th International Petroleum Technology Conference, Mar 26 - 28, Beijing, China.

6.3 Presentations

1. Geng, J., Bai, B., Thomas. S. "Study of the Relationship between Cationic Degree and the Performance of Nanoparticle Dispersion." 250th ACS National Meeting & Exposition. American Chemical Society, August 16-20, 2015, Boston, MA, USA.
2. Pu, J., Bai, B. Thomas, S. "Effect of metal ions on the swelling performance of the hydrogel in enhancing salt resistance." 250th ACS National Meeting & Exposition. American Chemical Society, August 16-20, 2015, Boston, MA, USA.
3. Long, Y. Chen, Z., Bai, B. "Interpenetrating network polymer gel for improving oil recovery," 250th ACS National Meeting & Exposition. American Chemical Society, August 16-20, 2015, Boston, MA, USA.
4. Chen, Z., Thomas, S., Bai, B. "Water free emulsion polymerization of co-polyacrylamides." 250th ACS National Meeting & Exposition. American Chemical Society, August 16-20, 2015, Boston, MA, USA.
5. Chen, Z., Thomas, S., Bai, B. "Polyacrylamide microgels and pore modeled oil recovery Performance." 250th ACS National Meeting & Exposition. American Chemical Society, August 16-20, 2015, Boston, MA, USA.
6. Bai, B. "Development and Prospect of Preformed Particle Gel for Conformance Control Technologies." Presented in the Conoco-Philips (10 companies) in Houston, Jan 9, 2014.
7. Muhammed, F.A., Bai, B. "Heavy Oil Recovery from Sandstone Reservoirs in the Mid-Continent Region Using Preformed Particle Gel Enhanced Surfactant." AAPG Annual Conference and Exhibition, Houston TX, 6-9 April 2014.
8. Farag, M.; Bai, B., Study and Pilot Test of Preformed Particle Gel Conformance Control Combined with Surfactant Treatment, RPSEA ONSHORE PRODUCTION CONFERENCE-Illinois Basin and Surfactant Flooding, April 30, 2014, Evansville, IN.
9. Bai, B. Transport of Millimeter-size Particles through Conduit-like Channels, 1st International EOR Conference, Changping, Beijing, 16-19 June, 2014.
10. Imqam, A., and Bai, B. "Experimental Methods to Evaluate Preformed Particle Gels." Presented to ConocoPhillips Conformance Control Research Group, Rolla, Missouri, August 21, 2013.

11. Muhammed, F.A., and Bai, B. "Forced Imbibition through the Combination of PPG and Surfactant." Presented to ConocoPhillips Conformance Control Research Group, Rolla, Missouri, August 21, 2013.
12. Bai, B. "Discussion on Preformed Particle Control Technology". Presented at the 2013 International Symposium on Oilfield Chemistry held in Qingdao, China, June 26-28.
13. Muhammed, F.A. "Coupling of Preformed Particle Gel and Surfactant for Improved Oil Recovery." Presented to Verde Oil Company, a small producer in Kansas, Savonburg, KS, July 29, 2013.
14. Muhammed, F.A., and Bai, B. "Study and Pilot Test of Preformed Particle Gel Conformance Control Combined with Surfactant Treatment." RPSEA Onshore Production Conference–Technological Keys to Enhance Production Operation, Wichita, Kansas, June 27, 2013.

6.4 Invited Talks

1. "Hearing How Preformed Particle Gels Can Control Water Production in Mature Oilfields." Presented in Mature Fields North America 2015 held in Houston, TX, Aug 25-26, 2015
2. "Particle Gels for Conformance Control". University of Texas-Austin, Graduate Seminar, March 3, 2014
3. Recent Development of Conformance Control Technologies, Northeastern University of Petroleum, Daqing, China, July 2013.
4. Recent Development and Prospect of Particle Gels for Conformance Control, Conoco-Philips, Houston, May 26, 2013.
5. Recent Development and Prospect of Particle Gels for Conformance Control, Baker-Hughes, Houston, May 27, 2013.

REFERENCES

1. Liang, J., and Seright, R.S. "Wall-Effect/Gel-Droplet Model of Disproportionate Permeability Reduction," paper SPE 59344 presented at SPE/DOE Improved Oil Recovery Symposium, 3-5 April 2000, Tulsa, Oklahoma. http://dx.doi.org/10.2118/59344-MS

2. Seright, R.S. "Conformance Improvement Using Gels," Annual Technical Report (U.S. DOE Report DOE/BC/15316-6), U.S. DOE Contract DE-FC26-01BC15316 (Sept. 2004).

3. Chauveteau, G. et al. "In-Depth Permeability Control by Adsorption of Soft Size-Controlled Microgels,"paper SPE 82228 presented at SPE European Formation Damage Conference, 13-14 May 2003, The Hague, Netherlands. http://dx.doi.org/10.2118/82228-MS

4. Bai, B., et al. "Conformance Control by Preformed Particle Gel: Factors Affecting Its Properties and Applications," SPE Reservoir Evaluation and Engineering Journal, 10 (4), 415-421. (2007a). http://dx.doi.org/10.2118/89389-PA

5. Bai, B., et al. "Preformed Particle Gel for Conformance Control: Transport Mechanism through Porous Media," SPE Reservoir Evaluation and Engineering Journal, 10 (2), 176-184. (2007b). http://dx.doi.org/10.2118/89468-PA

6. Coste, J.-P., et al. "In-Depth Fluid Diversion by Pre-Gelled Particles. Laboratory Study and Pilot Testing," paper SPE 59362 presented at SPE/DOE Improved Oil Recovery Symposium, 3-5 April 2000, Tulsa, Oklahoma. http://dx.doi.org/10.2118/59362-MS

7. Zaitoun, A., et al. "Using Microgels to Shutoff Water in Gas Storage Wells," paper SPE106042 presented at the International Symposium on Oilfield Chemistry, 28 February-2 March 2007, Houston, Texas. http://dx.doi.org/10.2118/106042-MS

8. Al-Anaza, H.A., and Sharma, M. "Use of a pH Sensitive Polymer for Conformance Control," paper SPE 73782 presented at the International Symposium and Exhibition on Formation Damage Control, 20-21 February 2002, Lafayette, Louisiana. http://dx.doi.org/10.2118/73782-MS

9. Huh, C., et al. "A Rheological Model for pH-Sensitive Ionic Polymer Solutions for Optimal Mobility-Control Applications," paper SPE 96914 presented at SPE Annual Technical Conference and Exhibition, 9-12 October 2005, Dallas, Texas. http://dx.doi.org/10.2118/96914-MS

10. Pritchett, J., et al. "Field Application of a New In-Depth Waterflood Conformance Improvement Tool," paper SPE 84897 presnted at SPE International Improved Oil Recovery Conference in Asia Pacific, 20-21 October 2003, Kuala Lumpur, Malaysia. http://dx.doi.org/10.2118/84897-MS

11. Frampton, et al. "Development of a Novel Waterflood Conformance Control System," paper SPE 89391 presented at SPE/DOE Symposium on Improved Oil Recovery, 17-21 April 2004, Tulsa, Oklahoma. http://dx.doi.org/10.2118/89391-MS

12. Cheung, S., et al. "A Swelling Polymer for In-Depth Profile Modification: Update on Field Applications. Presented at SPE Applied Technology Workshop of Chemical Methods o Reducing Water Production, San Antonia, Texas, USA, March 4-6.

13. Liu, Y., Bai, B., and Wang, Y. "Applied Technologies and Prospect of Conformance Control Treatments in China," Oil & Gas Science and Technology – Rev. IFP 65 (1), 1-20.

14. Dong, M., Ma, S., and Liu, Q. "Enhanced Heavy Oil Recovery through Interfacial Instability: A Study of Chemical Flooding for Brintnell Heavy Oil," Fuel Journal, 88 (6), 1049-1056.

15. Wang, D., et al. "Producing More Than 75% of Daqing Oil Field's Production by IOR, What Experiences Have Been Learnt?" paper SPE 77871 presented at SPE Asia Pacific Oil and Gas Conference and Exhibition, 8-10 October 2002, Melbourne, Australia. http://dx.doi.org/10.2118/77871-MS

16. Thomas, S. "Chemical EOR: The Past - Does It Have a Future?" SPE 108828-L, an SPE Distinguished Lecture during 2005-2006.

17. Wang, D., et al. "Sweep Improvement Options for the Daqing Oil Field." SPE 99441. SPE Reservoir Evaluation & Engineering Journal, 2006. http://dx.doi.org/10.2118/99441-MS

18. Stoll, W. M., et al. "Toward Field-Scale Wettability Modification-The Limitations of Diffusive Transport," SPE Reservoir Evaluation & Engineering Journal, 11 (3), 633-640, 2008.

19. Bai, B., et al. "Preformed Particle Gel for Conformance Control," RPSEA Annual Report, 2009.

20. Hao, Z, and Bai, B. "Preformed-Particle-Gel Transport through Open Fractures and Its Effect on Water Flow," SPE Journal, 2011. http://dx.doi.org/10.2118/129908-PA

21. Imqam, A., Bai, B., Al-Ramadan, M. et al. 2014a. Preformed Particle Gel Extrusion through Open Conduits during Conformance Control Treatments. SPE Journal. SPE-169107-PA. http://dx.doi.org/10.2118/169107-PA.

22. Wu, Y., et al. "An Experimental Study of Interaction between Surfactant and Particle Hydrogels," Polymer Journal, 01/2011.

23. Britt, K., et al. "Characterization of a Shallow Horizontal Fracturing Treatment in Western Missouri," paper SPE 102342 presented at SPE Annual Technical Conference and Exhibition, 24-27 September 2006, San Antonio, Texas, USA.

24. Liu, Q., et al. "Surfactant Enhanced Alkaline Flooding for Western Canadian Heavy Oil." Physicochemical. Eng. Aspects Journal, 2007; 293, p. 64–71.

25. Oldorp, K., et al. "Using Rheo-Optical Methods to Analyze the Waxing of Crude Oil," Thermo Fisher Scientific, Dieselstrasse 4, 76227 Karlsruhe, Germany Thermo Fisher Scientific, 25 Nimble Hill Rd, Newington, NH 03801.

26. Buckley, J.S., Liu, Y., Monsterleet, S. "Mechanisms of Wetting Alteration by Crude Oils," SPE Journal, 1998.

27. Bryan, J., and Kantzas, A., "Enhanced Heavy-Oil Recovery by Alkali/Surfactant Flooding," paper SPE 110738 presented at SPE Annual Technical Conference and Exhibition, 11-14 November 2007, Anaheim, California, U.S.A.

28. Emulsions, Microemulsions, and Lipid-based Drug Delivery Systems for Drug Solubilization and Delivery, Part II: Oral Applications. In Water-Insoluble Drug Formulation, Cannon, J.B et al. 2008

29. Topical non-steroidal anti-inflammatory drug (NSAIDs microemulsions: Rationale, review and future prospective, Vinod Singh et al. 2013

30. Gas/Liquid and Liquid/Liquid Interfaces, Proceedings of 2nd International Congress Surface Activity, J. T. Davies, 1957

31. Surfactants and subsurface remediation, Environment Science and Technology, West and Harwell, 1992

32. S.K. Mehta and G. Kaur, Microemulsions: Thermodynamic and Dynamic Properties, 2011

33. Fluorescence emission from petroleum; a valuable information source for petroleum analysis, Ryder et al, 2004

34. Olsen, D.K., and Johnson, W.I. "Feasibility Study of Heavy Oil Recovery in the Midcontinent Region (Kansas, Missouri, Oklahoma). Topical report performed under cooperative agreement No. FC2243FE60149.

35. Bai, B., et al. "Preformed Particle Gel for Conformance Control," DOE Final Report, March 2012.

36. Kokufuka, E., Zhang, Y.O., Tanaka, T., and Mamada, A. "Effects of Surfactants on the Phase Transition of Poly(N-isopropylacrylamide) Gel," Macromolecules, 1993, 26, 1053.

37. Gao, Y., Yeung, S.C.F.A, and Wu, C. "Interaction between Surfactant and Poly(N-vinylcaprolactam) Microgels," Macromolecules, 1999, 32, 3674-3677.

38. Zhao, F., et al. "Application of surface pressure drawdown curves of injection wells in profile modification using clay," Oil Drilling & Production Technology, 1994, 16(2):73-76.

39. Feng, Q., et al, "Application of fuzzy mathematics to block-wide injection profile control," Petroleum Exploration and Development, 1998, 25(3):76-79.

40. Liu, Y., et al, "Optimization Design for Conformance Control Based on Profile Modification Treatments of Multiple Injectors in a Reservoir," paper SPE 64731 presented at International Oil and Gas Conference and Exhibition in China, 7-10 November 2000, Beijing, China. http://dx.doi.org/10.2118/64731-MS

41. Bai, B., et al, "Field and Lab Experience With a Successful Preformed Particle Gel Conformance Control Technology," paper SPE 164511 presented at SPE Production and Operations Symposium, 23-26 March 2013, Oklahoma City, Oklahoma, USA. http://dx.doi.org/10.2118/164511-MS